Assessment of the application of permeable pile groins as coastal protection

A. C. Briele

Technische Universiteit Delft

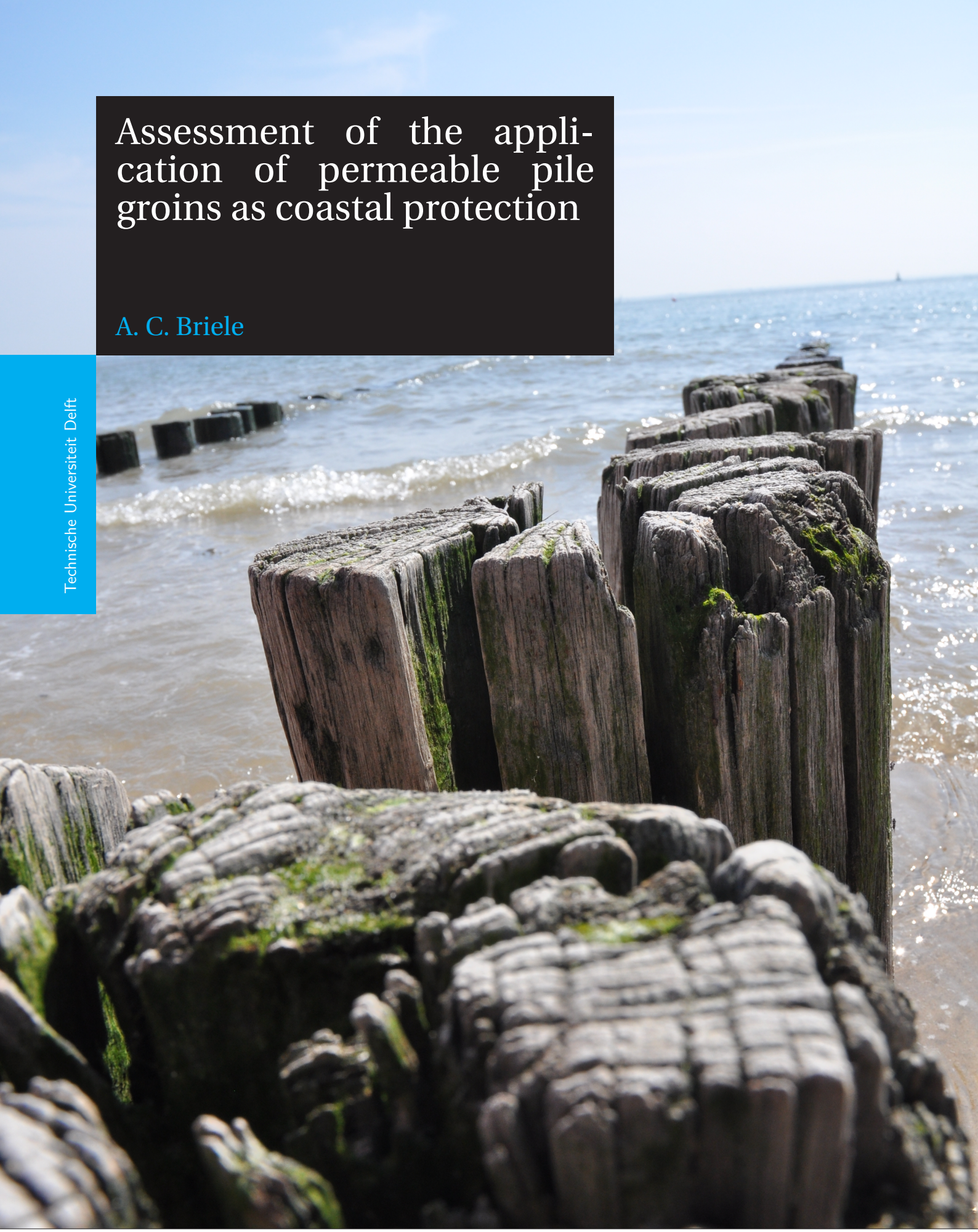

TU Delft Delft University of Technology

Witteveen + Bos

Challenge the future

Cover photo: A permeable double row pile groin in Vlissingen, The Netherlands - Taken at flood in May, 2014 - Carolin Briele

ASSESSMENT OF THE APPLICATION OF PERMEABLE PILE GROINS AS COASTAL PROTECTION

by

A. C. Briele

in partial fulfillment of the requirements for the degree of

Master of Science
in Civil Engineering

at the Delft University of Technology,
to be defended publicly on 17th of December, 2014 at 10:00 AM.

Supervisor:	Marcel Stive	
Thesis committee:	Prof. dr. ir. M. J. F. Stive,	TU Delft
	Prof. dr. ir. W. S. J. Uijttewaal,	TU Delft
	Dr. ir. M. Zijlema,	TU Delft
	ir. D. Dusseljee,	Witteveen+Bos

TU Delft Delft University of Technology

Witteveen+Bos

PREFACE

With this thesis, I finalize my Master's degree in Civil Engineering at the Delft University of Technology with specialization Hydraulic Engineering (Coastal Engineering). I would like to express my gratitude to those who supported me during the process of my graduation.
First of all, I would like to thank my committee members Marcel Stive, Wim Uijttewaal, Marcel Zijlema, Marije Smit and Daniël Dusseljee. Your guidance throughout the research and writing was of high valuable for me to develop my thesis and my skills on scientific research and reporting. Thank you for all your time and patience.
Further, I would like to thank TU Delft to provide the Master's studies that meet my interests perfectly and provide a scientific and motivating atmosphere to challenge myself and the future.
My gratidude also goes out to Witteveen+Bos who supported my research with guidance, computational capacity and valuable advise. It was a pleasure to be part of the group hydrodynamics and morphology. My special thank is directed at Maarten Janssen and Gert Klopman. Also, I would like to thank my fellow graduate students for the nice atmosphere.
Akash, Edgar and Arjan, I appreciate all the hours you gave to me to evaluate my report and my research. Thank you for all your input from a different point of view and all the time I spent processing your feedback.
Last but not least study related, I would like to thank IACES as responsible association that I was able to do my Master's degree in Delft. Thank you, Martijn and Joost, for awakening my interest in TU Delft and your support until I finally arrived.

In Delft, I had a wonderful time, meeting a lot of interesting Dutch and international students in such an open and encouraging atmosphere. Thank you for all the barbecues, rock 'n roll dances, concerts and drinks we had! Lisa, thank you for being the best room-mate I ever had. It was a pleasure to share talks and dinners and let me suffer in your sports classes.
Last but not least, I am very happy to have always had the support of my family, both on my studies and on personal development.

Carolin Briele
Delft, December 2014

SUMMARY

Permeable wooden pile groins have a long tradition as being part of the coastal protection in the Netherlands, as well as in Germany and the United Kingdom. They are built to protect beaches from eroding by reducing the current velocity along the beach and thus its ability to transport beach material. This type of groin is most popular among the population; in Zeeland (NL), they are incorporated into the national heritage. In scientific research however, they lack attention. More focus is set on beach processes themselves and on the (supposedly) more stable impermeable rubble mound groins. As several researches stress their potential as soft methods and their advantages over impermeable groins, this thesis intends to put their usage more into focus. By means of generic numerical research and a comparison to available laboratory data and analytical approaches, the understanding of this type of groins is enhanced. This thesis explores the usage of permeable wooden pile groins in coastal waters under the influence of current and wave forcing.

Both impermeable and permeable groins are able to reduce the sediment transport capacity and yield sediment accumulation. Impermeable groin are researched on reasonable well, as they are supposed to be more stable and their effects easier predictable. Important disadvantages are also originating from their impermeable structure: they deflect the approaching current causing strong offshore directed flows and large scale eddies between neighbouring groins. The paths of the sediment transportation will lead to a zig-zag profile of the shoreline, eventually causing erosion landward of the original shoreline and outflanking of the groin. Permeable groins reduce the original current velocity originating from the tide or breaking waves while not changing the general flow field. As a consequence, the sediment transport capacity reduces and dangerous rip-currents are prevented to a great extent.
The thesis provides insight into the theoretical behaviour of the flow field around groins based on available laboratory experiments and theoretical considerations. This is enriched by a numerical research. For the forcing by a current, an analytical model is developed which provides the global change in the waterlevel upstream and downstream of a stream. Further, the change in the velocity behind the groin and next to the groin can be obtained.
In numerical models available for hydraulic engineering and research, the direct implementation of permeable pile groins is not explicitly provided. For most large scale hydrodynamic and morphology models the flow around a groin is on a too small spatial scale to be of interest compared to the whole flow domain. However, there are tools available to approximate the effects of permeable groins. The effect of the groins on the hydrodynamics is evaluated by means of the numerical model SWASH (Simulating WAves til SHore). This relatively new model is developed with the intention to reproduce both small and large scale flows in shallow water. In SWASH, two possible tools are available of which one on basis of a Morison equation proved to be suitable for the representation of groins on a laboratory scale.
The numerical research evaluates the effect of permeable pile groins on the flow field when subject to a forcing by either a constant current originating from the tide, or the like, or from breaking waves. It is evaluated that many effects caused by the presence of groins on the flow field can be reproduced on a flat and an inclined (beach) bottom, both under a current or a wave forcing. For the wave forcing at a beach profile, a more detailed analysis is done on the effect on the flow field and bottom shear stresses under variations in the physical parameters. This study gives the range of boundaries under which permeable groins are applicable and their consequent effect on the flow field.

CONTENTS

List of Figures

List of Tables

List of Symbols

Latin

Symbol	Units	Definition
a	m	wave amplitude
A	m^2	area
A_b	m^2	area of bottom
A_D	m^2	area of obstacle normal to fluid
b	m	opening between piles
B	m	width
c	m	wave celerity
c_g	m/s	wave group celerity
c_0	m/s	deep water wave celerity
c_f	-	friction coefficient
c_p	m/s	phase speed
c_D	-	drag coefficient
c_S	-	Smagorinsky coefficient
C	$m^{1/2}/s$	Chézy coefficient
D	m	Diameter of a pile
E	m^2	wave energy
E_{tot}	m^2	total wave energy of a spectrum
f	Hz	frequency
F	N	force
F_D	N	drag force
Fr	-	Froude number
g	m/s^2	acceleration of gravity
G	N	weight force
G_s	N	weight force in s-direction
h	m	water depth
h_0	m	original water depth
h_b	m	water depth at wave breaking
h_{cr}	m	critical water depth
H	m	wave height
H_0	m	wave height at deep water
H_b	m	wave height at breaking
H_S	m	significant wave height
H_{RMS}	m	root mean square wave height
i	-	gradient
i_b	-	bottom gradient
i_w	-	water level gradient
k	1/m	wave number ($= 2\pi/L$)
k_s	m	Nikuradse roughness height
l_m	m	Prantl mixing length
L	m	wave length
L_0	m	deep water wave length
L_g	m	length of groin
L_s	m	groin spacing
m	$s/m^{1/3}$	Manning friction coefficient
M	N	Momentum
n	-	ratio group and deep water celerity
n	-	number of groins
N	-	number of piles
p		pressure

p_H		hydrostatic pressure
P	-	permeability
P	-	Mixing coefficient
P	m^3/s	Energy flux
q	m^2/s	specific discharge
q		non-hydrostatic pressure
Q	m^3/s	discharge
R	m	hydraulic radius
	depends	Resistance force
S	unit	radiation stress
$S_{ds,veg}$	unit	dissipation of energy by piles or vegetation
t	s	time
T	s	Wave period
u	m/s	velocity in x direction
u_*	m/s	shear stress velocity
v	m/s	velocity in y direction
v	m/s	longshore current velocity
v_0	m/s	approach velocity
v_0	m/s	maximal longshore current velocity
w	m/s	velocity in z direction
W	N	weight
x	m	distance along longshore axis
y	m	distance along cross-shore axis
z	m	distance along vertical axis

GREEK

SYMBOL	UNITS	DEFINITION
α	-	slope angle
δ		
γ	-	breaker index
Δx	m	grid size in x direction
Δy	m	grid size in y direction
ζ	m	surface elevation
η	m	water surface elevation within wave
η_b	m	water level set-down at wave breaking
η_{shore}	m	water level at the shore line
η_{max}	m	maximal water level set up
$\Delta\eta$	m	water level difference between η_{max} and η_b
θ	°	wave angle w.r.t. cross-shore axis if not indicated differently in the text
θ_b	°	wave angle at breaking
ν	m^2/s	dynamic viscosity
ξ	-	breaker parameter (Iribarren number)
ρ	kg/m^3	density
σ	Hz	(mean) wave frequency
τ	N/m^2	shear stress
τ_b	N/m^2	shear stress due to bottom friction
τ_p	N/m^2	shear stress due to presence of piles
ω	rad/s	angular frequency

LIST OF ACRONYMS

ACRONYM	DEFINITION
BDF	Backward Differentiation Formula
CFD	Computational Fluid Dynamics
CIRIA	Construction Industry Research and Information Association
ILU	incomplete LU-Decomposition
MSL	Mean Sea Level
PDE	Partial Differential Equation
RANS	Reynolds Averaged Navier Stoke's equations
RIZA	Rijksinstituut voor Integraal Zoetwaterbeheer en Afvalwaterbehandeling
SWASH	Simulating WAves till SHore

1

INTRODUCTION

1.1. BACKGROUND AND MOTIVATION

Coastal areas are attractive for human settlement. Nowadays, around half of the world's population lives within a band of 200km from the coast (10% of the land's surface) (Hinrichsen, 2011). Coastal management and protection are generally needed whenever (human) life, ecological or economical values are endangered by coastal processes or changes (Schiereck, 2004).
In order to protect the valuables, measures have been developed of which one is a permeable groin system. Groins are

Figure 1.1: A groin system in Hayling, UK, as a coastal protection system (Maritimejournal, 2014). Sediment accumulates in the groin fields.

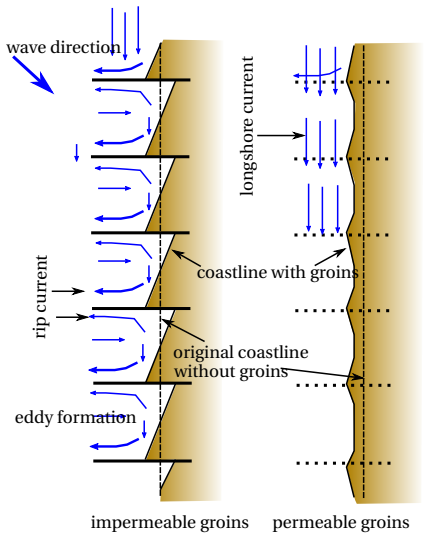

Figure 1.2: Schematic development of the coastline for a beach with impermeable (left) and permeable groins (right) compared to the original coastline.

structures (nearly) straight and orthogonal to the coastline. They are usually reaching until the end of the surf zone where waves start breaking, Their width is small compared to their length. Groins are most often used as a system out of several members with a certain distance between each other. The aim is to reduce the loss of beach material and eventually accumulate sediment within the groin cells (Figure 1.1). As groins are orthogonal to the coast, they interact with the longshore component of the flow along the coast and only contribute to a positive coastal development if most of the sediment loss is due to a longshore transport parallel to the coast, e.g. induced by a tidal wave or approaching waves. A groin system keeps the high current velocities away from the beach and thereby reduces the ability of the current to transport sediment. In a properly designed groin system, sediment accumulates and the coastline accretes towards the sea (Figure 1.2). In general, groins do not influence processes normal to the shoreline (cross-shore direction) significantly and are not able to reduce the impact on a coast by reducing the waveheight or triggering wave breaking. Therefore, they are not effective enough at a coast where most of erosion takes place in the cross-shore direction or under cross-shore storm events as the only measure. However, even when most of the erosion is taking place along the cross-shore direction, the profile within

a groin field can develop into a more dissipative beach form and be more stable under cross-shore storm conditions Trampenau (2000) as more wave energy is dissipated before erosion is initiated.
Groins can be designed from various materials, in a permeable or impermeable way. As the names suggest, the difference between these latter two types of groins is their permeability. Impermeable groins act as a hard obstacle to the flow, forcing a flow deflection and strong rip-currents. Permeable groins allow the current to pass through the openings between the piles while reducing the current velocity. The focus within this thesis lies on permeable groins made out of cylindric wooden piles, usually with a diameter of $D = 0.2$m to 0.3m. The permeability in this case is achieved by placing the piles with a certain distance to each other (Figures 1.3 and 1.4). For a comparison an impermeable rubble mound groin is given in Figure 1.5.

Figure 1.3: A permeable groin in Vlissingen at high water.

Figure 1.4: Two permeable groins with two rows each in Zeeland (Unknown).

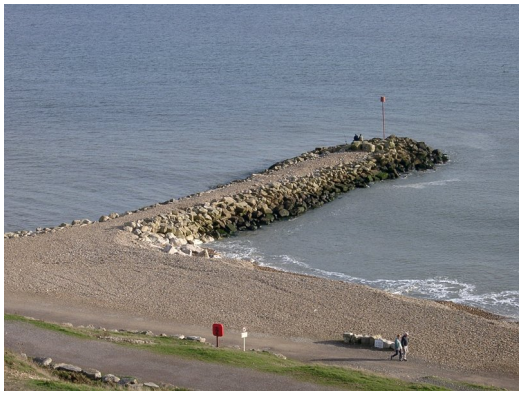

Figure 1.5: An impermeable rubble mound groin (Stacey, 2001).

One major shortcoming of an impermeable groin is the change they cause on the flow field and the erosion at the leeside of the groin. The flow within the groin cells can be described by one or more large scale eddies and rip-currents at the windward and leeward side of the groin (Figure 1.2). Rip-currents are usually strong currents normal to the coastline due to irregularities in the coastline or due to obstacles such as a groin. They can be a major reason for cross-shore sediment loss due their ability to transport sediment associated to their high offshore directed velocity. If the rip-currents reach far enough into the offshore, they eventually deposit the sediment outside the active beach profile, i.e. the part of the beach over which the material is deposited throughout the year. Further, their high velocity can be a threat to swimmer's safety (Komar, 1998). Erosion is taking place at the leeside of the groin due to a shortage in sediment availability as it accumulates windward of the groin. This behaviour leads to a so-called zig-zag profile and eventually leads to erosion landwards of the original shoreline (left part in Figure 1.2).
Permeable groins on the other hand are often described as an additional hydraulic resistance instead of an obstacle to the flow as they reduce the longshore current velocity while the qualitative flow field remains closer to the original one, i.e. only a minor part of the flow is deflected offshore in front of the groin and eddies are less probable to develop or with a lower velocity. If the groins are permeable enough (usually 30% or more), the coastline can develop parallel to the original one into the seaward direction without creating a zig-zag profile or feeding strong rip-currents. Though several authors[1] mention this type of groins as a good solution to protect the coast from eroding, little research has been conducted on permeable groins. Impermeable groins have been researched on a lot more. Permeable groin systems at the Dutch, German and British coast have basically been build on (engineering) guessing and experiences, less on theoretical background (Trampenau, 2000; Bakker et al., 1984)

[1] e.g. Fleming (1990a),Trampenau (2000), Bakker et al. (1984)

This thesis investigates the hydraulic flow field near groins based on a numerical study in comparison to available measurement data and theoretical values. A better understanding and prediction of the complex flow fields which develop around permeable groins allows to build groins based on more physical reasoning and to optimize the groin system related to flow fields, sediment movement and loss, safety and costs.

1.1.1. GROINS IN THE CONTEXT OF COASTAL PROTECTION

Coastal protection is the general term for measures taken to protect the coast from a loss of sediment and therewith the landwards lying areas. Protection is required when the coast itself or the surrounding area would be endangered by a retreat of the coastline and it is chosen to protect these values (Schiereck, 2004). A brief description of different ways to classify coastal protection is given to show the context of permeable pile groins as coastal protection. Possible ways are to indicate the general approach related to the structure (retreat, accommodate or protect), to identify the approach related to the impact (against the cause or the symptoms) or to the method itself (soft or hard methods).

Retreat, Accommodate or Protect The general approach related to the object to be protected can be divided in a retreat (i.e. further away from the coastline), an accommodation for the threat or the protection by measures (Bosboom and Stive, 2013).

Symptoms or cause The measures can be applied to eliminate the cause or the symptoms of the erosion. In the first case, one can think of a wave height and energy reduction, in the latter case of a sediment supply (Komar, 1998).

Soft or hard methods Coastal structures are often refered to as hard measures, while soft methods refer to more natural measures such as a sediment supply.

Groins as coastal protection Groins can be identified as a protection. As groins reduce the longshore current responsible for sediment transportation and reduce the wave heights under certain circumstances, they can be classified as a method against the cause. Many authors[2] refer to permeable groins as a soft method and to impermeable rubble mound groins as hard methods. This is as permeable groins function mainly by reducing longshore current velocities without altering streamlines as much as impermeable groins whereas impermeable groins are an insurmountable obstacle for waves and currents.

1.1.2. GROINS AND BEACH DEVELOPMENT

The choice of the type of protection clearly depends on the type of sediment available, i.e. if the sediment is rather fine or coarse (Fleming, 1990b). If the main part of the sediment is lost cross-shore, a groin system will not help preventing the loss (van de Graaf and Koster, 1990).
In general, groins are built to reduce the longshore current and thus reducing the longshore sediment transport. Depending on their permeability, the exact influence on the (re-)distribution of the current will be different, which leads to a different coastline development. Both permeable and impermeable groins are most commonly found in groups as their influence area is limited in space. By holding back sediment in one groin cell, they can cause downdrift erosion behind the groin, especially behind the last. By placing a group in certain ways, the downdrift erosion can be reduced.

Impermeable groins The basic idea of impermeable groins is to provide a coastal cell in which the sand is trapped and can be realigned with the dominant wave direction (Fleming, 1990b). When considering several of these cells, this leads to a "zig-zag" coastline (Figure 1.2). Especially behind the last groin or if the groins are too far apart, erosion can occur behind the groin leading to a loss of beach at the lee side of a groin (Fleming, 1990a).
Impermeable groins will lead to an offshore deflection of the longshore current, inducing rip-currents and erosion around the groin. Within the groin cells, one or more large scale eddies will develop. As the current is redirected around the groin, the longshore flow velocity just offshore of the groin will increase significantly.

Permeable groins Permeable groins have one significant advantage over impermeable groins. They do not block the longshore current completely, so that a part of the current can pass the groin without changing direction significantly. By this, the development of rip-currents, eddies within the groin fields and the currents seaward of the groin will be suppressed or at least reduced. As the piles are still an obstacle to the flow, minor rip currents can still develop, but are usually only found in front of the first groin (Trampenau, 2000) (see Figure 1.2). The zigzag profile will not develop, but a more straight coastline will remain, also allowing for an accretion of the whole coastline.
However, permeable groins seem to have short-comings when there is not a clear dominant wave direction, too severe storms and in case of an unfavourable relation of tide and waves. However, research from the 1980's onwards showed that

[2] e.g. Trampenau (2000)

permeable groins have more advantages than disadvantages if the proper boundary conditions are met. Yet, up until today, no clear design guidelines have been established for the use of permeable groins whereas there are for impermeable groins.

1.1.3. GROINS IN HISTORY AND SOCIAL PERCEPTION

The usage of groins as part of the coastal protection system has a long tradition. In the Netherlands, it can be dated back as to around 1540. In the 18th century an attempt on an improved usage took place which eventually led to valuable knowledge on the general sediment transport and an improved layout of the groins. However in the 19th century, due to economic reasons, they have been replaced by a new kind of groins: impermeable rubble mound groins (van Lyden, 2007).

In the 1960's, the first permeable groins have been built again to add to or substitute massive rubble mound groins. The experiences with these groins are summarized in Bakker et al. (1984) with the conclusion that under certain circumstances (Section A.1) permeable groins can and should be used, and that the observed failures could be explained and prevented. Though, from an engineering point of view, doubts remained due to failed permeable groins, these groins have been re-included into the Dutch landscape and appreciated. In the province of Zeeland, they have been included into the national heritage (Provinciale Zeeuwse Courant (2007), Boekblad.nl (2007)) and into the "Canon of Zeeland" which lists the 50 most important developments in the history of Zeeland (Geschiedeniszeeland, a,b; Kuipers and Francke, 2009).

In Germany, groins have been used as coastal protection since the early 19th century Trampenau (2000). Those groins have been build based on experiences with river groins and engineering estimation which partly led to insufficient designing as the processes in coastal waters are more complex than in river situations (Trampenau, 2000). This led to a "suspicion" especially against permeable groins in engineering practice. Also focussing on the general nearshore processes in hydraulic research led to an under-representation of groins in research Trampenau (2000).

1.2. OBJECTIVE

1.2.1. MAIN RESEARCH OBJECTIVE

The objective is to improve the understanding of the hydrodynamics around permeable groins and their physical and numerical reproducibility. It is investigated to what extend they can already be included into the existing numerical nearshore models. A better understanding of hydrodynamics around groins, based on analytical approaches and numerical simulation, makes it easier to predict the actual sediment transport and coastal development.

1.2.2. RESEARCH QUESTION

This thesis attempts to address the following questions:

What are the important hydrodynamic theories and concepts that have to be taken into account when analysing a groin system? In the literature study (Chapter 2), important concepts on coastal processes with and without groins are evaluated. Available guidelines on the usage of groins are presented.

How do coastal groins effect currents and water levels from a global and local viewpoint? It is to be evaluated, how the permeable pile groins effect the hydrodynamics, both on a conceptual and detailed local scale. For different boundary conditions, it is to be evaluated if an effect can be seen and under which conditions permeable pile groins are useful and optimal.

Can hydrodynamic processes around groin (fields) in coastal areas be reproduced? What are the possibilities to predict the influence of groins on the groin field by means of (simplified) analytical considerations and by means of numerical models?

What are advantages and possible shortcomings in numerical models? Numerical models are always an estimation of reality and physics. The application boundaries result from shortcomings or restrictions in the numerical model are to be evaluated.

What kind of research and development is further needed to evaluate permeable groins? On basis of the results, recommendations on potential further research are to be given.
Those questions are evaluated throughout the thesis and answered in Chapter 8.

1.3. APPROACH AND OUTLINE OF THE REPORT

To assess the application of permeable pile groins as part of the coastal protection system, they have been analysed under different forcing conditions based on a literature study, analytical considerations, a numerical model and comparison to available measurements.
This thesis starts with a review on important processes on hydrodynamics and morphology at and near the surf zone that can be associated with the functioning of a groin system, for both with and without the interaction with groins (Chapter 2). Available guidelines and important researches are presented in Appendix A.
An analytical approach to evaluate the variation in the flow velocity and water levels is found in Chapter 3. This model is based on the Morison equation for a current forcing.
A description of the model used (SWASH) to simulate the hydrodynamics around the groins by The SWASH team (2013) can be found in Chapter 4, laboratory measurements for the calibration and validation of the model in Chapter 5.
The groins have been analysed for a current-only forcing (Chapter 6) and for a wave-only forcing inducing a longshore current (Chapter 7). In both forcing situations, the groins have been implemented into the numerical model by means of several methods available to evaluate the present possibilities inside the numerical model SWASH. For the current-only forcing, a more detailed study on the turbulence model is done. For the wave case, a numerical study on the longshore current is presented (Appendix B) as well as a study on physical boundary conditions. For both types of forcing, a validation of the numerical model is done to prove its ability to reproduce the undisturbed flow before, in a second step, the groins are implemented.
In Chapter 8, the findings are summarized and recommendations concerning groin modelling and design as well as further research are given.

2

THEORETICAL BACKGROUND

2.1. INTRODUCTION

The important concepts related to the usage of groins are illustrated starting with the definition of terms and the coordinate system conventions used in this thesis. This chapter further describes coastal processes related to waves (Section 2.3) and the interaction of groins with waves and currents (Section 2.4). The chapter commences with concepts related to turbulence models (Section 2.5) and bottom friction concepts (Section 2.6). Some of the most important guidelines and experiments concerning groins are listed in Appendix A.

2.1.1. DEFINITION OF TERMS, CONVENTIONS

In this thesis, the axis system used is Cartesian with the x-axis in alongshore direction and the y-axis normal to the shore, originating at the shoreline at still mean sea level[1]. The vertical z-axis is defined downwards, originating at still water level. The shoreline itself is defined as the line alongshore until where the water reaches. The bottom slope angle is defined as the angle between still water and the averaged beach bottom. The angle of the approaching waves θ is defined with respect to the cross-shore axis y in clockwise direction.

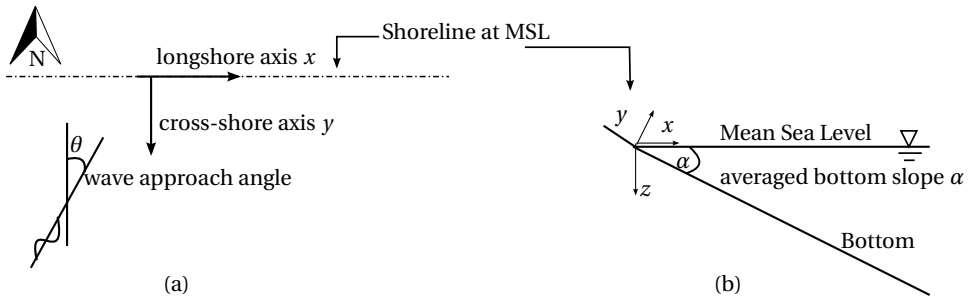

Figure 2.1: Conventions of orientation and coordinate system, (a) shows a topview (b) shows a cross-section.

2.2. GROINS

2.2.1. DEFINITION OF GROINS

A groin is a coastal structure built to reduce longshore current velocities and protect the beach from eroding. Groins are usually built straight and orthogonal to the coastline. The straight groin is most commonly used in Germany and the Netherlands. A groin system contains several groins in a row, with a spacing between the groins of L_s, potentially variable alongshore. The groin length L_g is usually maximal until the breaker line of the waves against the erosion associated with wave energy and mass transport (e.g Fleming, 1990a). Figure 2.2 shows the principle groin terminology.

[1] Often, the coordinate system changes when dealing with waves (x-axis normal to the coast). For convenience, within the thesis only one coordinate convention is used, except when explicitly mentioned.

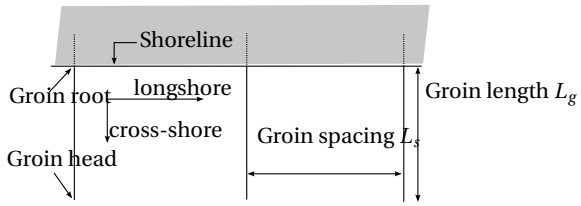

Figure 2.2: Definitions of a groin and groin fields as used within this thesis.

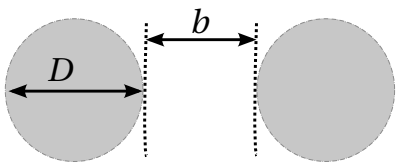

Figure 2.3: Definition of the permeability of a pile groin.

2.2.2. PERMEABILITY OF PILE GROINS

Groins can be either impermeable or permeable. Permeable groins act as an additional hydraulic resistance to the current rather than as a complete blockage (as impermeable groins).
Permeable groins are, in addition to their length and groin spacing, defined by their permeability. The permeability is achieved by openings in the groin. In case of (wooden) piles as material, the permeability P is defined as the free space between the piles b over the distance between the middle of two piles:

$$P = \frac{b}{D+b}\,, \tag{2.1}$$

with D the diameter of the usually cylindric pile (Figure 2.3).

2.3. COASTAL PROCESSES

The most important concepts of nearshore water movements and processes waves undergo approaching the shore and their analytical description are presented. Of interest are those processes that eventually lead to wave breaking and the initiation of the longshore current and the set-up and set-down of the mean water level.

2.3.1. WAVES AND WAVE RELATED CURRENTS

Waves approaching the coastline are subject to transformation in the intermediate and shallow water depths due to shoaling, refraction, diffraction and other (non-)linear transformations. As a consequence, waves eventually steepen until they cross a threshold steepness and break. Breaking waves exert a force on the water body initiating a longshore current.

LINEAR WAVE THEORY

The regular sinusoidal wave can be described by means of its wave length L, height H and phase speed c, see e.g. Holthuijsen (2007). The relation between those three parameters is:

$$c = \frac{L}{H}\,. \tag{2.2}$$

An important concept is the transformation waves undergo when travelling from deep water through intermediate to shallow water (and vice versa). Waves change their height, speed and length while the period remains the same.
A simple first approach to describe the wave transformation is the Airy wave theory (Komar, 1998). It is a simple linear relationship for a horizontal bottom assuming no losses due to friction and a much smaller wave height than waterdepth and wavelength, and it also describes the behaviour on a sloping bottom quite well (Komar, 1998).
The water surface elevation $\eta(x,t)$ can be described as:

$$\eta(x,t) = \frac{H}{2}\cos(kx-\omega t)\,, \tag{2.3}$$

in which $k = 2\pi/L$ is the wave number and $\omega = 2\pi/T$ the angular frequency, e.g. Holthuijsen (2007).
The wave energy E and the energy flux of the waves P remain the same without dissipation and can be described as (Holthuijsen, 2007):

$$E = \frac{1}{8}\rho g H^2, \text{and } P = Ecn = (Ecn)_\infty = \text{constant} \tag{2.4}$$

with n the ratio of group speed to phase speed $n = c_g/c_p$ (Holthuijsen, 2007).

SHOALING

When waves approach shallow water, they will transform their characteristics except from their period and energy. By comparing the energy flux at deep and shallow water, the following relation can be derived:

$$\frac{H}{H_0'} = \left(\frac{1}{2n}\frac{c_0}{c}\right)^{1/2}, \tag{2.5}$$

in which the index 0 indicates the wave characteristics at deep water (Komar, 1998). The shoaling process is used to explain the wavebreaking due to a high steepness of the waves yielding eventually to a longshore current.

REFRACTION

Waves tend to become parallel to the depth contours, describable by Snell's law:

$$\frac{\sin\theta_1}{c_1} = \frac{\sin\theta_2}{c_2} = \text{constant}, \tag{2.6}$$

with θ the angle of the approaching waves to the cross-shore direction and c the phase speed of the waves (Figure 2.4). Refraction occurs due to the difference in wave speed at different waterdepths (Komar, 1998). At a smaller waterdepth, the wave will travel slower forcing the wave to turn into the direction of the smaller waterdepth as the ratio of angle and phase speed remains constant. The wave crest will therefore tend to align with the shoreline, especially in case of a straight coastline with parallel depth contours (Komar, 1998). In practice, waves approaching with an angle to the cross-shore direction at deep(er) water will keep an angle when they are breaking and when they are close onshore and give rise to the longshore current.

DIFFRACTION AND SHADOW ZONE

Along obstacles such as groins, the wave train is interrupted creating a shadow zone behind it. The waves will bend at the edge of the obstacle into the shadow zone towards the obstacle (Komar, 1998), see Figure 2.5. The shadow area will be subject to less wave energy. Analytical description proved to be not straightforward as it cannot be directly implemented or only with a high order (Holthuijsen, 2007).

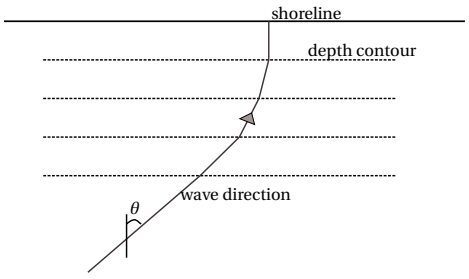

Figure 2.4: Refraction of waves at a beach with parallel depth contours: Waves tend to turn to the shore, adapted from Holthuijsen (2007).

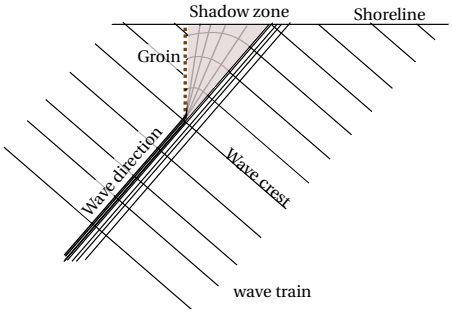

Figure 2.5: Diffraction of waves at a beach with a constant depth: Waves tend to turn to the obstacle but with a reduced wave height, adapted from Holthuijsen (2007).

WAVE BREAKING

Due to shoaling, waves are getting steeper until they reach a point when they are too steep and break, i.e. the ratio of waveheight over wavelength is too large to be sustainable. As this behaviour is not implicitly included in the shoaling formula, an additional formula has to be defined (dissipation model) (Bosboom and Stive, 2013).
The basic formula is of the type as obtained by Miche (1944)

$$\gamma = \left[\frac{H}{L}\right]_{max} = 0.142\tanh(kh), \tag{2.7}$$

based on the Stoke's wave theory for a horizontal bottom (in Bosboom and Stive, 2013). The Iribarren number

$$\xi = \frac{\tan\alpha}{\sqrt{H_0/L_0}} \tag{2.8}$$

relates the slope of the bottom α to the slope of the waves H_0/L_0 (Schiereck, 2004) and creates categories of different breaker types. According to Battjes (1974), the greatest possible steepness of the waves before they break depends on the type of breaker, i.e. on the Iribarren number. The most common types for breakers at the Dutch and German coast are spilling breaker, i.e. that the slope is flat with respect to the wave (Bosboom and Stive, 2013). According to Bosboom and Stive (2013), literature suggests that the breaker index lies around $\gamma = 0.6$ to 0.8 for spilling breakers.

SURF ZONE

The surf zone is defined as the part between the shoreline and the initiation of wave breaking (Figure 2.6).

RADIATION STRESS

Longuet-Higgins and Stewart (1964) have defined the radiation stress as the depth-integrated and wave-averaged flow (or flux) of momentum due to the presence waves, thus the excess momentum flux due to the presence of waves (Bosboom and Stive, 2013). The radiation stress is responsible for wave forces on the water yielding to differences in the mean water level (set-up and set-down) and the wave-induced longshore current in the surf zone and can be used to approach them mathematically.
The radiation stress can be divided into normal and shear components. In case waves are normal incident to the coastline, only the normal components persist. This would theoretically be expected due to refraction. In case of real waves, they will not generally enter normal to the coast but keep an angle to it. In this case, they introduce a shear radiation stress component which is responsible for the longshore current. This longshore current is considered as one of the forcings on the permeable piles in this thesis.
The components of the radiation stress are given by:

$$S_{xx} = E\left(n - \frac{1}{2} + n\cos^2\theta\right), \quad S_{yy} = E\left(n - \frac{1}{2} + n\sin^2\theta\right), \text{normal components} \tag{2.9}$$

$$S_{xy} = S_{yx} = En\cos\theta\sin\theta, \qquad \text{shear components} \tag{2.10}$$

for a wave approaching the coast with an angle θ w.r.t the shore-normal axis x.

SET-UP AND SET-DOWN

The set-up and set-down of the mean sea level results from breaking waves. The change in the averaged sea level results in a slope and a pressure gradient to balance the onshore component of the radiation stress (Komar, 1998, citing Longuet-Higgins and Stewart (1964)). As the set-up can be significantly, it can influence the hydrodynamics around (permeable) groins as it influences whether piles are emerged or submerged. The maximum in set-up is found behind the shoreline. Just at the point of wavebreaking, a depression in the sea level occurs: the set-down.
The analytical solution is based on a pressure gradient balancing the radiation stress in the surf zone:

$$-\frac{\mathrm{d}}{\mathrm{d}x}\left[\left(n - \frac{1}{2} + n\cos^2\theta\right)E\right] = \rho g h \frac{\mathrm{d}\eta}{\mathrm{d}x}, \tag{2.11}$$

It is assumed that the shallow water equations hold, where $n = 1$ and waves approach normal to the shore giving $\theta = 0°$. The resulting equation is integrated from the point of breaking to the place of maximal set-up, where $h = 0$m is found (Bosboom and Stive, 2013). This gives the maximal set-up with

$$\eta_{max} = \eta_b + \frac{3}{8}\gamma H_b. \tag{2.12}$$

The value for the set-down in the shallow water approximation is calculated based on Longuet-Higgins and Stewart (1962) (as cited by Bosboom and Stive, 2013) with

$$\eta_b = -\frac{1}{16}\frac{H_b^2}{h_b} = -\frac{1}{16}\gamma H_b. \tag{2.13}$$

The set-up difference in water level is then

$$\Delta\eta = \frac{3}{8}\gamma H_b. \tag{2.14}$$

In this approach, the influence of the bottom friction and the Coriolis force is assumed to be small compared to the wave forcing and are therefore excluded for simplicity: In Apotsos et al. (2007), it was shown that this approach may lead to an underestimation of the set-up (as cited in Bosboom and Stive, 2013). Further, this simplified model assumes that waves are approaching normal to the shore. For waves approaching with an angle different than shore-normal, the term $\cos^2\theta$ of equation 2.11 theoretically leads to a lower value. This simplified approach to verify the order of magnitude of the set-up and setdown in numerical models.

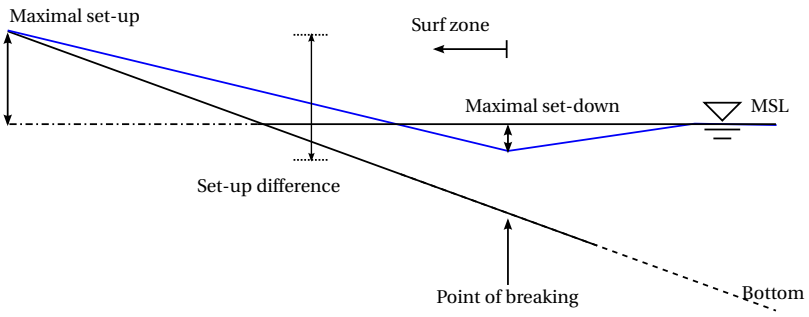

Figure 2.6: Definition of the set-up and set-down of the mean water level.

THE LONGSHORE CURRENT

The longshore current is one of the main forcing mechanisms permeable pile groin are supposed to interact with and reduce. In the surf zone, a net transport can be found in the wave direction as the waves will usually keep a certain angle deviating from shore-normal. This current initiated by breaking waves is directed in the longshore direction of the coast. Averaging the velocities over a certain time (in practise a couple of wave periods) results in the longshore current which is parallel to the coast.

In order to evaluate the forcing on the groin, the longshore current needs to be computed precisely which is difficult. For the longshore current, analytical formulae are available for the theoretical behaviour without horizontal mixing. For a longshore current found under natural conditions at the coast, various formula exist that need calibration by field measurements. The formulae developed to describe the longshore current are based on the shear component of the radiation stress concept. The range of the longshore current profile and velocity is given to validate the range of the computed longshore current analytically.

When not taking the viscosity and horizontal momentum exchange into account, the maximum value for the longshore current is theoretically found at the breaker line (Bosboom and Stive, 2013) - when considering viscosity or a more random wave field, a more realistic profile is found. The processes around mixing and turbulence will smooth out the profile: The maximum velocity becomes less and will shift landwards while it will also widen into outside of the surf zone. This is the same principle as described in Section 2.4.2 and Figure 2.10b. The extent of the mixing is discussed in Longuet-Higgins (1970a).

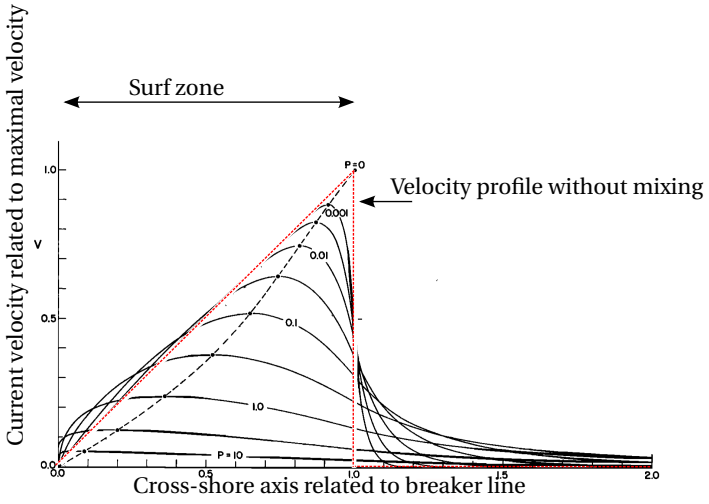

Figure 2.7: Influence on the longshore current for different mixing values P(adapted from Longuet-Higgins, 1970b). The line for a mixing value of $P = 0$ indicates the theoretical velocity profile without horizontal mixing.

The theoretically maximal velocity can be derived analytical when assuming lateral dispersion is not taking place and using a simple breaking model ($\gamma = H/h$ = constant). It is further assumed that, as there is no excess momentum of wave energy before wavebreaking, the current velocity reduces immediately to zero offshore of the breaker line. This is

illustrated by the line for $P = 0$ (i.e. without horizontal mixing) in Figure 2.7. According to Bosboom and Stive (2013), this yields the velocity profile:

$$V(x) = \frac{5}{16}\pi \frac{H_b}{c_f} g \frac{\sin\theta_0}{c_0} \frac{h}{h_b} \tan\alpha \text{ ,theoretical longshore current profile wthout mixing} \tag{2.15}$$

where H_b is the wave height at breaking, θ_0 the angle of the waves at deep water with respect to the cross-shore, c_0 the phase velocity at deep water, h the local waterdepth, h_b the waterdepth at wavebreaking and $\tan(\alpha)$ the cross-shore slope of the beach bottom.
Longuet-Higgins (1970a) found a slightly more complicated formula for the longshore current. This value is the maximal velocity found in the longshore current profile:

$$v_0 = \frac{5\pi}{16}\gamma\varsigma^2 \frac{S}{C_f}\sqrt{gH_b}\sin\theta_b\cos\theta_b \text{ ,maximal velocity} \tag{2.16}$$

as cited in Komar (1998). C_f is a bottom roughness coefficient, H_b the wave height at breaking and θ_b the angle of the approaching waves at breaking w.r.t the cross-shore, ς a coefficient depending on the breaker parameter γ, and S the beach slope.
In the research on the longshore current, the velocity at the breaker line and in the middle of the surf zone is found to be of interest. The velocity in the middle of the surf zone is approximately half of the maximal velocity without mixing for almost all mixing parameters as shown in Longuet-Higgins (1970b), compare Figure 2.7. For a realistic mixing, the maximal velocity corresponds further roughly to the velocity in the middle of the surf zone (Komar, 1998). Combined with available measurements often at that locations, several formulas have been developed at that location. Of these variety of formulas, the one by Komar (1979) is in good agreement with measurements (Komar, 1998).
The longshore current velocity in the middle of the surf zone is given by Komar (1979):

$$\bar{v}_l = 1.17\sqrt{gH_b}\ \sin(\theta_b)\ \cos(\theta_b) \text{ ,current velocity in the middle of the surf zone} \tag{2.17}$$

with H_b the wave height at breaking and α_b the angle of the waves at breaking.

2.3.2. RIP-CURRENTS

Rip-currents are strong and narrow currents that flow (close to) normal to the shore towards the sea (Komar, 1998). These rip currents can be generated at a natural beach without obstacles when the shoreline supports the development of rip-currents (Holthuijsen, 2007). Rip-currents can also develop when longshore currents encounter an obstacle, e.g. a groin. For waves arriving with an angle different than normal from the shore generate a stronger rip current at the wave incident side of the structure (The COMET programme, 2012). These rip-currents are weaker or even absent in the presence of permeable groins (Trampenau, 2000).
Rip-currents are able to reach significant flow velocities and carry considerable loads of sediment with it causing erosion of the beach (see Section 2.3.4). Additionally, these rip currents can be troublesome for swimmers (Komar, 1998) due to their high offshore directed velocity.

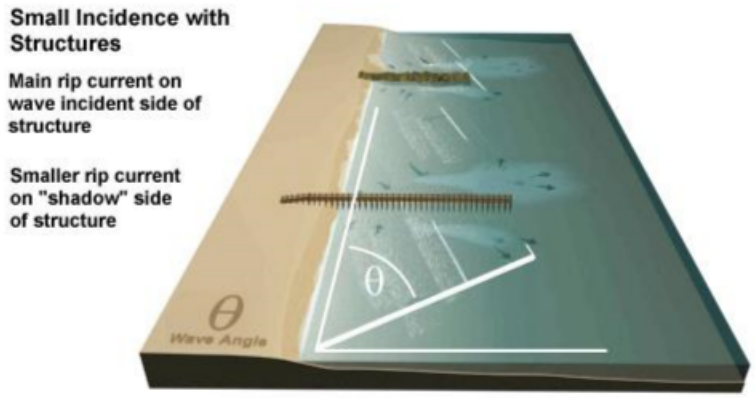

Figure 2.8: Small wave angle with shoreline structures and subsequent rip-current formation (adapted from The COMET programme, 2012).

2.3.3. TIDAL CURRENTS

The tidal current is induced by the movement of the tidal wave along the coast. This slowly varying current in time has slightly different effects on the beach processes: The tidal current may be responsible for transporting sediment along the beach. The tidal current especially effects the transport of sand in the lower parts of the nearshore profile as the its velocity decreases towards the shoreline and the beach material (shingle) near the shoreline requires a higher shear stress before it gets stirred up and transported (Fleming, 1990a).
Depending on the direction, the tidal current can either enhance or reduce the longshore current due to waves and thus enhance or reduce the sediment transport (Bosboom and Stive, 2013).
The water level differs throughout the tidal circle at the coast. The difference between high water and low water can vary from a few centimetres to several meters (around 2m at the Dutch coast). The water level determines if the piles are submerged or emerged which changes the forcing acting on the piles (RIZA, 2003a; Fleming, 1990a).

2.3.4. SEDIMENT TRANSPORT

INITIATION OF MOVEMENT AND TRANSPORT

Generally speaking, there are two phases in the sediment transportation: The stirring up of material and the transportation of material in either cross-shore or longshore direction. These two direction are often separated as the effect on the beach profile can be significantly different depending on the transportation direction.
For bedload material, it is assumed that it is only available for sediment transport once it is subject to a shear stress higher than a critical value (Bosboom and Stive, 2013) based on the principles by Shields (1936).
The shear stress τ_b can be expressed as a function of the shear velocity at the bottom u_*,

$$\tau_b^2 = u_*^2 \, \rho \, , \tag{2.18}$$

with ρ the density of water. The shear velocity is a dimensionless friction coefficient and is depending on the actual velocity (Schiereck, 2004).
Many approaches assume that the amount of transported sediment can directly be expressed as a function of the bed shear stress (Bosboom and Stive, 2013). The higher the velocity is, the higher is thus the shear stress and the possibility that bed material is made available for transportation. If the velocities of the flow field at the beach are reduced (e.g by a groin system), the actual sediment transportation can be reduced. For the transportation in the two directions, many (non-trivial) formulae are developed (Bosboom and Stive, 2013).

IMPORTANCE OF RIP CURRENTS

In the presence of groins, rip-currents are usually developing (Section 2.3.2). Due to their high velocity, they are able to make available and transport a high amount of sediment. They are able to deposit this sediment outside the so-called morphologically active zone if they reach far enough offshore. This reduces the material of the beach and causes erosion. It is therefore desirable to minimize the rip-current velocity if placing an obstacle to the flow.

2.4. INTERACTION OF FLOW AND PILES

For the understanding of the interaction between water and groins, several important concepts are illustrated on the interaction of water with a single pile of a permeable groin, and the interaction of groins with currents and with waves.

2.4.1. MORISON EQUATION

To be able to understand pile groins, the behaviour around one single pile is reflected. The forces of waves and currents on a slender structure such as a pile can be described by the Morison equation which consists of an inertia part for the oscillating flow and a drag part for the current flow. To be allowed to use a Morison type of equation, the diameter D of the cylinder is supposed to be much smaller than the wavelength L,

$$\frac{D}{L} < 0.1 \text{ to } 0.2 \quad \text{, typical application range for Morison equation (Journée and Massie, 2001)} \tag{2.19}$$

The Morison type of equation reads

$$F(t) = \frac{\pi}{4} \rho C_M D^2 \frac{\delta u}{\delta t}(t) + \frac{1}{2} \rho C_D D \cdot u(t) \, |u(t)| \, , \tag{2.20}$$

where C_M is a coefficient of mass, C_D a coefficient of drag, D the pile diameter, ρ the density of water and u the velocity Morison et al. (1950). The two coefficients C_M and C_D are to be determined, which can be done via several approaches yielding a range of results and insecurity in the exact value (Journée and Massie, 2001).

KEULEGAN CARPENTER NUMBER

One way to determine the (approximate) value for the coefficients is given by the Keulegan Carpenter Number (KC-number) by Keulegan and Carpenter (1958) which can be used to determine the importance of the inertia and the drag term (Journée and Massie, 2001): For a large KC number, i.e. a current only situation, the inertia term may be neglected. For a low KC number (KC < 3), the drag part may be neglected. For KC-numbers in between (i.e. current and waves are important), both terms have to be used, while for a certain range (3 < KC < 15), the drag term may be linearised. The Keulegan number itself is defined as a ratio of the water displacement amplitude x_a over the pile diameter D (Journée and Massie, 2001):

$$KC = 2\pi \frac{x_a}{D} \text{ , or } KC = \frac{u_a \cdot T}{D} \tag{2.21}$$

with T the oscillating flow period.

REYNOLDS NUMBER

The Reynolds number is a dimensionless ratio of the inertia and the viscous forces and may be express by:

$$Re = \frac{uD}{\nu} \tag{2.22}$$

with D the diameter of the pile and ν the kinematic viscosity, introduced by Stokes (Battjes, 2002). The Reynolds number gives insight in the interaction of the pile and the flow field. Depending on the Reynolds number, three stages are identified: ideal fluid ($Re = 0$), strong-viscous fluid ($Re \leq 1$) and weak viscous fluid ($Re \geq 1$) (Battjes, 2002) which strongly determines the flow field around and behind the pile. The fluid under consideration in this thesis is a weak viscous fluid.

DRAG COEFFICIENT

The drag coefficient of rigid structures is depending on the flow characteristics expressed in the KC-number and the Re-number. According to Suzuki et al. (2013), it is often difficult to determine a drag coefficient or a bulk drag coefficient for a cylinder cluster. For the research in this thesis, a drag coefficient of $C_D = 1.5$ is used, suggested for trees by RIZA (2003a).

2.4.2. FLOW FIELD AROUND PILES

For viscid fluids, turbulence and eddies develop behind piles, which can be described by the so-called Von Karman street (Battjes, 2002). Depending on the Reynolds number, the eddies have different characteristics, e.g. symmetric or asymmetric (Figure 2.9).

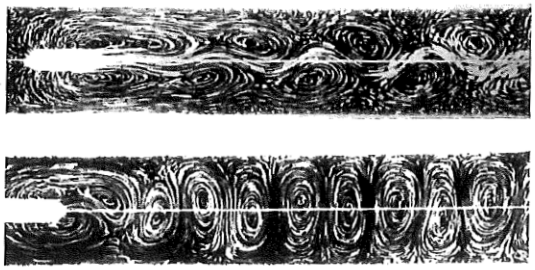

Figure 2.9: Exemplary flow field behind an obstacle creating vortices for different Reynolds numbers, $Re = 57$, (upper figure) and $RE = 95$, (lower figure) (Rosenhead and Schwabe (1930) in Zdravkovich, 2003).

Further, a so-called wake flow develops behind the pile (Figure 2.10a). This implies that there is a velocity gradient of the main flow characteristics present. At this interface, a transfer of mass and momentum is present which is referred to as turbulent viscosity ν_t (Uijttewaal). Further behind a row of multiple piles, two streams with a different velocity are present. Between those two streams, a transfer of mass and momentum will take place and will eventually lead to a flow field with one common mean velocity, Figure 2.10b (Uijttewaal).

Additionally, the turbulent behaviour varies with the number of piles. Contra a priori expectations, it is less straight forward than using theories for one pile only on row or clusters of piles (Zdravkovich, 2003): The exact behaviour depends on multiple factors such as the distance between the piles. The vortices caused by the individual piles will influence each other. The velocity between the piles will increase depending on the distance of the piles.

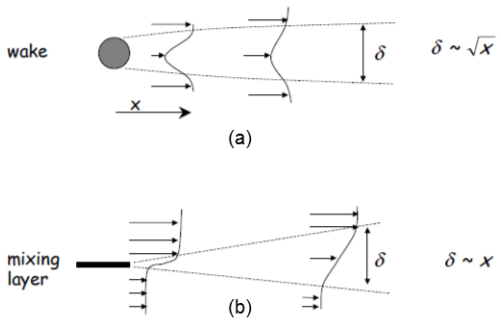

Figure 2.10: Free shear flow. (a) shows the flow field behind a single pile, (b) shows the mixing of two streams with a different mean velocity. Both flow fields tend to even out the velocity differences. (Adapted from Uijttewaal).

2.4.3. WAVE DISSIPATION BY CYLINDERS

The dissipation of wave energy by cylinders ϵ_v can be described by means of an integration of the force F in time (over a wave period T) and in space (over the waterdepth h):

$$\epsilon_v = \overline{\int_{-h}^{-h+\alpha h} Fu\, dz} \tag{2.23}$$

2.4.4. PERMEABLE GROINS AND WAVES

Groins itself only have a limited influence on the wave energy itself as the waves are arriving with a too small angle towards the groin. This holds especially for permeable groins with less area to interact with the waves. For waves not approaching normal to the shoreline, diffraction around the groin will occur (Fleming, 1990a).
Groins do influence currents that originate e.g. from the tide or wave induced. In general, the longshore currents should be reduced by one groin in the same way as in case of a current only-situation. However, behind the groin, the longshore current receives energy from the breaking waves, also the horizontal mixing is more due to the turbulent kinetic energy due to the wave breaking. As a consequence, the velocities behind the groin will reach the original velocities much faster than in a current only situation (Trampenau, 2000).
Figure 2.11 shows the theoretical longshore current redistribution when interacting with a permeable groin: Landwards of the groin, the velocity is decreased, seawards it increases. The main component will remain longshore directed.

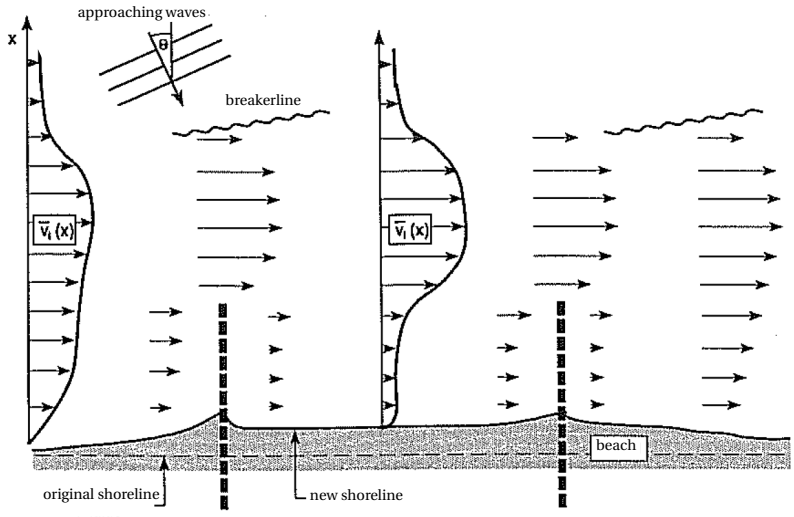

Figure 2.11: Schematic changes in the longshore current velocity profile in the presence of permeable groins, adapted from Trampenau (2000).

2.5. TURBULENCE MODELING

A velocity field can usually be described by the mean flow characteristics and the turbulent fluctuations. By means of decomposing the velocity vector in those two components, the Reynolds averaged Navier-Stokes equations are developed. Due to their non-linearity, they are difficult to analyse analytically. To close those equations, an expression for the so-called Reynolds stresses needs to be found which describe the fluctuating part of the velocity vector (Uijttewaal).
Those Reynolds stresses can be expressed by means of the turbulent viscosity ν_t for which numerous approaches are available out of which the constant eddy viscosity, the mixing length, the Smagorinsky and the $k-\epsilon$ models are described.

2.5.1. CONSTANT EDDY VISCOSITY

The constant eddy viscosity model assumes the viscosity to be a product of the velocity and a length scale. This model is valid for a two dimensional approach or limited vertical resolution. The eddy viscosity ν_t can be described by the term

$$\nu_t(x,y) = \frac{U_0(x)\delta(x)}{R_T}, \tag{2.24}$$

in which $U_0(x)$ is the characteristic velocity scale and $\delta(x)$ the characteristic lengthscale of the mean flow and R_T a turbulent Reynolds number (Pope, 2000).

2.5.2. MIXING LENGTH ACCORDING TO PRANDTL

The mixing length approach according to Prandtl assumes that the velocity is described by means of a velocity difference over the distance l_m over which the mixing is taking place (Uijttewaal). The length l_m is consequently called the mixing length. The viscosity can then be described as

$$\nu_t = l_m^2 \left| \frac{\partial \langle U \rangle}{\partial y} \right|, \tag{2.25}$$

in which $\langle U \rangle$ is the mean velocity vector Pope (2000). In this model, the viscosity is determined by the length scale of mixing which is to be determined per flow situation.

2.5.3. k-EPSILON MODEL

The k-epsilon model is a so-called two-equation model, i.e. one equation is provided for the turbulent kinetic energy k and one for the energy dissipation ϵ. Out of this two transport equation of turbulent quantities, the lengthscale, the timescale and the viscosity can be derived Pope (2000).
The transport equation for k reads:

$$\frac{\overline{D}k}{\overline{D}t} = \nabla \cdot \left(\frac{\nu_t}{\sigma_k} \nabla k \right) + \wp - \epsilon, \tag{2.26}$$

with $\wp$ the production of turbulent energy. The transport equation for ϵ reads:

$$\frac{\overline{D}\epsilon}{\overline{D}t} = \nabla \cdot \left(\frac{\nu_t}{\sigma_\epsilon} \nabla k \right) + C_{\epsilon 1} \frac{\wp \epsilon}{k} - C_{\epsilon 2} \frac{\epsilon}{k} \tag{2.27}$$

For which, according to Rodi (1987) cited in Ma et al. (2013), the standard values for the model constants are:

$$C_1 = 0.09,\ C_{\epsilon 1} = 1.44,\ C_{\epsilon 2} = 1.92,\ \sigma_k = 1.0,\ \sigma_\epsilon = 1.3. \tag{2.28}$$

The viscosity then follows to be:

$$\nu_t = C_1 \frac{k^2}{\epsilon}. \tag{2.29}$$

Ma et al. (2013) suggests to use the modified expression by Rodi (1987) for the inclusion of terms related to vegetative drag. Those read in their conservative form for the transport equation of k:

$$\frac{\partial Dk}{\partial t} + \nabla \cdot (D\mathbf{u}k) = \nabla \cdot \left[D \left(\nu + \frac{\nu_t}{\sigma_k} \right) \nabla k \right] + D \left(P_s + C_{fk} P_v - \epsilon \right) \tag{2.30}$$

The transport equation for ϵ reads:

$$\frac{\partial D\epsilon}{\partial t} + \nabla \cdot (D\mathbf{u}\epsilon) = \nabla \cdot \left[D \left(\nu + \frac{\nu_t}{\sigma_\epsilon} \right) \nabla \epsilon \right] + \frac{\epsilon}{k} D \left(C_{1\epsilon} \left(P_s + C_{f\epsilon} P_v \right) - C_{2\epsilon} \epsilon \right), \tag{2.31}$$

in which u is the velocity vector, P_s is a shear production term and P_v the production term of turbulence due to the presence of vegetation. For the constants applicable in the presence of vegetation, a value of $C_{fk} = 0.07$ and $C_{f\epsilon} = 0.16$ is advised based on calibration by Shimizu and Tsujimoto (1994) (cited in Ma et al., 2013).

2.5.4. LARGE EDDY SIMULATION: SMAGORINSKY MODEL

The Smagorinsky model is a Large Eddy Simulation (LES) which averages in space instead of time (as done in the constant eddy viscosity and mixing length approach) (Uijttewaal). With this averaging, the effect of the small scale turbulences responsible for energy loss is included and only the large sales have to be solved on the grid.

$$\nu_t = (c_s \Delta_f)^2 \sqrt{2S_{ij}^2}\,, \qquad \text{with} \tag{2.32}$$

$$S_{ij} = \frac{1}{2}\left(\frac{\delta v_i}{\delta x_j} + \frac{\delta v_j}{\delta x_i}\right), \tag{2.33}$$

in which c_s is the Smagorinsky constant, Δ_f the filter width (corresponding to the mesh size), and $\bar{v_i}$ and $\bar{v_j}$ the averaged velocity into the directions x_i and x_j. The Smagorinsky constant is usually between 0.1 and 0.2 and has to be determined according to the flow field. The mixing length corresponds to the product of $c_s \Delta_f$ (Uijttewaal).

2.6. BOTTOM FRICTION

Friction is one of the most important concepts of how flows are balanced and losing energy. It is highly complex term and formulas have been developed based on measurements and empirical relationships. In current conditions, often a Chézy formula is used. When including waves, a Manning approach or a dimensionless friction coefficient may be used. Those approaches can be related to each other.
The friction concepts used in this thesis are:

Roughness height k_s in [mm] The Nikuradse roughness height is the actual roughness found on the ground due to the sediment or others. It is expressed in [mm].

Chézy friction parameter C in [$m^{1/2}/s$] The Chézy friction coefficient is especially important for the Chézy formula:

$$u = C\sqrt{Ri}\,, \tag{2.34}$$

with C the Chézy coefficient, R the hydraulic radius and i the slope of the energy head (e.g. Bezuyen et al. (2011)). The actual Chézy value is depending on the waterdepth. It can be related to the Nikuradse roughness height via:

$$C = 18\log\left(\frac{12h}{k_s}\right), \tag{2.35}$$

in which h the local waterdepth (Bezuyen et al., 2011). This coefficient is in fact a smoothness factor and more suitable for a current situation with a bottom constant in cross-shore direction

Dimensionless friction coefficient c_f The dimensionless friction coefficient c_f is used in context of the bed shear stress (Bosboom and Stive, 2013):

$$\tau_b = \rho c_f |u| u \tag{2.36}$$

with ρ the density of water. This friction factor can be expressed by means of Chézy or other friction approaches. Related to Chézy , it reads (Bezuyen et al., 2011):

$$c_f = \frac{g}{C^2}\,. \tag{2.37}$$

Manning friction parameter m in [$s/m^{1/3}$] The friction approach based on Manning is often used in the context of waves and beaches, as a constant Manning coefficient takes into account the effect of the local waterdepth. A lower waterdepth with the same roughness of the bed exerts more friction on the flow. The friction coefficient by Manning m can be related to the one of Chézy by:

$$m = \frac{H^{1/6}}{C}\,. \tag{2.38}$$

3

ANALYTICAL MODEL FOR CURRENT AND GROIN INTERACTION

3.1. INTRODUCTION AND MOTIVATION

Based on simplified analytical formulae, an approach is developed to provide insight into the behaviour of a current when approaching a permeable pile groin. This chapter shows the development of this model and the assumed simplification (Section 3.2 and 3.3), the output (Section 3.4) and its application boundaries (Section 3.5).

3.2. ANALYTICAL CALCULATION WITHOUT PILES

When dealing with the current only situation, it can be approached as an open channel flow. The starting point is the balance based on the momentum for a sloping bottom (in flow direction) without groins. The bottom is cross-shore uniform. The balance on a volume of water in open channel flow reads:

$$F_1 + \Delta G_s = F2 + \Delta R\,, \tag{3.1}$$

$$\Delta F = i_b \Delta G - \Delta R\,, \tag{3.2}$$

where ΔF is the resulting force due to water pressure and discharge, i_b the bottom slope, ΔG is the weight force and ΔR the resistance force due to bottom friction (Figure 3.1). The term $i_b \Delta G$ (i.e. the part of the weight force driving the force down the slope) vanishes as there is no slope in longshore direction.

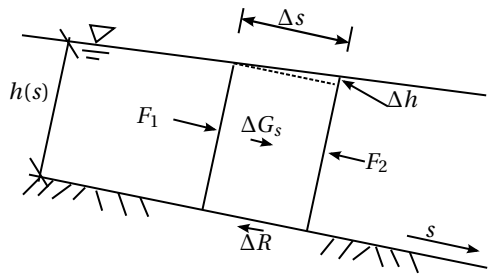

Figure 3.1: Forces on a column of water for a current from the left to the right (based on Battjes, 2002).

By means of substituting open channel flow geometry and the Froude number, this results in the open channel flow equation. For a flat bottom, it can be evaluated analytically. The driving force of the current is a pressure gradient due to a slope in the water surface in that case. The resulting differential equation is:

$$\frac{dh}{ds} = \frac{-c_f \cdot q^2/gh^3}{1 - \alpha \cdot q^2/gh^3}\,, \tag{3.3}$$

with α a dimensionless coefficient, q the specific discharge per unit width, g the acceleration of gravity, s the coordinate of the stream (Battjes, 2002)
Substituting the critical waterdepth $h_{cr}^3 = q^2/g$[1] into equation 3.3 yields (Battjes, 2002):

$$\frac{dh}{ds} = -c_f \frac{h_{cr}^3}{h^3 - h_{cr}^3} \,. \tag{3.4}$$

The integration with respect to s results in:

$$\frac{1}{4}h^4 - h_{cr}^3\, h + c_f\, h_{cr}^3\, s = \frac{1}{4}h_0^4 - h_{cr}^3\, h_0 + c_f\, h_{cr}^3\, s_0 \,. \tag{3.5}$$

Using the continuity equation and assuming a constant discharge over the domain, the velocity at the two boundaries can be calculated:

$$q = v \cdot h \,, \tag{3.6}$$

in which q is the specific discharge [m^2/s], v the velocity found for the local waterdepth h.

3.3. ANALYTICAL CONSIDERATION INCLUDING PILES

The aim is to add an additional term for the resistance force due to the presence of piles. In equations 3.3 to 3.5, only the bottom friction is included. A simplified approach to represent the force on a slender pile in flow over the whole waterdepth can be found in:

$$F_D = c_D \cdot \frac{1}{2}\rho u^2 A_D \,, \tag{3.7}$$

in which c_D is the drag coefficient of the piles, ρ the density of the fluid, u the undisturbed velocity and A_D the area of the obstacle (i.e the pile) normal to of the fluid. This is the current only part of the Morison equation (equation 2.20). In a current only situation with a high KC-number, the drag force is dominant and the inertia term can be neglected (Journée and Massie, 2001). This approximation has also been suggested for emergent vegetation RIZA (2003b).

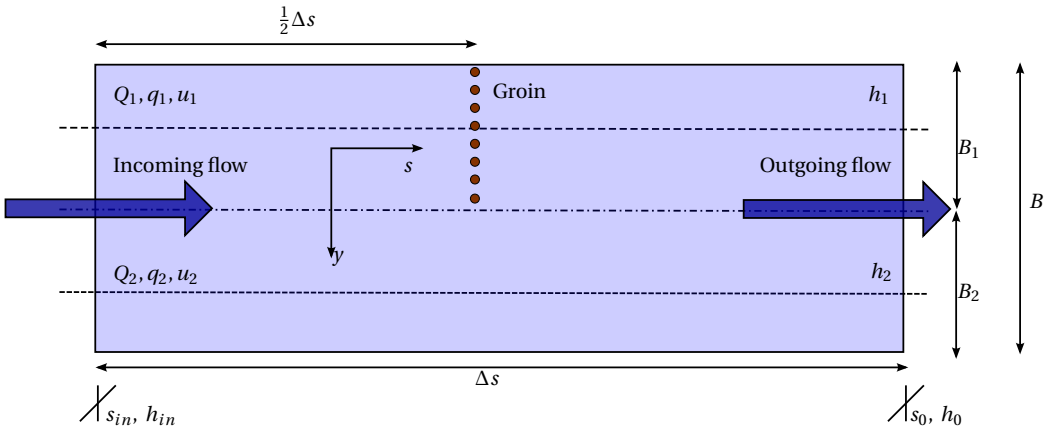

Figure 3.2: Schematization of the domain with two streams for the current situation.

[1] The critical waterdepth is defined as the depth separating supercritical flow from subcritical flow, e.g. Battjes (2002)

3.3.1. WATERLEVEL WITH PILES

Figure 3.2 shows the scheme for a two-streams approach. The flow will be estimated by two one dimensional streams, one disturbed by a groin (stream 1) and one undisturbed (stream 2). It is simplified assuming that the bottom is flat in cross- and longshore direction and that the two streams have the same width $B_1 = B_2 = \frac{1}{2}B$.
In the given case, the area A_D of equation 3.7 is approximated by half of half of the width of the domain B times the waterdepth h to simulate a permeability of the groin of $P = 50\%$ as defined in Section 2.2.2. This takes into account that the permeability of the groin is $P = 50\%$ of the groin and furthermore that the groin is only on half of the domain.

$$A_D = \frac{1}{2} \cdot \frac{1}{2} Bh \,. \tag{3.8}$$

A further simplification is to spread the force over the width B and length Δs of the domain and translating it into an averaged bottom shear stress. This shear stress due to piles reads:

$$\tau_p = c_D \, \frac{1}{2} \rho \, u^2 \, \frac{1}{4} \, B \, h \, \frac{1}{\Delta s \, B}. \tag{3.9}$$

With this simplified approach, the two resistance forces along the streams (i.e. due to bottom friction and due to piles) can be combined. The force is spread over the whole domain as there is exchange of momentum and flow in the horizontal plane. When being far enough away from the groin, the water level elevation are considered to be constant again along the cross-shore axis. By this, the approach reduces to a one-equation model for the water level consideration. The bottom shear stress due to bottom roughness reads (Bosboom and Stive, 2013):

$$\tau_b = c_f \rho u^2. \tag{3.10}$$

The sum of the shear stress and the force respectively read:

$$\Sigma\tau = \tau_p + \tau_b = c_D \cdot \frac{1}{2} \rho u^2 \cdot \frac{1}{4} \cdot h \cdot B \frac{1}{\Delta s B} + c_f \rho u^2 \,, \tag{3.11}$$

$$\Sigma\Delta R = \left(c_D \cdot \frac{1}{2} \rho u^2 \cdot \frac{1}{4} \cdot h \cdot B \frac{1}{\Delta s B} + c_f \rho u^2 \right) \cdot B \cdot \Delta s \,. \tag{3.12}$$

This can be substituted into the balance in equation 3.2:

$$\Delta F = -\Delta R \,, \tag{3.13}$$

$$\rho g A \left(1 - \mathrm{Fr}^2\right) \Delta h = - \left(c_D \frac{1}{8} \rho u^2 \frac{h}{\Delta s} + c_f \rho u^2 \right) B \Delta s \,, \tag{3.14}$$

$$\Delta h = \frac{u^2 \left(c_D \frac{1}{8} \frac{h}{\Delta s} B + c_f B \right)}{g h B \left(1 - \mathrm{Fr}^2\right)} \Delta s \,, \tag{3.15}$$

substitution of $u = q/h$ and $\mathrm{Fr}^2 = q^2 / \left(g h^3\right)$ yields

$$\Delta h = - \frac{\frac{q^2}{h^2} \left(c_D \frac{1}{8} \frac{h}{\Delta s} + c_f \right)}{g h \left(1 - \frac{q^2}{g d^3} \right)} \Delta s \,. \tag{3.16}$$

The discharge is assumed to be constant over time and space for a steady flow, so the critical water depth can be evaluated by $h_{\mathrm{cr}}^3 = q^2 / g$.

$$\Delta h = - \frac{h_{\mathrm{cr}}^3 \frac{1}{h^2} \left(c_D \frac{1}{8} \frac{h}{\Delta s} + c_f \right)}{h \left(1 - \frac{h_{\mathrm{cr}}^3}{h^3} \right)} \Delta s \,, \text{yielding} \tag{3.17}$$

$$\frac{\delta h}{\delta s} = - \frac{h_{\mathrm{cr}}^3 \left(c_D \frac{1}{8} \frac{h}{\Delta s} + c_f \right)}{h^3 - h_{\mathrm{cr}}^3 \,.} \tag{3.18}$$

After integration with respect to s, it yields:

$$\frac{1}{4} h_{in}^4 - h_{\mathrm{cr}}^3 h_{in} - \frac{1}{4} h_0^3 + h_{\mathrm{cr}}^3 h_0 = -c_f h_{\mathrm{cr}}^3 \, (s_{in} - s_0) - c_D \frac{1}{8} h_{in} \, h_{\mathrm{cr}}^3 \frac{1}{\Delta s} (s_{in} - s_0) \,. \tag{3.19}$$

This equation gives the global water level difference between the upstream water level h_{in} and downstream water level h_0. Due to the non-linear nature of this equation, it has to be solved iteratively. The hydraulic input to this formula will be the discharge by means of the critical water depth h_{cr} which is assumed to be constant along s, and the water level downstream h_0. The obtained output will be the water level at the upstream boundary (Figure 3.3). The distance $(s_{in} - s_0)$, and the resistance coefficients c_D and c_f are physical model constants.

3.3.2. VELOCITY DISTRIBUTION AMONG THE TWO STREAMS

Aside from the water levels, the influence on the flow velocities and discharges is necessary to describe the effect of a groin. This approach delivers a global impression on the changes in velocity and discharge when pile groins are obstacles to the flow. In the presence of piles, the water discharge will redistribute in such a way that the least resistance is to overcome. More discharge will flow in the part that is not disturbed by the piles as the flow resistance is lower.
Far enough away from the obstacle at the upstream and downstream boundary, the water level is constant along the cross-shore due to horizontal mixing. Thus, the global pressure gradient driving the flow is nearly the same for both parts with and without piles. An estimation of how the flow is distributed is attempted by comparing the flow resistance terms to the discharge and velocity term. By this, the system consists of two 1D paths, one containing an additional flow resistance due to the groin, one not (Figure 3.2).
The flow resistance for the part with and without groins read respectively:

$$R_1 = c_f\ \rho\ u_1^2\ B_1\ \Delta s + c_D\ \frac{1}{2}\rho u_1^2\ \frac{1}{2} h\ B_1 \frac{\Delta s}{\Delta s}\,, \qquad \text{with groins} \tag{3.20}$$

$$R_2 = c_f \rho u_2^2 B_2\ \Delta s \qquad \text{without groins.} \tag{3.21}$$

The width of the two streams is assumed to be equal: $B_1 = B_2$. The velocities computed are averaged velocities over the simplified stream. It is assumed that those values approximate the velocities behind the groin field in the non-averaged situation.
The relation between the friction terms then is:

$$\frac{R_1}{R_2} = \frac{c_f \rho u_1^2 B_1 \Delta s + c_D\ \frac{1}{4}\rho u_1^2 \frac{h}{\Delta s}\ B_1 \Delta s}{c_f \rho\ u_2^2\ B_2\ \Delta s}\,, \tag{3.22}$$

$$\frac{R_1}{R_2} = \frac{c_f u_1^2 + c_D\ u_1^2 \frac{1}{4} \frac{h}{\Delta s}}{c_f u_2^2}\,. \tag{3.23}$$

This ratio is related to the discharge in the two streams. As the width and the water level of the two streams are (approximately) the same, it can be reduced to the relation of the velocity.

$$\frac{R_1}{R_2} = \frac{c_f u_1^2 + c_D\ u_1^2 \frac{1}{4} \frac{h}{\Delta s}}{c_f u_2^2} = \frac{u_2}{u_1}\,. \tag{3.24}$$

The total discharge can be described as

$$Q_1 + Q_2 = Q_{tot} \tag{3.25}$$

$$u_1 B_1 h + u_2 B_2 h = u_{av} B h \tag{3.26}$$

Assuming only an insignificant influence of the width and the water level as $B_1 \approx B_2$ and $h_1(x) \approx h_2(x) \approx h(x)$, equation 3.26 reduces to

$$\frac{u_1 + u_2}{2} = u_{av}\,. \tag{3.27}$$

The combination of equations 3.24 and 3.27 can be solved to determine the averaged velocities in longshore direction for both streams (Figure 3.4).

3.4. PRINCIPLE MODEL OUTPUT

The total model output of this analytical approach is the change in water level at the upstream and downstream boundary, and the flow velocities in the two streams.

WATER LEVEL

The water level at the upstream boundary $h_{in,piles}$ can be evaluated and set in comparison with the downstream water level h_0 and the upstream water level in a stream undisturbed by a groin $h_{in,no\ piles}$ (Figure 3.3a). In his way, the effect on the change in water level Δh over the distance Δs can be evaluated in dependency of different parameters (e.g. the incoming discharge, the bottom roughness or drag coefficient of the piles, Figure 3.3b).

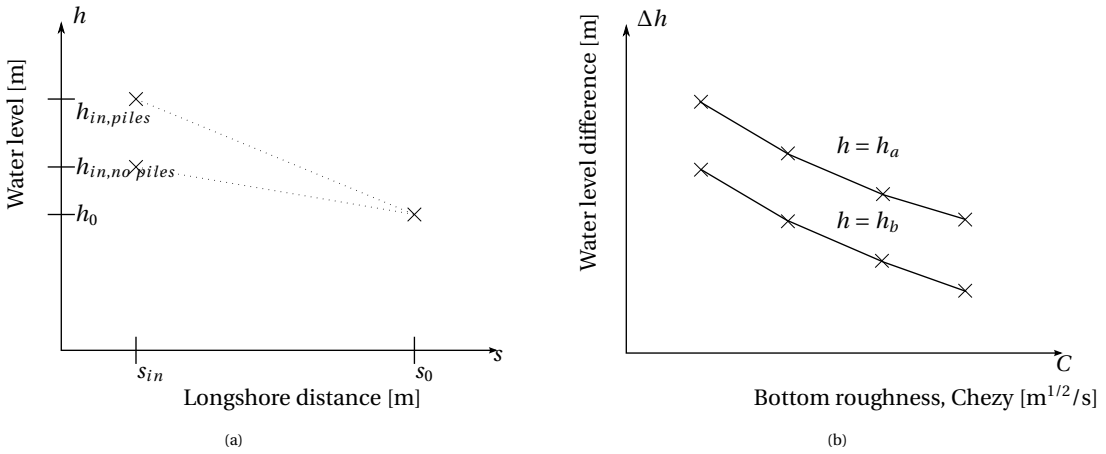

Figure 3.3: Possible output analysis from analytical approach (equations 3.5 and 3.19) for the water levels. (a) illustrates the interpretation of the upstream water level under the influence of piles to a situation without piles for a single fixed parameter set. (b) illustrates the comparison for the dependency of parameter sets, exemplary varying the waterdepth and bottom roughness.

VELOCITY

The velocity obtained are averaged velocity for each stream. Those velocities can be evaluated as absolute velocities or as relative ones by setting them in comparison to the undisturbed approach velocity u_0. For the undisturbed flow, the velocity will increase towards the downstream boundary (Figure 3.4a). This velocity is constant in cross-shore direction. In vicinity of the groin, the velocity behind the groin will decrease compared to the approach velocity; the velocity next to the groin will increase (Figure 3.4b). This increase and decrease in velocity can be computed for different sets of parameters (Figure 3.4c)

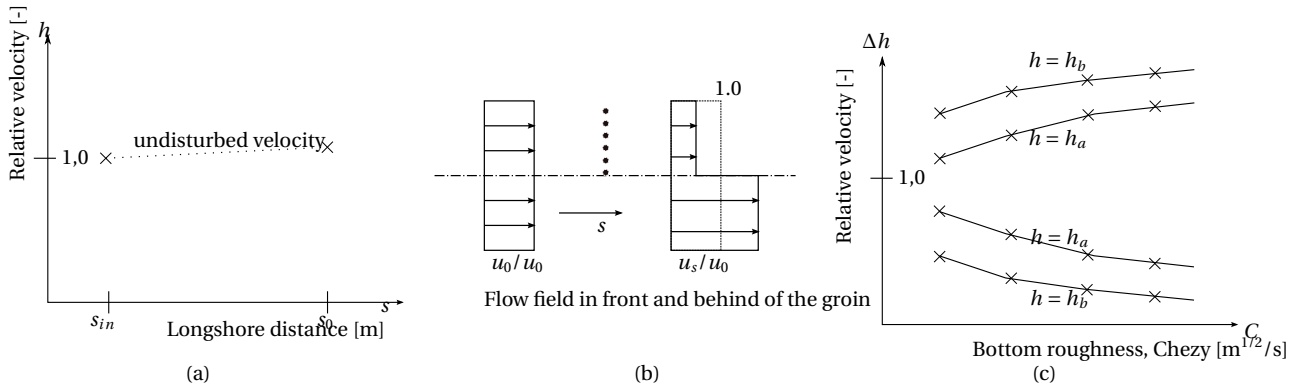

Figure 3.4: Possible output analysis from analytical approach (equations 3.24 and 3.27) for the velocities. (a) illustrates the interpretation of the upstream velocity under the influence of piles to a situation without piles for a single fixed parameter set. (b) illustrates the comparison for the dependency of parameter sets, exemplary varying the waterdepth and bottom roughness. Both figures are set in comparison to the approach velocity at the upstream boundary u_0.

3.5. APPLICATION BOUNDARIES OF THE MODEL

This analytical approach provides a first estimate of the effect of pile groins on the water level and the velocity field. The influence of varying the bottom roughness, the drag of the piles, the waterdepth and the discharge can be approximated. Due to assumptions and simplifications, the model has application boundaries discussed below.

(1) The model is based on the assumption of one dimensional streams. As a results, local effects in the water level and velocity cannot be displayed such as piling up of water in front of the groin or velocity increase between the piles. Information on velocities and mixing in cross-shore direction cannot be provided.
(2) This model is developed using a simplified flat bottom. A sloping bottom will influence the flow field. First, there is a weight force towards the larger depths (offshore directed) (Bosboom and Stive, 2013). Second, the longshore velocity is influenced as it depends (a) on the waterdepth via the continuity assumption and (b) on the bottom roughness which plays a higher role at smaller waterdepths.
(3) Further, waves are not included. The sloping bottom and shallow water depths will cause wave transformation complicated for analytical models. The breaking waves will cause a longshore current that is not constant along the cross-shore and thus more complicated than the constant current assumed in the model.
(4) Behind the piles, turbulent motion is present. Taking the energy cascade (e.g. Pope, 2000) into account, some energy will get lost reducing the flow velocity. The energy loss is generally low, and should not have an important influence on the computed velocity.
(5) The presence of the piles will effect the area available for the discharge, however in this model it is assumed to be insignificant; In reality it is expected to have a certain effect. The piles do reduce the width of the stream. However, as only one groin is under consideration, the total amount of piles is limited. Further, the velocity field under consideration is somewhat behind the groin where the whole stream width is available again.

Considering the application boundaries, a more detailed study is advised to be done by means of a numerical model. With a numerical model, flows in cross-shore direction, wave effects and less simplified assumption of the groin can be included. Further, more details of the flow field and water level over the domain can be obtained.

4

NUMERICAL MODEL APPROACH

As indicated in Section 3.5, a numerical model can give more insight in the flow field in more detail than a simplified analytical approach. Within this thesis, the numerical model SWASH (Simulating WAves til SHore) is being used. A reasoning for this choice is given in Sections 4.1 and 4.2. The concept of SWASH is given in Section 4.3 with the general concept in Section 4.3.1 and an elaboration on turbulence models (Section 4.3.2) and wave energy dissipation by piles (Section 4.3.3).

4.1. MOTIVATION NUMERICAL RESEARCH

A numerical model can give more insight in the flow field in more detail than a simplified analytical approach. Once enough trust is given to a model and a specific model set-up to reproduce physics, a numerical research can be used to identify the effect of varying boundary conditions and environmental parameters. This validation can be done by comparison to results from laboratory measurements or analytical considerations. Compared to laboratory experiments, they can be less expensive as the required time and material decreases. Further they can also give results on a smaller spacial and temporal resolution or on a larger scale.

4.2. CHOICE OF NUMERICAL MODEL

There are different types of numerical models available for numerical research in hydraulic engineering. Due to different reasons all of those models are subject to application boundaries. Those models and their restrictions and discussed to evaluate the most promising model for the scope of this thesis.

DEMANDS ON THE NUMERICAL MODEL

When considering the nearshore zone where groins are supposed to be built, it has to be dealt with small-scale effects present in the nearshore zone and around structures which needs to be included in the model. This thesis deals with flow fields around single and multiple groins. This restricts the spacial resolution of the numerical grid and which processes can be included. Processes on a scale smaller than the resolution of the grid and their effects on the flow field have to be schematised to be included.
The model needs to be able to compute the propagation of currents along the domain. Further, wave transformation has to be available and resulting currents. A research on a small laboratory scale is the scope of this report. However, to properly analyse the effect of groins in reality, an extension to nature scale should be possible. When applying groins, often a groin field is applied. Therefore the spatial scale should be allowed to be chosen large also in nature scale. For a morphological study, sediment transport and correlated processes need to be included.

AVAILABLE MODELS AND CHOICE OF MODEL

Different types available for simulating hydraulics at a coastal situation are circulation and coastal flow models, Boussinesq-type of models, Computational Fluid Dynamic models and wave-flow models.
Circulation and coastal flow models are often developed for large scale flows and are less suitable for small scale effects such as the simulation of surface waves, small scale flows around hydraulic structures, e.g. due to the hydrostatic pressure assumption (The SWASH team, 2014). For the present, research especially wave transformation and small scale flows around hydraulic structures such as piles are of interest.
Boussinesq type of models consists of a set of equations for surface water waves with the limits of incompressible, inviscid flows and weak non-linearity and weak dispersion (Kirby, 2003). Boussinesq type of models can therefore not be used immediately for an accurate prediction of breaking waves (The SWASH team, 2014) which are expected to be present and of major influence on the flow field in this study.

Detailed processes around piles can be simulated in Computational Fluid Dynamics (CFD) models. Those models can be used for a detailed three dimensional flow analysis around small structures. However, a high resolution is required. Combined with a demand on a large spatial sclae, this could probably lead to a high omputational costs. (Deltares, 2014) Those model application boundaries of the different models have been taken into account for the development of SWASH which is designed to solve wave and flows in coastal waters on large and small scale. It can take into account small-scale flows around hydraulic structures both for flow and waves (The SWASH team, 2014). The SWASH model can be used to approximate very short or breaking waves accurately. This gives the model advantages in the present simulation compared to Boussinesq-type of models and large flow field models. With this idea in mind, it has been chosen to use the SWASH model to verify if this model is able to evaluate nearshore flows in interaction with permeable groins.
The profile development due to erosion and sedimentation is not yet implemented into the SWASH model so that the profile development is not included in the research. For the scope of the present research this is less of a disadvantage as first the hydrodynamics need to be computed well enough. The bottom shear stress can be computed inside the model SWASH which is one of the important concepts when dealing with sediment transport.

4.3. THE SWASH MODEL

SWASH by The SWASH team (2013) is being developed at the Delft University of Technology to simulate wave and flow phenomena. SWASH is supposed to be a "multi-tool" on small and large scale flows, waves and interactions between waves, currents and structures. According to the manual, SWASH is able to „simulate non-hydrostatic, free-surface, rotational flows and transport phenomena in one, two or three dimensions“(The SWASH team, 2014). It is based on the non-linear shallow water equations including non-hydrostatic pressure. It can simulate wave transformations, e.g. due to non-linear wave-wave interactions, wave-structure or wave-vegetation interactions (The SWASH team, 2014).

4.3.1. GOVERNING EQUATIONS

SWASH can be used in a Cartesian framework. It is based on the unsteady incompressible Reynolds-averaged Navier-Stokes equations, in the given application in the Eulerian form (without Coriolis and baroclinic effects). The model can be evaluated in depth averaged or fully three dimensional mode. In the depth averaged mode (for simplicity), the momentum equations are given by:

$$\frac{\delta u}{\delta t} + u\frac{\delta u}{\delta x} + v\frac{\delta u}{\delta y} + g\frac{\delta \zeta}{\delta x} + \frac{1}{h}\int_{-d}^{\zeta}\frac{\delta q}{\delta x}dz + c_f\frac{u\sqrt{u^2+v^2}}{h} = \frac{1}{h}\left(\frac{\delta h\tau_{xx}}{\delta x} + \frac{\delta h\tau_{xy}}{\delta y}\right), \text{ and} \tag{4.1}$$

$$\frac{\delta v}{\delta t} + u\frac{\delta v}{\delta x} + v\frac{\delta v}{\delta y} + g\frac{\delta \zeta}{\delta y} + \frac{1}{h}\int_{-d}^{\zeta}\frac{\delta q}{\delta y} + c_f\frac{u\sqrt{u^2+v^2}}{h} = \frac{1}{h}\left(\frac{\delta h\tau_{xy}}{\delta x} + \frac{\delta h\tau_{yy}}{\delta y}\right). \tag{4.2}$$

The continuity equation is given by:

$$\frac{\delta \zeta}{\delta t} + \frac{\delta hu}{\delta x} + \frac{\delta hv}{\delta y} = 0 \tag{4.3}$$

with x, y, z the coordinates, while z is define positive in upwards direction and t the time. u, v, w are the velocity components in x, y and z-direction respectively.

The numerical approximation used based on an explicit and second order accurate difference is strictly mass and momentum conservative Zijlema et al. (2011). The grid is a classical staggered Arakawa C-grid, where the unknowns water level ξ and velocity u are computed at alternating points. The pressure p is decomposed into a hydrostatic p_H and non-hydrostatic part q while assuming a zero atmospheric pressure. Within the Cartesian frame and axis x, y, z, the pressure gradient reads:

$$p = g(\eta - z) + q = p_h + q\,, \tag{4.4}$$

in which g is the acceleration of gravity. The hydrostatic balance is given by:

$$\frac{\delta p_h}{\delta z} = -g\,. \tag{4.5}$$

For discretizing the pressure term, the so-called Keller Box scheme is used. This scheme takes into account the effect of non-hydrostatic pressure with small number of layers. The Keller box is used for the approximation of the vertical gradient of the non-hydrostatic pressure accurately. It is different to the other most common used schemes as it is edge based instead of centre based (Stelling and Zijlema, 2003).
Layers can be implemented in two ways into the model: With a fixed height in [m] or as a percentage of the local water-depth (a combination is possible) following the bed level.

4.3.2. TURBULENCE

As described in Section 2.5, viscosity of water and turbulence determines the exchange of momentum in the horizontal and vertical plane. In SWASH, several models can be chosen to include viscosity:

Constant eddy viscosity A constant value for the eddy viscosity is used (in m^2/s) according to equation 2.24. In SWASH it can be applied in the horizontal plane.

Smagorinsky The Smagorinsky model as described in Section 2.5.4 is be applied. The input parameter is the Smagorinsky constant c_s constant over the domain. The standard value is $c_s = 0.2$. In SWASH it can be applied in the horizontal plane.

The Prandtl mixing length uses the theorem by Prandtl (Section 2.5.2). The input is a mixing length l_m in [m] constant over the domain. In case of waves, this value is advised to be in the order of the wave height. In SWASH it can be applied in the horizontal plane.

The $k-\epsilon$ model uses the $k-\epsilon$ model (see Section 2.5.3) adapted for the presence of vegetation. The coefficients `[cfk]` related to the turbulent kinetic energy k and coefficient `[cfe]` related to the dissipation rate ϵ in the presence of groins are used with the standard values of `[cfk]` = 0.07 and `[cfe]` = 0.16 based on the analysis for turbulence around vegetation (Shimizu and Tsujimoto (1994) in Ma et al., 2013). In SWASH, it can be applied in the vertical plane.

4.3.3. WAVE DISSIPATION DUE TO PILES

For the vegetation model in SWASH, Suzuki et al. (2013) assumes a gathering of rigid and vertical vertical cylinders and a model based on the Morison equation (equation 2.20) and wave dissipation by cylinders (equation 2.23).
Though for waves in reality, the inertia term does play a role (unlike for sinusoidal waves if integrated over one wave cycle), Suzuki et al. (2013) concludes that the influence should be limited and is excluded from the model. Equation 2.20 holds for a single pile and is extended in the SWASH model for a cluster of piles by including the number of piles N_v:

$$F' = \frac{1}{2}\rho \widetilde{C}_D b_v h_v N_v u|u| \quad \text{in } [\mathrm{N/m^2}], \tag{4.6}$$

with $\widetilde{C}_D$ the drag coefficient of the piles, b_v the with of the piles, h_v the waterdepth and u the flow velocity. The practical version inside the SWASH model (replacing h_v by h_v/h) is added to equations 4.1 and 4.2 at the right hand side.

5

AVAILABLE DATA FOR CALIBRATION AND VALIDATION

5.1. INTRODUCTION AND OUTLINE

To evaluate the performance of a numerical model, results can be compared to laboratory data. Two experiments are referred to. Reniers (1999) conducted research on the longshore current behaviour induced by a wave forcing without the presence of groins (Section 5.3). This data source is used to validate the development of breaking waves and the longshore current inside the model SWASH based on laboratory scale. Trampenau (2000) conducted a research on groins under the influence of a current-only forcing and a wave-only forcing inducing a longshore current (Section 5.2):

Data source	Current forcing	Wave forcing	Groins	Description Section	Results Section
Trampenau (2000), currents	x		x	5.2	6.5, 6.6, 6.7, 6.8, 6.9
Trampenau (2000), waves		x	x	5.2	7.4, 7.5
Reniers (1999)		x		5.3	7.2

5.2. TRAMPENAU (CURRENT OR WAVE ONLY FORCING)

As described in Appendix A.4, Trampenau (2000) conducted research on permeable and impermeable groins on laboratory scale and in nature. The experiments in the laboratory are based on typical beach situations in the Baltic Sea and reduced to laboratory scale based on Froude scaling.

5.2.1. SET-UP OF THE EXPERIMENT

The basin had an approximate size of $l_x = 26$m in longshore direction and $l_y = 14$m normal to the main flow direction. The actual area used differs for the current and for the wave case.
In the experiments, two principle situation are considered: A current-only forcing and a wave-only forcing. The latter one induces a longshore current.
The groins are simulated by wooden piles with a diameter of 1cm. The beach is a sloping bottom with an averaged slope of 1:55.
For both the current and wave forcing, several tests have been conducting with varying parameters of the forcing and of the groin. Those parameters are:

- For current forcing:
  - Approach velocity ($v_0 = 0.03$ to 0.12m/s)
  - Permeability ($P = 0$ to 50%)
  - Number of groins ($n = 1$ to 3)
- For wave forcing:
  - Wave angle to cross-shore ($\theta = 20°, 30°, 40°$)
  - Permeability ($P = 0$ to 50%)
  - Number of groins ($n = 1$ to 2)
  - Length of the groin L_g compared to width of the surf zone: $L_g = 0.66$ to $1 \times L_s$

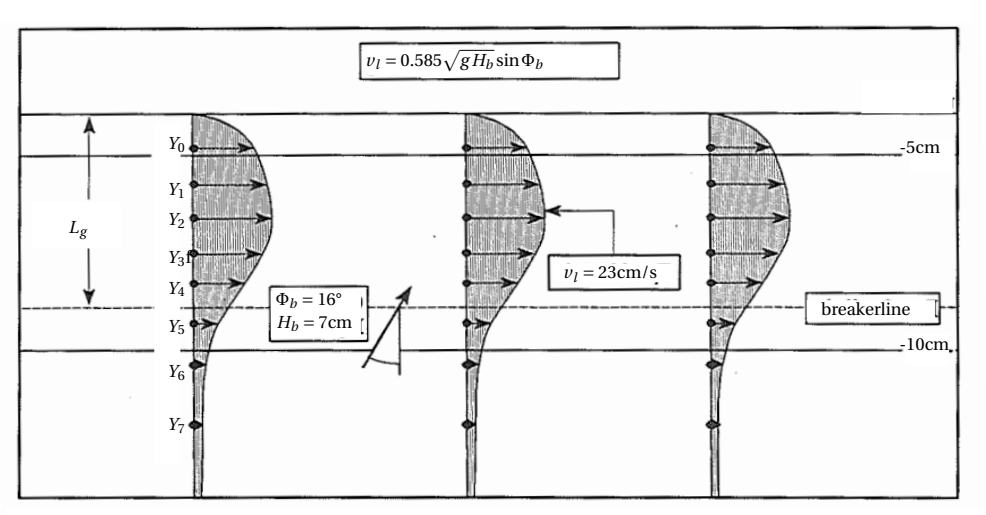

Figure 5.1: Longshore current according to Trampenau (2000) for the situation without groins. The formula is a variation of equation 2.17 for the averaged current in the middle of the surf zone.

5.2.2. MEASUREMENTS AND AVAILABLE DATA

In the experiments, velocities and water levels were measured at seven points in the flow case and eight in the wave case. The measurement devices have been placed on a movable bridge so it could be measured at any desired location w.r.t. the longshore axis (Figure 5.2).

It is not clear where exactly above the ground the velocities have been measured, but it is estimated in this thesis that it was about 30% of the waterdepth above the bed level as this value approximates the mean velocity fairly (see Reniers, 1999). In order to determine the mean longshore current, the velocity has been averaged over 60s. Trampenau (2000) also provides a figure on the undisturbed longshore current (Figure 5.1).

In the publication, Trampenau (2000) provides mainly relative velocities compared to the undisturbed flow which is due to the nature of his research and objective. Absolute velocities are provided as vector figures, but are difficult to interpret and digitize (Figures 5.2 and 5.1).

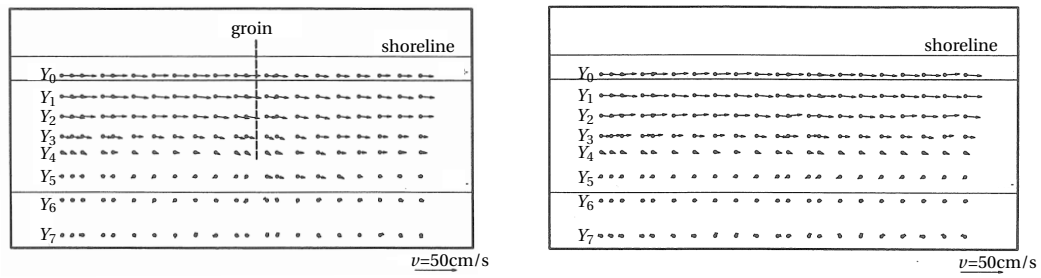

Figure 5.2: Velocity measurements at several measurements points by Trampenau (2000) for the situation without piles (right) and for a groin with a permeability of 50% (left). This specific measurements are given for the wave forcing with a waveheight of $H = 0.05$m.

5.3. RENIERS, WAVES

Reniers and Battjes (1997) conducted research on the longshore current due to waves at a barred beach on a comparable scale as Trampenau (2000) did. The focus lay on the longshore current itself so that detailed measurements are available on different features of the current. The main experimental scales are:

- Beach slope: $\alpha \sim 1:20$
- Beach profile according to Figure 5.3b
- Regular waves
- Wave height $H \sim 7-10$cm
- Wave period $T \sim 1-2$s
- Water depth at wave maker $h \sim 0.55$m
- Basin size ~ 33m × 12m – 33m
- The roughness height of the bottom has been estimated to be $k_s = 0.0005$m
- Width of the bar: ~ 2.5
- Height of the bar: ~ 0.1m

Regular waves were generated at the top left side of the basin by a wave maker. The area of interest were the closest 12m onshore which were observed by measurement devices on a mobile carriage (Figure 5.3b).
As results, the longshore current velocities, wave heights and averaged water level were obtained for several different sets of the above mentioned characteristics (e.g. Figure 5.4). Also a non-barred beach was tested, but did not lead to reliable results on the longshore current due to limitations in the measurement devices.

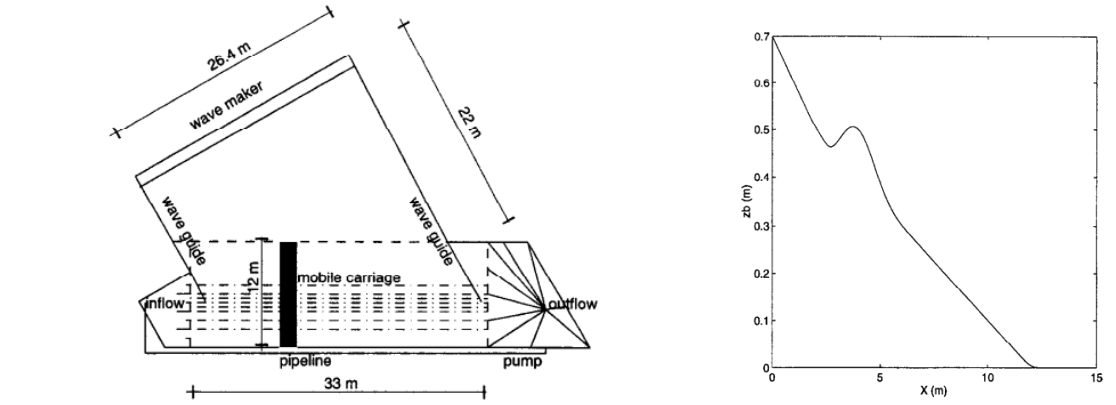

(a) Set-up of the test basin (topview)

(b) Bottom profile

Figure 5.3: The experimental set-up of Reniers (1999) (left) and the bottom profile in the cross-shore direction (right).

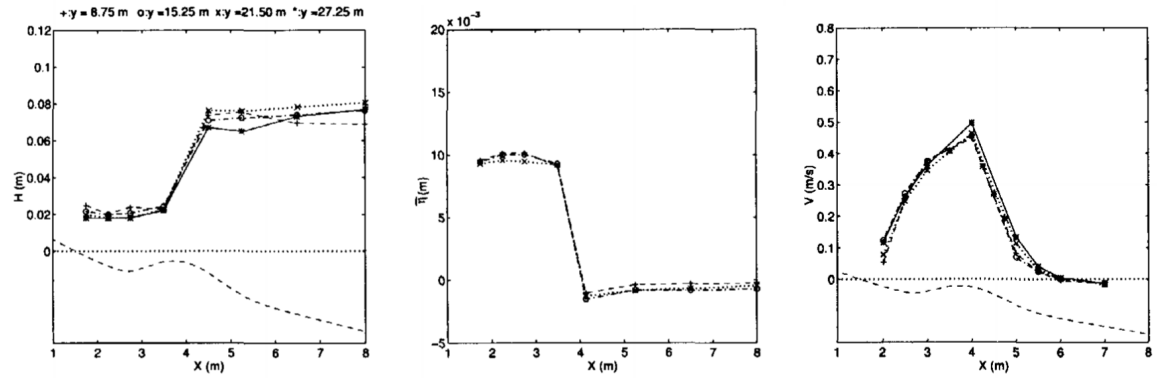

Figure 5.4: Results for experiment SA243 by Reniers (1999), the left figure shows the waveheight, the middle figure shows the setup of the mean water level, and the right figure shows the mean flow velocity in longshore direction.

6

CALIBRATION AND VALIDATION: CURRENT ONLY FORCING

6.1. INTRODUCTION AND OUTLINE

This chapter explores the effect of permeable groins under a current only forcing for different model approaches and boundary conditions. SWASH is used to evaluate different settings of model choices concerning the implementation of the piles, turbulence models and hydraulic boundaries. First, the general set-up of the analytical and numerical model is described (Section 6.2). Section 6.3 lists the important simulations referred to in this Chapter. In Sections 6.4 up to 6.9, the results for different aspects are described. Conclusions and recommendations are presented in Section 6.10.

6.2. MODEL SET UP

The general set-up of the testcases is on laboratory scale. On this scale, the analytical approach as described in Chapter 3 and the SWASH model are evaluated and compared to measurements of the laboratory experiment by Trampenau (2000) (Section 5.2).

6.2.1. DOMAIN

The grid is rectangular with a length of l_x = 25m longshore and l_y = 10m cross-shore. The grid size in the numerical testcases is $\Delta x = \Delta y$ = 0.025m or 0.05m. The domain in relation to the bottom files is illustrated in Figure 6.1. For the comparison of SWASH to the analytical model without the presence of piles, a one dimensional model is used in the SWASH computations with a length of l_x = 25m.

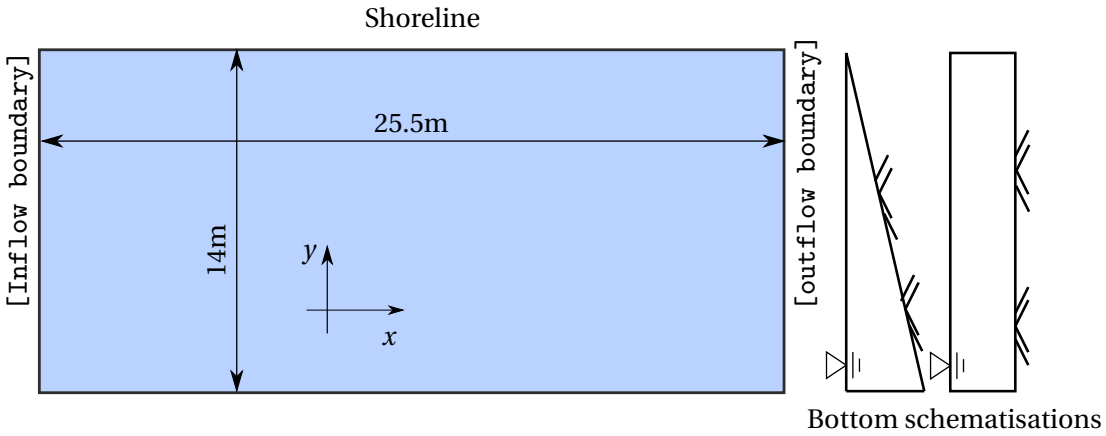

Figure 6.1: Principle of the SWASH domain for the current computations including the domain, the bathymetry and the boundary conditions.

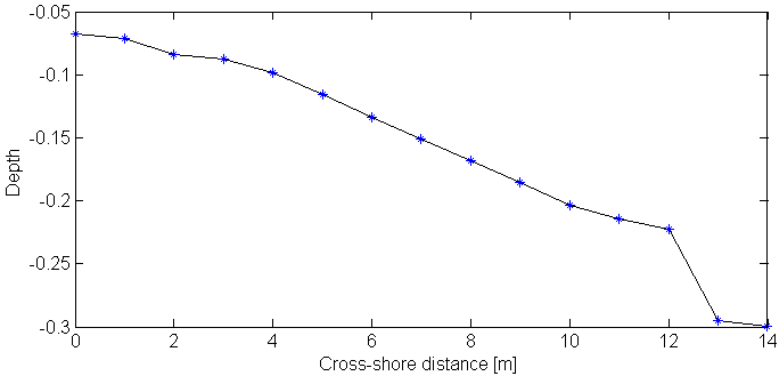

Figure 6.2: Bathymetry of the sloping beach profile.

6.2.2. BATHYMETRY

SIMPLIFIED CASE

A rectangular bottom with a depth of $h = 0.10$m and $h = 0.30$m is used for the comparison of the numerical model to the analytical approach. The bottom is alongshore uniform (Figure 6.1).

CASE TRAMPENAU

In the simulations comparing results to the measurements of Trampenau (2000), the bottom is sloping to imitate a beach and alongshore uniform. The bathymetry is illustrated for the cross-section in Figure 6.2.

6.2.3. GROINS

Next to the boundary conditions, the implementation of the piles in the numerical model is of major importance. The piles can be implemented in several manners:

- as stiff cylinders described by their height, diameter and drag coefficient (the vegetation module in SWASH),
- exception values or
- as a permeable (rubble mound) groin/ breakwater.

The physical characteristics of the piles are a diameter of d=0.01m and their height is larger than the waterdepth (emerged piles).

PILES AS CYLINDERS (VEGETATION)

In the SWASH model, piles (called vegetation in SWASH) can be prescribed as stiff cylinders by a combination of the height `[height]`, the diameter `[diamtr]`, the number of stems per m^2 `[nstems]` and the drag coefficient `[drag]`.
The vegetation module uses a Morison type of equation to evaluate the dissipation of energy (Section 4.3.3). The vegetation is defined at the corners of the computational grid. It can be defined as a subgrid feature (averaged) or in such a way that it is more resolved on the grid.
To reach a permeability of $P = 50\%$ with piles of a diameter $D = 0.01$m, 5,000 plants have to be set per m^2. The cells should be blocked completely (theoretically), when the velocity component has to calculate with 10,000 stems/m^2. The used value for the velocity will be the interpolated value of the grid corners. A value of 5,000 at each grid corner will result in an averaged situation of 5,000 stems per grid cell, i.e. a permeability of $P = 50\%$ not resolved on the grid. The same result is reached for a schematiziation 10,000-0-10,000-0 etc. In order to reproduce a permeability of $P = 50\%$ with the vegetation stems visible on the grid, the input should read 20,000-0-0-0-20,000-0-0-0-20,000 etc.
One disadvantage of implementing the vegetation on the grid is the high resolution that is required. In order to reach a diameter of 1cm, a grid size of 0.5cm is needed. This is computationally expensive, especially under these flow conditions that require a large spin-up time. To reduce the computational time, the grid is fixed to a size larger than the piles. The cells thus contain in fact a cluster of piles. In Section 6.8.1, the effect of variations in the schematization of the groin are illustrated.
The drag coefficient c_D is determined to be $c_D = 1.5$. This is based on the reasoning for larger trees in RIZA (2003a).

IMPLEMENTATION AS EXCEPTION VALUES

In SWASH and most other hydraulic models, it is possible to include exception values. All cells containing a certain value (e.g. in the bathymetry file) will be excluded from the computation. In this way, those cells are an impermeable obstacle to the flow.

IMPLEMENTATION AS RUBBLE MOUND GROIN

It is possible to include a rubble mound groin into the simulation. This requires the specification of the height of the structure, the diameter of the stones and the porosity. This option is not under consideration as there are several unrelated parameters not directly linked to a pile groin. Additionally, it is advised (The SWASH team, 2014) to spread the groin at more than one cell. This requires a small resolution of the grid. Therefore this option is not included in the comparison.

6.3. OVERVIEW OF SIMULATIONS

To analyse the different approaches under current forcing (analytical approach, numerical modelling and laboratory experiments) and their relation to each other, different sets of testcases have been analysed.
For a flat bottom, the analytical approach (Chapter 3) is compared to the SWASH model, both without and with the presence of groins (Sections 6.3.1 and 6.3.2 respectively). For a bottom inclined in the cross-shore direction, results from numerical simulations are compared to measurements by Trampenau (2000).

6.3.1. FLAT BOTTOM: ANALYTICAL MODEL AND SIMPLIFIED SWASH MODEL

To solve the equations 3.5 and 3.19, two boundary conditions are supposed to be known: the discharge upstream (which is constant over the domain) and the water level downstream. These formulas can then be solved for the upstream water level. For a known discharge, the velocity at the up- and downstream boundary can be calculated for the case without groins by means of the continuity equation (equation 3.6).
For the basic sizes given by Trampenau (2000), this formula is tested on sensitivity on variations in the parameters bottom roughness (represented by Chézy C) and the water level.

The input parameters are:

- Length of the stream: $s_0 - s = s_0 = 25\text{m}$
- Water level at downstream boundary: $h_0 = 0.1\text{m}, 0.2\text{m}$ and 0.3m
- Estimated average velocity: $u = 0.12\text{m/s}$ leading to discharges of $q = 0.012\text{m}^2/\text{s}, 0.024\text{m}^2/\text{s}$ and $0.036\text{m}^2/\text{s}$ respectively.

This leads to the simulations presented in testseries A (Table 6.1). In case without piles, a 1D model is used as the analytical approach is also one-dimensional.

Table 6.1: Testseries A: Simulations for analytical formula without piles in SWASH and the analytical approach for a flat bottom.

Testcase	Friction [$\text{m}^{1/2}/\text{s}$]	Waterdepth [m]	SWASH	analytical method
A1	$C = 50$	0.1	X	X
A2	$C = 60$	0.1		X
A3	$C = 70$	0.1	X	X
A4	$C = 80$	0.1		X
A5	$C = 90$	0.1	X	X
A6	$C = 100$	0.1		X
A7	$C = 50$	0.2	X	X
A8	$C = 60$	0.2		X
A9	$C = 70$	0.2	X	X
A10	$C = 80$	0.2		X
A11	$C = 90$	0.2	X	X
A12	$C = 100$	0.2		X
A13	$C = 50$	0.3	X	X
A14	$C = 60$	0.3		X
A15	$C = 70$	0.3	X	X
A16	$C = 80$	0.3		X
A17	$C = 90$	0.3	X	X
A18	$C = 100$	0.3		X

6.3.2. FLAT BOTTOM WITH GROINS: ANALYTICAL FORMULA AND SWASH MODEL

For the case including groins, a 2D SWASH model is used with depth averaged velocities and compared to the analytical model (Table 6.2). A sensitivity analysis is done for the flat bottom on the turbulence models (Table 6.3). For the Prandtl mixing length it is advised to use a mixing length in the scale of the most important mixing. For the set-up given, two lengths can be identified: the size of the piles and the depth of the water which leads to a mixing length coefficient of $l_m = 0.01\text{m}$ and $l_m = 0.1\text{m}$.

Table 6.2: Testseries B: Simulations in SWASH and the analytical formula to compare their results. One groin is implemented for each testcase with a permeability of P=50%. The bottom is flat.

Testcase	Friction [$m^{1/2}/s$]	Waterdepth [m]	SWASH	analytical method
B1	$C = 50$	0.1	X	X
B2	$C = 70$	0.1	X	X
B3	$C = 90$	0.1		X
B4	$C = 50$	0.2		X
B5	$C = 70$	0.2		X
B6	$C = 90$	0.2		X
B7	$C = 50$	0.3	X	X
B8	$C = 70$	0.3	X	X
B9	$C = 90$	0.3		X

Table 6.3: Testseries C: Simulations to compare the effect of horizontal turbulence models for a flat bottom ($h = 0.10$m) with a bottom roughness represented by Chézy $C = 90 m^{1/2}/s$ in the numerical model SWASH. The length of the groin ($L_g = 5$m cover half of the cross-shore width of the domain).

Testcase	Turbulence model	Value
C1	No turbulence model	-
C2	Smagorinsky	$c_s = 0.2$
C3	Prandtl mixing length	$l_m = 0.01$m
C4	Prandtl mixing length	$l_m = 0.1$m
C5	Constant eddy viscosity	

6.3.3. SLOPING BEACH BOTTOM: SWASH MODEL AND MEASUREMENTS

SWASH simulations with a sloping bottom are compared to the experiments by Trampenau (2000).
The effect of the vertical turbulence model combined with the number of layers is evaluated (Table 6.4) and results presented in Section 6.7.1. Further, the effect of the implementation of the groins is evaluated (Table 6.5) and described in Section 6.8.1.
Related to the environmental parameter, the number of groins has been varied. A groin field with three groins has been tested by Trampenau (2000) and is compared to numerical simulations in Section 6.9.

Table 6.4: Testseries D: Simulations to compare the effect of multiple layers and vertical turbulence models for a sloping bottom in the numerical model SWASH.

Testcase	Groins included	Number of layers	Horizontal turbulence model	Vertical turbulence model
D1	No	1	None	None
D1	Yes	1	Smagorinsky	None
D2	Yes	4	Smagorinsky	None
D3	Yes	4	Smagorinsky	k-epsilon

Table 6.5: Testseries GR: Simulations to compare the effect of the resolution of the piles for a sloping bottom with a bottom roughness represented by Chézy $C = 90 m^{1/2}/s$ in the numerical model SWASH. The length of the groin ($L_g = 5$m covers half of the cross-shore width of the domain).

Testcase	Module	Description
GR1	Morison	A coarser grid (0.1x0.1m) with big vegetation ($D = 0.2$m)
GR2	Morison	A finer grid (0.05x0.05cm) with medium vegetation ($D = 0.1$m)
GR3	Morison	A finer grid (0.01x0.01cm) with big vegetation ($D = 0.2$m)
GR4	Morison	A finer grid (0.05x0.05m) with small vegetation ($D = 0.01$m) not resolved on the grid
GR5	Exception value	Exception values used every other cell
GR6	Exception value	Two exception values followed by two flow cells
GR7	Exception value	A cluster of exception values next to each other imitating a circle

6.4. ANALYTICAL AND SIMPLIFIED SWASH MODEL WITHOUT GROINS

The comparability of the analytical formula on the water levels without groins (equation 3.5) and the SWASH results is analysed. In SWASH, a 1D simulation is done, as the analytical formula is a 1D approach. A set of nine settings for different roughness and waterdepth values is evaluated in SWASH and compared to results obtained by the analytical formula.

GENERAL FLOW FIELD

The general flow field is as described in Section 3.2 for a flat bottom without groins. The current in the basin is driven by the pressure gradient, while the pressure due to the water level decreases from the inflow to the outflow boundary. As the water level decreases towards the downstream boundary and the continuity equation holds along the stream, the velocity increases downstream (Figures 3.3a and 3.4a).

COMPARISON FORMULA AND SWASH COMPUTATIONS

For the comparability of the analytical approach and the SWASH computations, the difference in water level and in the velocity between the upstream and downstream boundary is analysed. From the upstream to downstream boundary, the water level decreases and the velocity increases. Figure 6.3a shows the water level difference between the boundaries, Figure 6.3b the variations in the velocity. For both variables, the calculated values with the analytical approach and the SWASH model coincide well. The results show that the depth of the bottom has a significant influence on the water level gradient and velocity gradient along the stream as it determines how much the flow is influenced by the bottom friction. From this result, it can be concluded that the usage of the numerical model is appropriate on this laboratory scale with the chosen values for the numerical resolution.

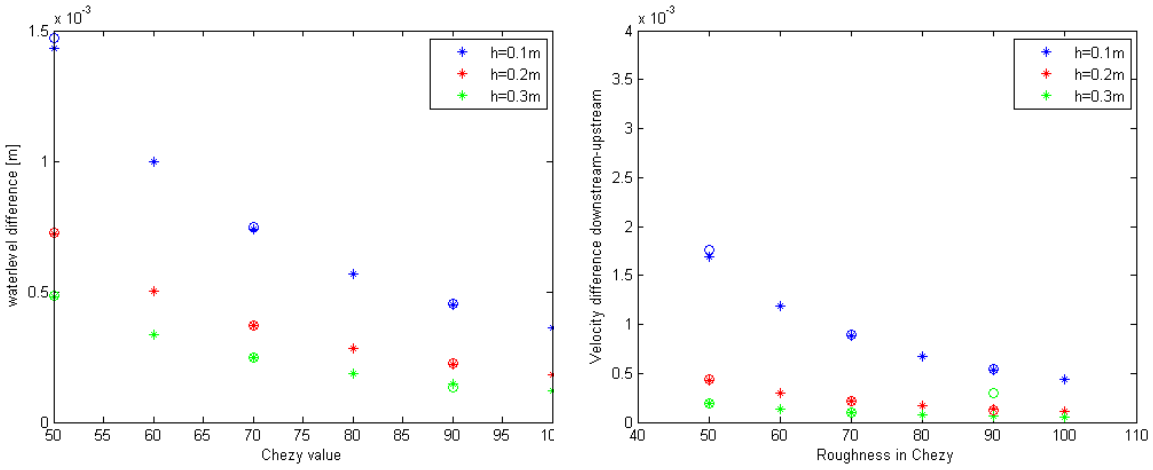

(a) Water levels

(b) Velocities

Figure 6.3: The differences in water level (a) and velocities (b) between the upstream and downstream boundary for a flat basin with a longshore length of $l_x = 25$m. Asterisks indicate the results by the analytical formula 3.5 in (a) and 3.6 in (b), circles the results by a 1D SWASH calculation. The water level decreases from up to the downstream boundary, the velocity increases from the up- to the downstream boundary.

6.5. ANALYTICAL FORMULA AND SWASH RESULTS WITH ONE GROIN

For a flat basin with one groin, the water level difference and velocity distribution is evaluated and compared between the analytical approach (equations 3.19, 3.24 and 3.27) and the numerical computations with the SWASH model. As the analytical approach is simplified, it is important to observe the same qualitative development, influence of factors and the order of magnitude of the results. The SWASH computation is on a 2D grid, the analytical one consists of one 1D stream for the water level (equation 3.19) and two 1D streams for the velocities (according to equations 3.24 and 3.27). The grid resolution of the numerical model in this setting is set to $\Delta x = \Delta y = 0.025$m.

GENERAL FLOW FIELD

The flow field in the numerical results is described. As in the setting without groin, the water level gradient drives the flow. The groin is an obstacle to the flow, leading to a piling up of water windward of the groin and a water depression leeward of the groin (Figure 6.5a). This piling up of water results in an additional pressure gradient in cross-shore direction leading to an offshore directed current windward of the groin. Behind the groin, the pressure gradient is directed landward but leads to a weaker current as the pressure gradient difference is spread of a wider width. The flow is mainly directed into the longshore direction with a small component in the cross-shore direction due to the blockage and the water level gradient in the cross-shore direction (Figure 6.4).

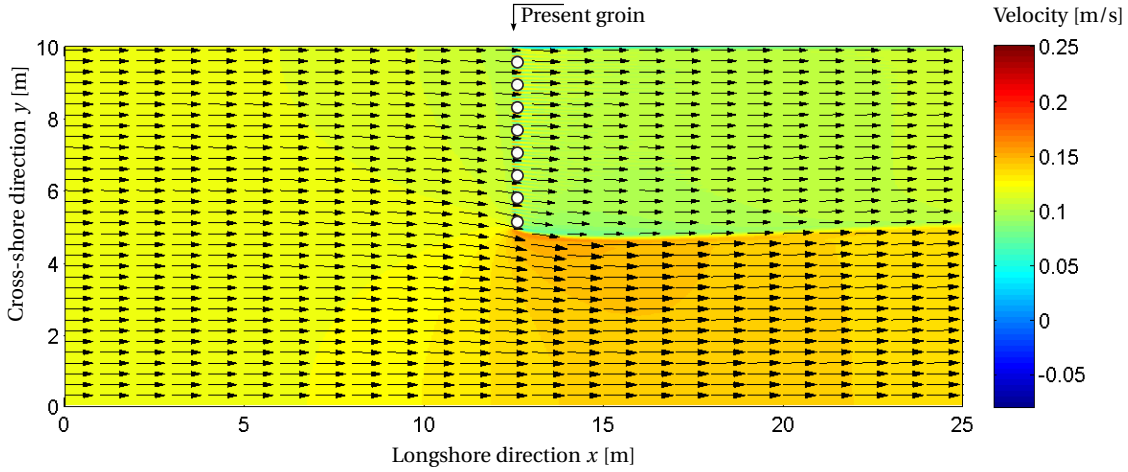

Figure 6.4: Flow pattern obtained from SWASH results around the groin under current forcing for testcase B1 with $C = 50\text{m}^{1/2}/\text{s}$ and a waterdepth of $h = 0.1\text{m}$.

WATER LEVEL

In the analytical approach, it is assumed that the water level at the upstream and downstream boundary is constant along the cross-shore direction due to horizontal mixing. This can be observed in the SWASH computations as well; the water level at the two boundaries is constant along the cross-shore direction (Figure 6.5a).
Figure 6.5b illustrates the water level difference between the upstream and downstream boundary for the formula and for the SWASH computation. It shows qualitatively the same result, the order of magnitude is about the same. In SWASH, the water level difference is higher than in the analytical consideration. This suggests that in the SWASH computation, the flow resistance is higher. This can be explained as the SWASH computation takes more processes into account that lead to energy dissipation such as by turbulence and by flow into the cross-shore direction that are not covered in the analytical approach (see Section 3.5). Though the absolute values are differing for the two approaches, the rate of increase and decrease in the water levels as a function of the Chézy value or of the waterdepth is the same for the analytical computation and the SWASH simulations (Table 6.6). As the numerical computations allow for a 2D approach, local water level differences can be observed, i.e. the water piling up in front of the groin and depressing behind the groin as illustrated Figure 6.5a.

Table 6.6: Influence of the waterdepth and bottom roughness on the difference in water level up- and downstream. The value $\Delta(\Delta h)$ in [mm] gives the difference of the water level difference between the boundaries for either the bottom roughness or the waterdepth while holding the other variable constant, for both the analytical formula and the SWASH computation.

$\Delta(\Delta h)$ in [mm]	Formula	SWASH
Chézy $C = 50/70\text{m}^{1/2}/\text{s}$ & $h = 0.1\text{m}$	0.6889	0.6820
Chézy $C = 50/70\text{m}^{1/2}/\text{s}$ & $h = 0.3\text{m}$	0.2350	0.2680
$h = 0.1\text{m}$ / 0.3m & Chézy $C = 50\text{m}^{1/2}/\text{s}$	0.9442	0.9112
$h = 0.1\text{m}$ / 0.3m & Chézy $C = 50\text{m}^{1/2}/\text{s}$	0.4903	0.49721

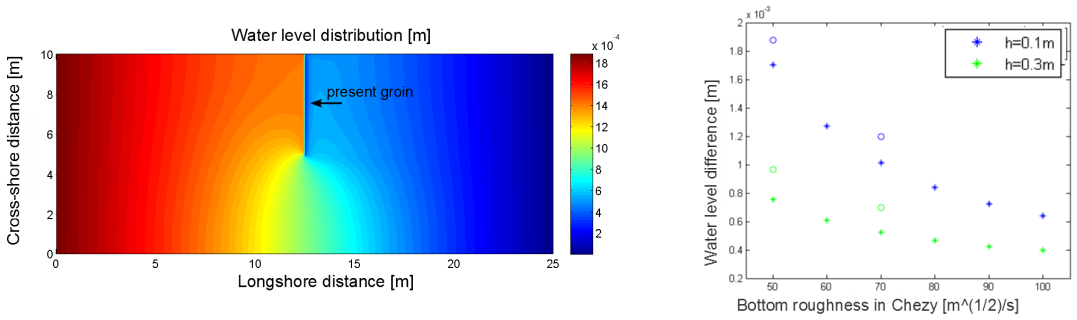

(a) Waterlevel distribution for testcase B1

(b) Water level differences

Figure 6.5: Water level distribution over the domain. The left Figure shows the waterlevel distribution exemplary for testcase B1 with $h = 0.1$m and a Chézy value of $C = 50\text{m}^{1/2}/\text{s}$ from the topview. The right Figure shows the water level differences between the two boundaries with one groin, comparing SWASH (circles) and formula (asterisks), testseries B.

VELOCITY

The relative velocity is compared between the analytical approach and the SWASH computation. The relative velocity is the disturbed velocity compared to the approach velocity u_0 with $u_0 \approx 0.012\text{m/s}$.
The influence of the groin on the velocity is qualitatively the same for the numerical computations and for the evaluation of the formula. Figure 6.6a shows the velocity distribution between the two streams for the SWASH and analytical computations for two different water levels ($h = 0.1$m and $h = 0.3$m). The velocities presented are the downstream velocities of both streams related to the velocity of the situation without groins (compare Section 3.4). The upper part is the stream without groins, the lower one for the stream with piles. The bottom is more important for the distribution of the velocity in case of the analytical formula (visualized in the larger vertical distance between the relative velocities).
Figure 6.6b compares the velocity output from SWASH for the two streams when averaged over the whole length of the domain which is closer to the idea of the analytical considerations. Also in this case, the velocities for the cases under consideration show a good matching.

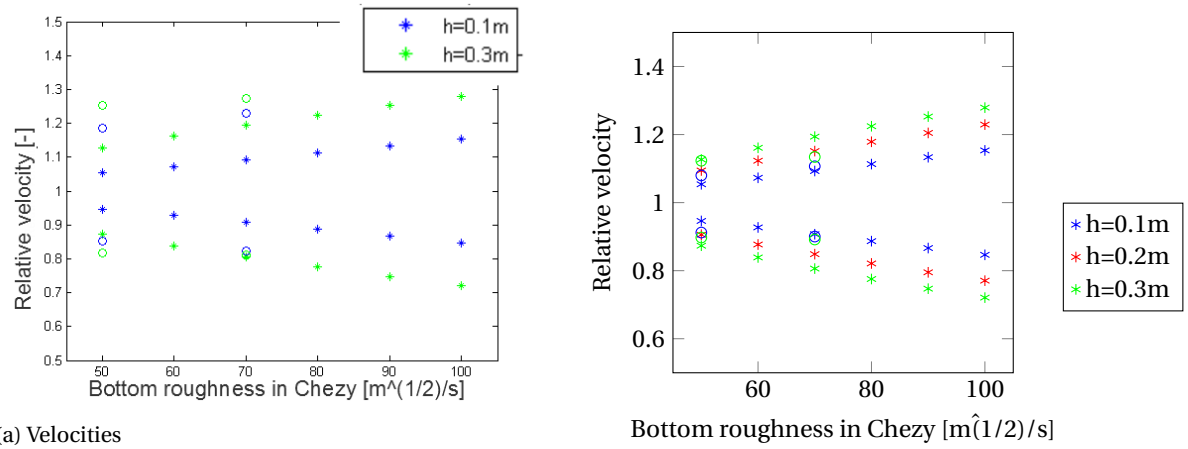

(a) Velocities

Figure 6.6: Relative velocity in the disturbed and undisturbed stream, comparing SWASH (circles) and formula (asterisks). For the SWASH model, (a) uses the averaged velocity per stream, (b) uses the velocity downstream of the groin only. The velocity of the disturbed testcase is set in relation to the approach velocity $u_0 = 0.12\text{m/s}$.

CONCLUSIONS

For the simplified case and a flat bottom, the performance of the SWASH model and the analytical approach have been evaluated concerning the flow field, water level and velocity profile distribution. For a case without groins, good consistency is found between the two methods. When including one groin, good consistency can be found in the effect of the undisturbed waterdepth and the bottom friction on the water level difference at the boundaries due to the presence of the groin. The absolute values however vary from each other. The velocity is more difficult to compare due to the difference in approach (1D in the analytical and 2D in SWASH). While the analytical approach gives only one value per stream, SWASH gives varying velocities over the whole domain on a 2D grid. Both when averaging the velocity over the domain in SWASH and when only comparing the SWASH velocity at the end of the domain, reasonable results are obtained compared to the analytical approach.

6.6. SLOPING BOTTOM: COMPARISON SWASH AND MEASUREMENTS TRAMPENAU FOR ONE GROIN

In this comparison, the sloping bathymetry in cross-shore direction has been used to simulate the beach (Figure 6.2). To evaluate the influence of the piles on the flow, the relative velocity is of interest, i.e. the velocity at a certain point in space under influence of the groin compared to the undisturbed velocity at that same point. For the inclined beach, the undisturbed velocity varies orders of magnitude in the cross-shore direction and a reference case of undisturbed flow is simulated. For the relative velocities, the numerical computations are compared to the measurements.

6.6.1. REFERENCE CASE WITHOUT PILES

The reference case without piles is used to obtain relative velocities of the disturbed flow compared to the undisturbed flow. The outflow boundary is prescribed as a constant water level. The inflow boundary is prescribed as a discharge boundary, varying along the cross-shore direction leading to a uniform distribution of the water level and the longshore velocity (Figure 6.7).

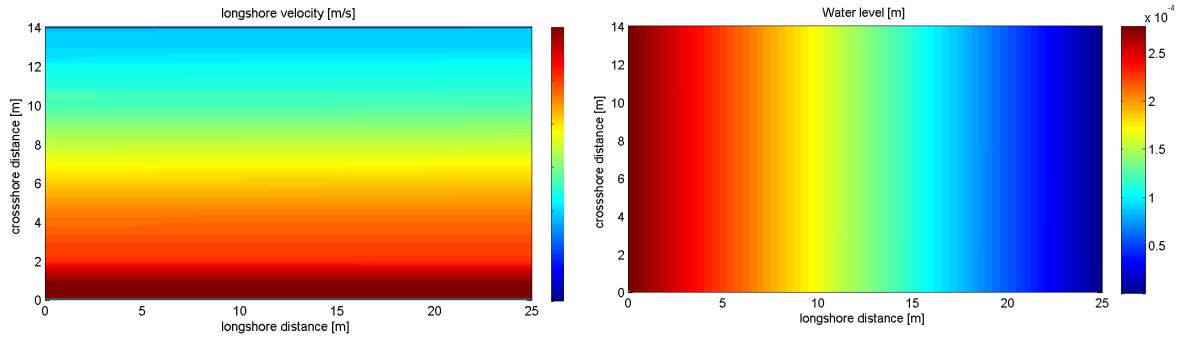

(a) Velocity

(b) Water level

Figure 6.7: Velocity (left) and water level (right) distribution for undisturbed flow: Reference values obtained by SWASH.

6.6.2. RESULTS

The setting for testcase D1 is evaluated on the velocity field. Due to the presence of the piles, fluctuations in the flow field are present behind the groin. Averaging the flow velocity in space, the relative velocity behind the groin reaches 72% of the original velocity. In the measurements, the relative velocity behind a groin with a permeability of $P = 50\%$ is found with about 73%. The relative velocity seawards of the groin only minorly lower in the simulations than in the measurements. It reaches up to 120% of the original velocity, while in the measurements, the relative velocity is up to 129% (Figure 6.8).

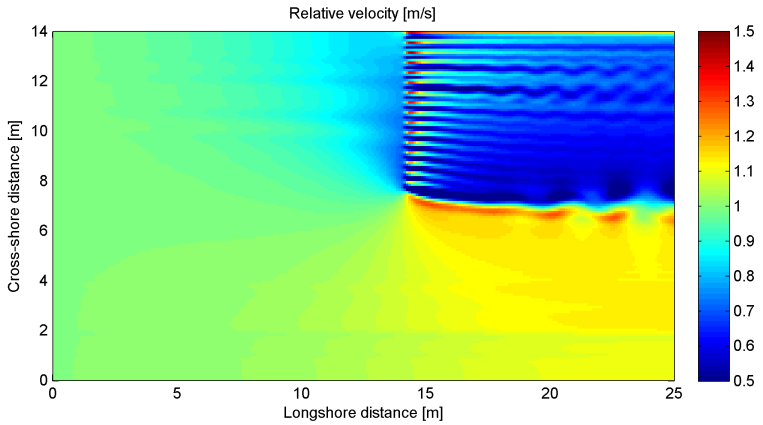

Figure 6.8: Relative velocity field for a sloping bottom under the influence of a groin, SWASH results for testcase D1 compared to the velocity field as in Figure6.7a.

6.7. EFFECT OF TURBULENCE MODELS

The piles of the groin are obstacles to the flow. Especially around them and leewards, a lot of turbulence and mixing is to be expected. In a numerical model, the mixing is to be included via approximations (Section 2.5). In SWASH, a distinction has to be made for horizontal viscosity models and vertical viscosity models. In the horizontal space, three models are available: A constant eddy viscosity and the Prandtl mixing length approach and the Smagorinsky model. In the vertical, two approaches are possible: a constant background viscosity and the k-epsilon model (or a combination). Furthermore, the dynamic viscosity of water can be prescribed in SWASH.

6.7.1. ANALYSIS HORIZONTAL MIXING ON FLAT BOTTOM

It has been observed that the velocity recovers later in the numerical simulation than in the results of the experiments. This suggests that there is more horizontal mixing in the experiments than in the numerical simulations. Therefore, other turbulence models are included into the model set-up: No turbulence model, the constant eddy viscosity and the Prandtl-mixing length, next to te Smagorinsky model.
Testseries C (Table 6.3) has been simulated to compare the results of the SWASH computations due to variations in the turbulence model. For this, a bottom friction Chézy value of $C = 90\text{m}^{1/2}/\text{s}$ and a waterdepth of $h = 0.10$m are used. The groin is resolved on the grid with a length of $L_g = 5$m (half of the domain width).
For the Prandtl mixing length it is advised to use a mixing length in the scale of the most important mixing. For the set-up given, two lengths can be identified: the size of the piles and the depth of the water which leads to a mixing length coefficient of $l_m = 0.01$m and $l_m = 0.1$m. The latter mixing length also coincides with the resolution of the grid.

RESULTS

Except for the mixing length of $l_m = 0.1$m, the averaged velocity of the different simulations stays in the same range with only minor differences, compare Figure 6.9. The averaged velocity behind the groin is lowest for this case. The effect of reducing the energy of the flow is larger than smoothing the velocity profile and exchanging momentum of disturbed and undisturbed stream.

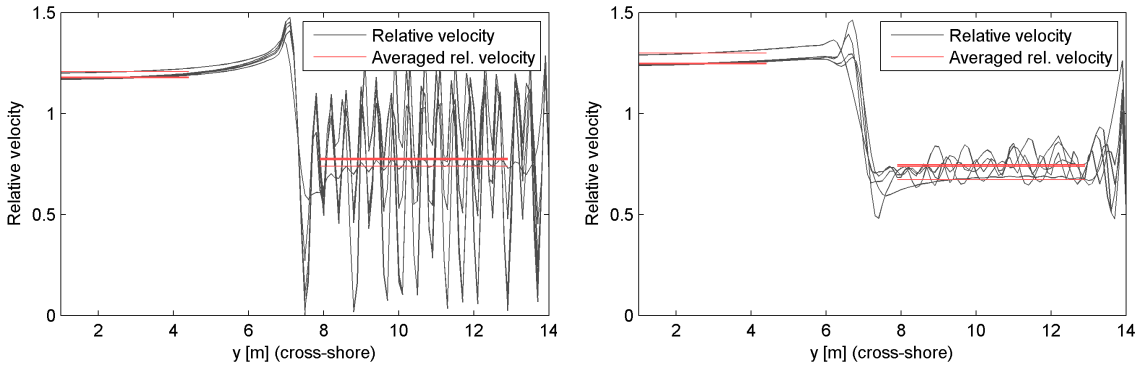

(a) $x = 15$m

(b) $x = 20$m

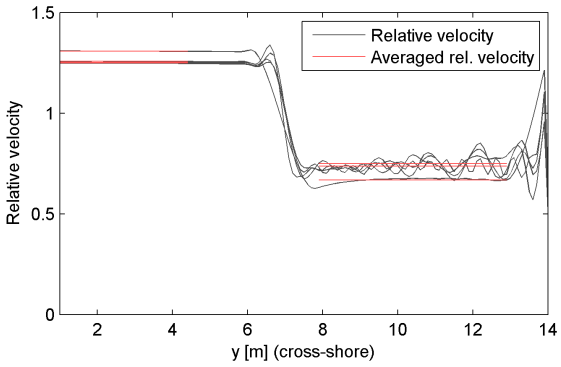

(c) $x = 25$m

Figure 6.9: Relative velocity (black) for a flat bottom ($h = 0.10$m) at $x = 15$m (a), $x = 20$m(b) and $x = 25$m(c). Several turbulence models are compared. Though the fluctuations vary (significantly), the averaged velocities (red) are close to each other. Using a Prandtl-mixing length of $l_m = 0.1$m shows the lowest averaged velocity.

The simulations using the Prandtl-mixing length model and the eddy viscosity model give approximately the same result

in quantitative and qualitative manner. The magnitude of the peak velocities are close to the simulation without turbulence model. The run with the Smagorinsky model is clearly different from the other runs. It has more peaks, but their amplitude is less.
Comparing the velocities at the different cross-sections, the mean velocities are close to each other, but the deviations vary per model. Further downstream of the groin, the differences in the velocity deviations are diminishing.
This testseries gives insight into the principal effect and importance of the turbulence model. In the available measurement data, no detailed data was available to cover the needed resolution in space and time to verify those results. For further interest in the turbulent flow behind the groin, a laboratory experiment with a fine measurement resolution is advised.

6.7.2. ANALYSIS VERTICAL MIXING ON SLOPING BOTTOM

For the sloping beach bottom, the effect of using multiple layers is evaluated. For a three dimensional approach, the usage of a vertical viscosity model is possible: The k-epsilon model. The following simulations are used to compare the effect of a three dimensional approach. A friction of Chézy with $C = 90\text{m}^{1/2}/\text{s}$ has been used, the groins are resolved on the grid reaching $L_g = 3.5\text{m}$ into the domain. The parameters of the k-epsilon model are chosen with the standard values of $k = 0.07$ and $\epsilon = 0.16$ (Section 4.3.2).

RESULTS

Just leeward of the groin, a significant influence on the velocity profile of the choice of the vertical turbulence models and number of layers cannot be seen. When using multiple layers, the velocity differences in the stream with the groin smooths out earlier if including the k-epsilon model than if not including it. This is to be expected as turbulences smooths out velocity deviations. Further, the exchange between the two layers behind the groin starts earlier for the simulation including a vertical turbulence model. In simulation D3 (without k-epsilon model), a drop in velocity can be seen left (in cross-shore direction) of the high velocity next to the groin at the cross-sections at $x = 20\text{m}$ and $x = 25\text{m}$ (Figure 6.10). This drop is not seen in any other simulation, leading to conclude an unrealistic behaviour. The smoothing and the drop in velocity next to the groin suggests to use a vertical turbulence model when applying multiple layers. A further observation is that the slope of the beach enhances the exchange between the two streams downstream of the groins. With an inclining beach, the two streams begin to exchange momentum earlier than for a flat bottom at about $x = 17\text{m}$.

6.8. DISCUSSION ON THE IMPLEMENTATION OF THE GROIN

The piles of the groin are implemented in two different ways: Using a dissipation model based on the Morison equation or as exception values. For both approaches, slightly different resolutions of the groin can be achieved. Those are discussed in the following section.

6.8.1. INFLUENCE OF THE GRID-SIZE AND VARIATION IN THE DISSIPATION MODEL

MODEL SET-UP

In the simulation described so far, an approximate resolution of the piles on the grid is used. Due to the small pile diameters compared to the grid size, they are eventually not truly resolved on the grid but the numerical cells contain either a cluster of piles next to cells not containing piles. In this section, the effect of several ways implementing the vegetation in the current situation is described, the testcases described are (Table 6.5):

- A simulation with a coarser grid ($\Delta x \times \Delta y = 0.1\text{m} \times 0.1\text{m}$) (GR1)
- A simulation with a finer grid ($\Delta x \times \Delta y = 0.05\text{m} \times 0.05\text{m}$) (GR2)
- A simulation with a finer grid ($\Delta x \times \Delta y = 0.05\text{m} \times 0.05\text{m}$) with a clustering in such a way that more cells in a row are containing piles and reach the same theoretical distribution as GR1 (GR3)
- A simulation with a finer grid ($\Delta x \times \Delta y = 0.05\text{m} \times 0.05\text{m}$) with small vegetation ($D = 0.01\text{m}$) averaged over the whole length of the groin (GR4)

RESULTS

The larger pile clusters in testcase GR1 impose more resistance on the flow and lead to a higher fluctuation of velocity behind the groin. The mean velocities behind the groin is lower than the one with smaller stems (GR2 and GR3). A third effect is that the velocity for the larger resolution smooths out later in longshore distance (Figure 6.11).

Comparing the setting with a small grid and larger vegetation (GR3) to the other runs, the velocity is higher in the region with the groins, and the eddies behind the groin stay longer inside the flow, but there is more exchange in the flow at the interface of the two streams. With the latter setting the increase in velocity next to the groin is less pronounced. Thus, earlier offshore, the velocity is near the undisturbed velocity. The mixing of the two streams also occurs earlier, however it requires a higher resolution of the grid and is computationally more expensive (Figure 6.12).

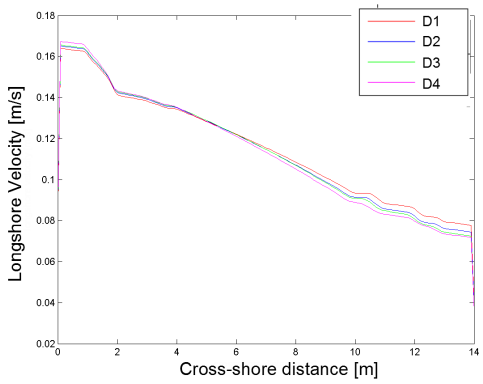

(a) $x = 5$m

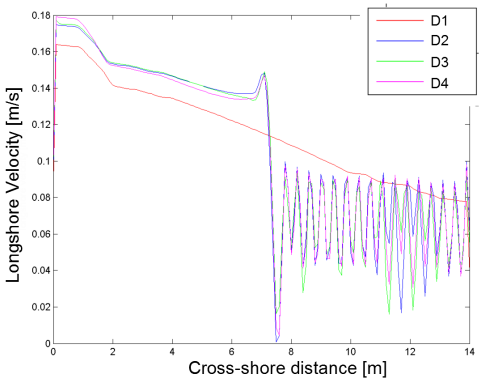

(b) $x = 10$m

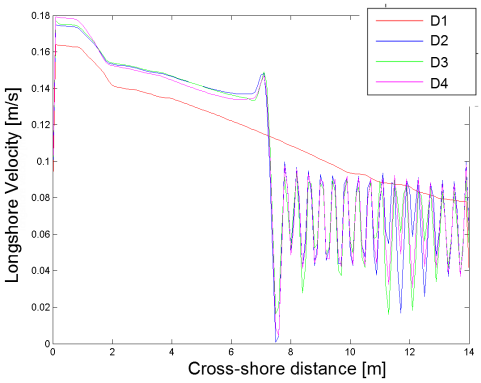

(c) $x = 15$m

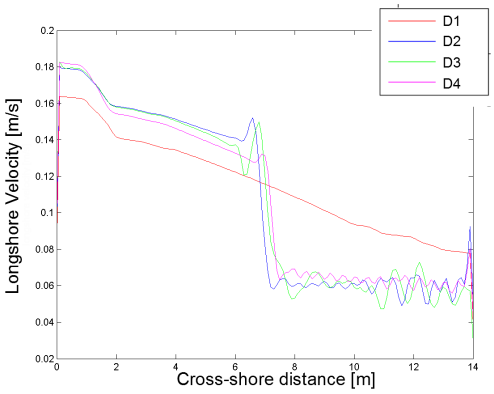

(d) $x = 20$m

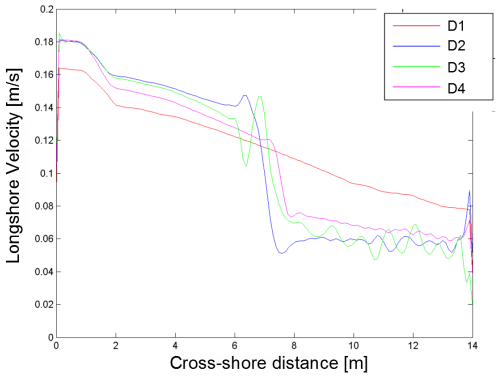

(e) $x = 25$m

Figure 6.10: Velocity distribution for comparison influence of vertical layers, at several cross-sections. SWASH results for testseries D.

A comparison with a simulation with vegetation not resolved on the grid (testcase GR4), but an averaged permeability of about $P = 50\%$ over the whole length of the groin shows relation to the fine grid with the fine vegetation (Figure 6.13). The exchange of the two streams behind the groin is similar. The difference is the behaviour immediately in front and behind the groin. No vortex can be seen and the velocity decreases more. In front of the groin, no deflection of the flow towards the offshore is observable. This behaviour is understandable as SWASH translates the drag force into a mean deceleration of the flow. Though the diameter of the piles could not be achieved as the grid resolution due to computational costs, the clustering of piles imitating permeability is given preference over an averaged field if applied to a groin situated at a beach.

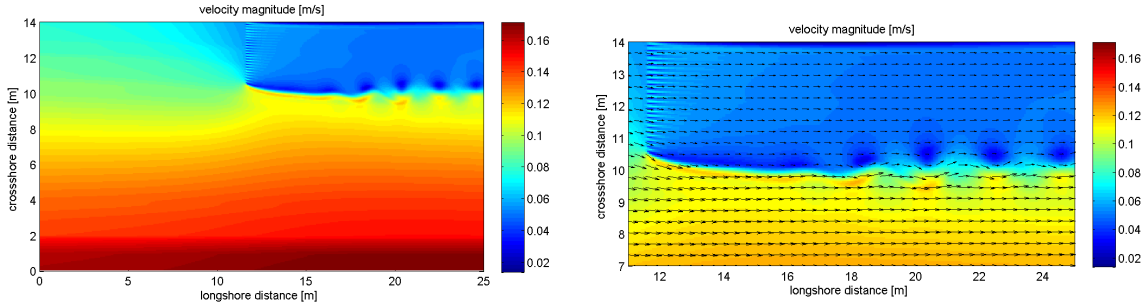

(a) (b)

Figure 6.11: Velocity field for the fine grid and fine vegetation. (b) shows a zoom and flow directions for testcase GR2.

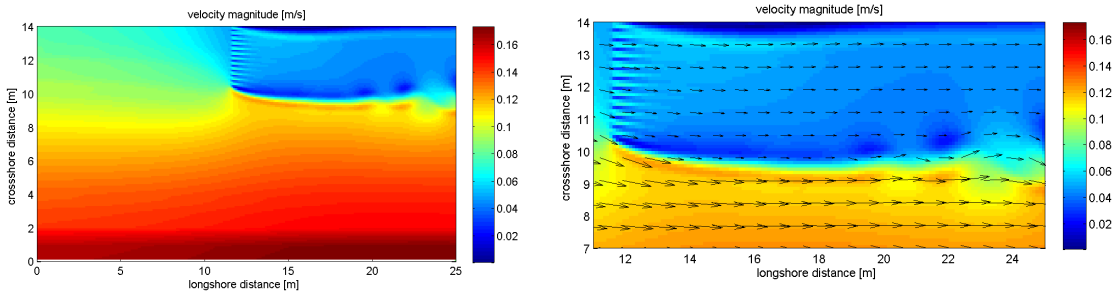

(a) (b)

Figure 6.12: Velocity for the coarse grid and coarse vegetation, (b) shows a zoom and flow directions for testcase GR1.

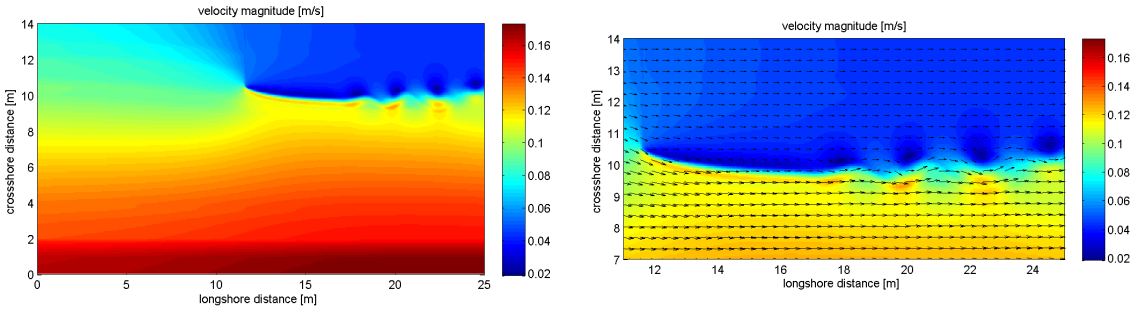

(a) (b)

Figure 6.13: Velocity for the coarse grid and averaged vegetation, (b) shows a zoom and flow directions for testcase GR4.

6.8.2. USING EXCEPTION VALUES

MODEL SET-UP

Another option to implement the stems is to exclude certain cells from the calculation as so-called exception values in the bottom file. By this, the cells stay dry in any case. Positively, the computational time generally decreases when excluding cells from the computation. Compared to the Morison method, the velocity in these points is zero and the piles can be placed accurately and visibly. As a disadvantage, the Morrison drag-effects might not be properly taken into account. Further, the physical diameter of the piles is small compared to the present resolution of the grid. Using exception values will lead to the blockage of a cell which is bigger than the actual pile. A resolution of the grid smaller than or just as the pile diameter is found to be computational too expensive.
To identify effects of the usage of exception values as piles, the following simulations are discussed (Table 6.5):

- Exception values used every other cell (GR5)
- Two exception values followed by two flow cells (GR6)
- A cluster of exception values next to each other imitating a circle (GR7)

RESULTS

With respect to the velocities, there are some differences visible comparing all testcases with exception values to the Morison module. The velocity at the northern boundary reduces and eventually becomes negative: A large scale eddy is present (Figure 6.14b). In the third simulation with bigger stems (GR7), the velocity between the piles is much higher compared to using the Morison model due to the fact that more water has to flow through the gaps. In the Morison approach, the cells containing pile clusters did not block the discharge completely. The mixing of the stream can be observed downstream of the groin. The drawback is that - though the vegetation can easily be implemented in a bathymetry file - it requires a smaller grid than $\Delta x \times \Delta y = 0.01\text{m} \times 0.01\text{m}$ (the diameter of the pile) to resolve the piles of the experiment. Already with that resolution, the calculation time increases significantly and doesn't seem to be computational feasible any more. It should be attempt to provide a grid smaller than the piles, so that the excluded cells can be clustered together and provide a more circular pile. This would require a further refining.
Using exception vales with a permeability of $P = 50\%$ leads to a recirculation close to the shore which is not visible in the runs with vegetation and the experiments by Trampenau (2000) (Figure 6.14b and 6.15b). This implies a higher effective permeability as this recirculation is observed in the experiments and literature for groins with a lower permeability.
Testcase GR7 shows vortex streets behind the groin. It is explainable that it happens for this specific simulation: The piles are rather large (about $D = 0.70\text{m}$), so the effect of the piles itself persists longer in longshore direction (Figure 6.14b).

This brief exploration showed that the usage of exception values is not appropriate as it leads to a lower effective permeability of the groin: Though theoretically the permeability is higher, the flow shows flow characteristics obtained for a flow disturbed by a groin with a lower permeability.

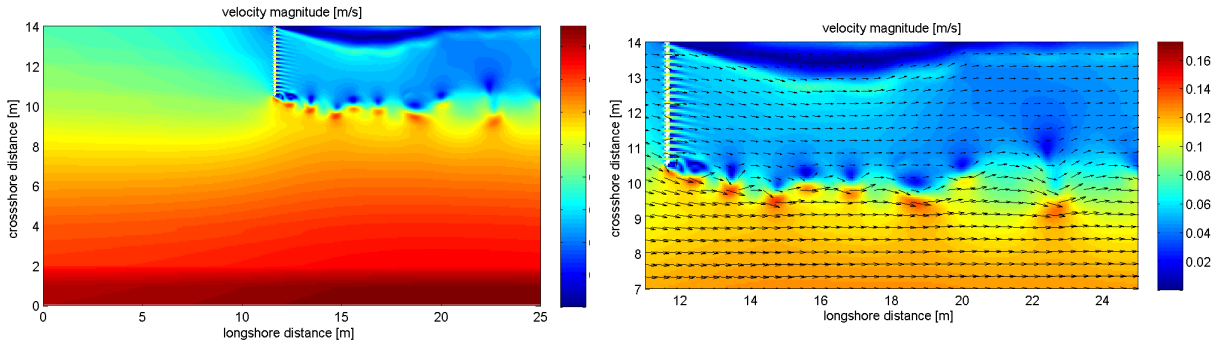

(a) (b)

Figure 6.14: Velocity for piles represented by two dry cells (GR6), (b) shows zoomed in and velocity vectors.

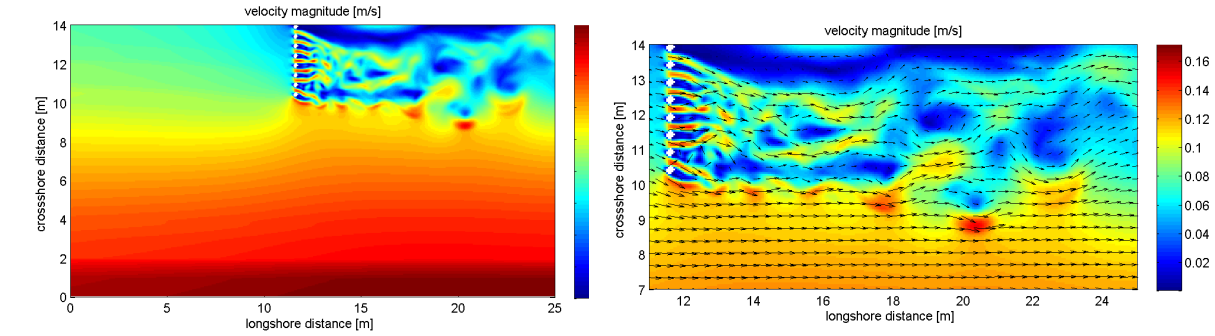

(a) (b)

Figure 6.15: Velocity for piles represented by multiple dry cells (testcase GR7). (b) shows a zoom in and velocity vectors.

6.9. COMPARISON SWASH AND MEASUREMENTS TRAMPENAU FOR THREE ROWS OF PILES

MODEL SET-UP

Related to the environment parameter, the number of groins has been varied. A groin field with three groins has been tested by Trampenau (2000).
They are placed with a distance of L_s = 4m to each other. In the numerical set-up, the groins are placed at x = 11.50m, 15.50m and 19.50m. The grid size of $\Delta x = \Delta y = 0.05$m is used. The groins have a permeability of about $P = 50\%$ with the same principle of resolution on the grid as described in Section 6.2.3. The size of the piles are $D = 0.01$m. They reach L_g = 3.5m far from the shoreline. The domain has slightly been extended in x-direction (l_x = 27.5m instead of 25m). As horizontal turbulence model, the Smagorinsky model with a value of $c_S = 0.15$ is chosen.

RESULTS

Figure 6.16 shows the longshore velocity component of the flow, averaged over time (t = 120s). It can be seen that the velocity reduces from groin to groin and starts increasing again somewhat behind the last groin. The relative velocity profiles of the numerical simulation are compared to the ones of the experiment. The reduction of the velocity behind the groins is coinciding (Figure 6.17). Averaging the relative velocity of the numerical simulations in cross-shore direction leads to the same averaged velocity as in the experiments (Table 6.7). The value of the relative velocity next to the groin cross-shore is close to each other. For the first groin, the location is about the same. The cross-shore location of the maximal velocity at the second and third groin is closer to the groin in the experiments than in the numerical simulation. The maximal velocity off-shore of the groin reduces earlier in the numerical simulations.

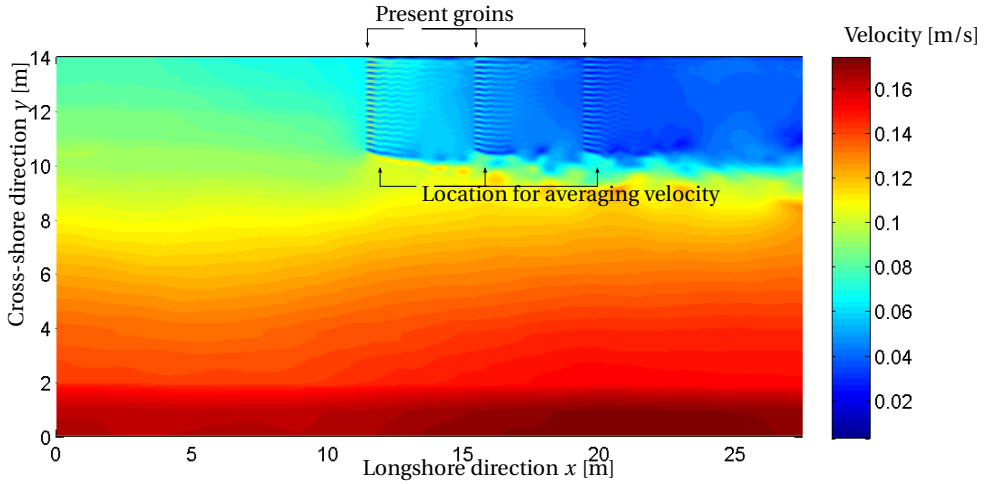

Figure 6.16: Longshore velocity for three groins as obtained with numerical simulations by SWASH, topview.

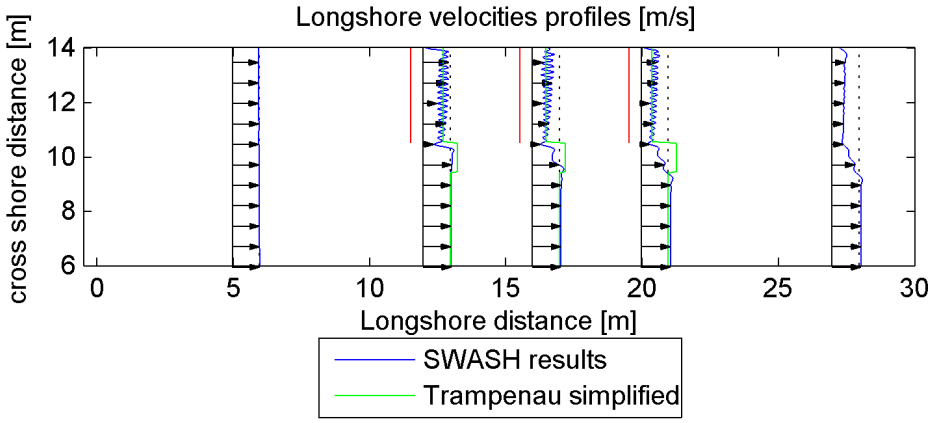

Figure 6.17: Compare the relative longshore velocity profiles leewards of the three groins of the SWASH computation with the measurements by Trampenau (2000). The permeability is $P = 50\%$.

Table 6.7: Comparison of the relative velocity 0.5m leeward of the groins (see Figure 6.17), only the part including the groin is evaluated.

	Groin 1		Groin 2		Groin 3	
	Trampenau	SWASH	Trampenau	SWASH	Trampenau	SWASH
Velocity (relative) [-]	0.73	0.75	0.52	0.55	0.41	0.45
Velocity undisturbed [m/s]		0.0846		0.0846		0.0846
Velocity behind groins (absolute) [m/s]		0.0634		0.0468		0.0377

6.10. CONCLUSIONS AND RECOMMENDATIONS

The comparison of the numerical results to analytical results and to measurements showed that it is possible to compute the effect of permeable pile groins under the forcing of currents on the flow field. Different possibilities of implementing the groins have been tested with the conclusion that a resolution on the grid of the piles appears to be the most promising. The disadvantage is the rather fine grid resolution required, but a slightly coarser grid than theoretically needed still gives results close to measurements. The velocity recovers earlier in the experiments than in the numerical simulations suggesting a lack of mixing in cross-shore direction. A sensitivity analysis on the turbulence model in case of the settings based on the measurements by Trampenau (2000) showed that the mean velocity is hardly effected. For a further analysis on the fluctuations, experiments with a higher spatial and temporal resolution are recommended in a future study. With the Morison approach, the discharge is not completely blocked, so a real physical interpretation is more difficult and the quantitative velocity just around the piles to be considered with more care.

7

CALIBRATION AND VALIDATION: WAVE FORCING

7.1. INTRODUCTION AND OUTLINE

In this Chapter, the implementation and the development of the longshore current in undisturbed circumstances is described, followed by a comparison of the relative velocities for a groin with a permeability of $P = 50\%$. The longshore current has been evaluated for two available measurement data sets: (1) Comparing a longshore current simulation with the measurement data published in Reniers and Battjes (1997) and Reniers (1999) for a situation without groins in Section 7.2; and (2) evaluating longshore current simulations excluding and including groins based based on data by Trampenau (2000) in Sections 7.3 to 7.5.
For the simulation of the profile based on the measurements by Trampenau (2000), analytical expectations and simulations for the longshore current are evaluated first before the groins are included. The testseries based on the laboratory experiment of Reniers (1999) is intended as a validation of the numerical model use on the small under a wave-forcing inducing a longshore current. The analytical considerations for the case of Trampenau are intended as a further validation of the results for the testseries based on this experiment. The detailed sensitivity of the SWASH model in case of the wave simulation is further elaborated in Appendix B.
Concerning the groins, the way of implementing is varied and calibrated to match best with the measurements. For the setting fitting the best, groin and forcing parameters are changed (Section 7.6).

7.2. COMPARING SWASH TO LABORATOY DATA ON LONGSHORE CURRENTS: RENIERS CASE

On the longshore current itself, several studies have been conducted of which one is by Reniers and Battjes (1997) on a similar laboratory scale as in Trampenau (2000) (Section 5.3). The focus and scope of these experiments on the longshore current was often to identify mechanisms and interaction with a bar and shear instabilities of the longshore current. This data puts emphasis on the current velocities and is used as a validation of the longshore current computed by SWASH with the intended settings in the model set-up with groins comparing to the measurements by Trampenau (2000).
The case `SA243` is used to compare the numerical results with the measurements obtained in the laboratory experiments with the following settings:

- `SA243`
- Barred beach
- Water depth $h = 0.55$m at wave making boundary
- Regular waves:
  - Wave Height $H = 0.08$m
  - Wave Period $T = 1.0$s

The roughness height is estimated by Reniers and Battjes (1997) with $k_s = 0.0005$m. The Chézy value is obtained by evaluating equation 2.35 for a local waterdepth of $h = 0.55$m at the wave making boundary with $C = 73\text{m}^{1/2}/\text{s}$. This corresponds to a Manning coefficient of $m = H^{1/6}/C = 0.0124\text{s}/\text{m}^{1/3}$ (equation 2.38).

7.2.1. MODEL SET-UP

The wave basin as described in Section 5.3 has been simplified to a rectangular domain of the size $l_x = 33$m and $l_y = 22.85$m with a grid size of $\Delta x = \Delta y = 0.05$m. The bottom is sloping with an average slope of $\tan\alpha = 1:20$ to a maximal

waterdepth of $h = 0.55$m at the wave maker. It includes a bar 2m away from the shoreline (Figure 5.3b).

7.2.2. RESULTS

For the case under consideration, the results on the waveheight H_{SIG}, the longshore current velocity and the mean waterlevel are illustrated and compared to the measurements in Figure 7.1. This has been evaluated for both friction approaches (Manning and Chézy).
The wavebreaking takes place at the same location above the bar visualized by the drop in waveheight. A second breaker line is present close to the shore. This was also found in the experiments by Reniers and Battjes (1997). The maximal longshore current velocity is about equal and at the same cross-shore location. The current velocities close to the shore do coincide less.
The waterlevel set-up difference in case of the laboratory experiments is about 11 to $12 \cdot 10^{-3}$m, in case of the SWASH computation about $8.3 \cdot 10^{-3}$m. Comparing the wave height H_{SIG}, the one behind the bar is around 1.4cm in case of the SWASH computation and 2cm in case of the experiments. In front of the bar, the wave height is found between 6.5 to 7.5cm for the computations and 6.5 to 8.0cm for the experiments.
The longshore current profile and the mean water level are partially different for the two friction approaches. This

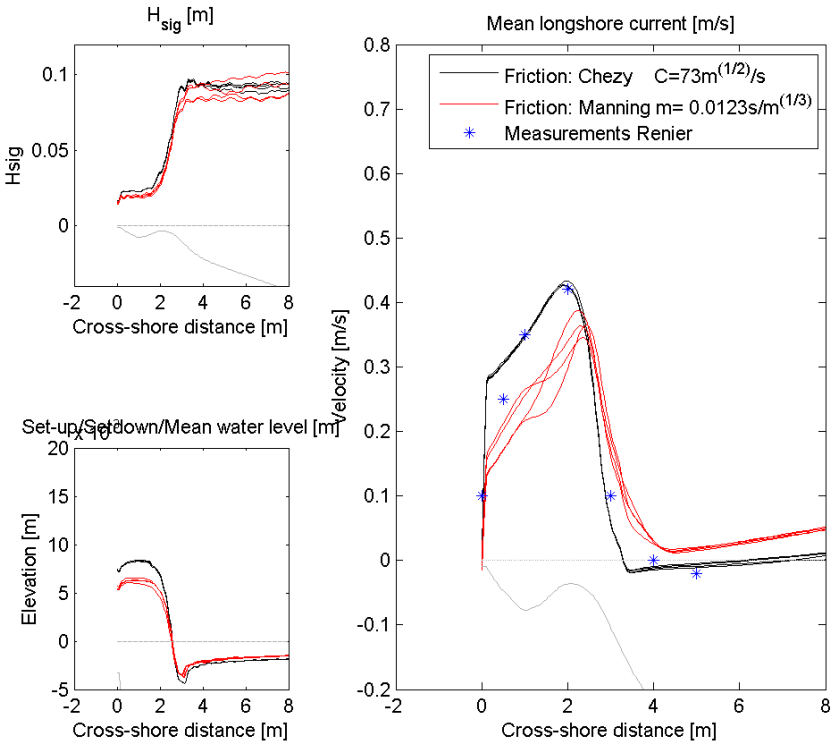

Figure 7.1: Wave height H_{RMS}, water level-setup and longshore current velocity at several cross-sections obtained by SWASH simulations with different friction approaches (solid lines) compared to the results by Reniers and Battjes (1997) (points) for the test `SA243`.

stems from the nature of these two approaches when both values are chosen to be constant throughout the domain, namely that the bottom onshore gets more effective roughness in case of the approach following Manning (Section 2.6). Therefore the velocity of the longshore current is lower than when using Chézy. In a coastal application, preference is given to the approach by Manning. Though the magnitude of the peak velocity is approach better for the simulation using the Chézy approach, the profile of the measurements coincides better with the simulation using Manning's approach. A sensitivity analysis would show the most proper value to obtain results even closer to the measurements.

This consistency between the numerical model and the measurements leads to confidence that SWASH can be used for a research on longshore currents and groins on this small laboratory scale with the chosen numerical set-up.

7.3. COMPARING NUMERICAL RESULTS TO MEASUREMENT DATA: TRAMPENAU CASE

The physical set-up and the results of the experiment by Trampenau (2000) are described in Section 5.2.

7.3.1. NUMERICAL MODEL

Figure 7.2 gives the principle idea of how the model is set-up for the wave case based on the experiments by Trampenau (2000).

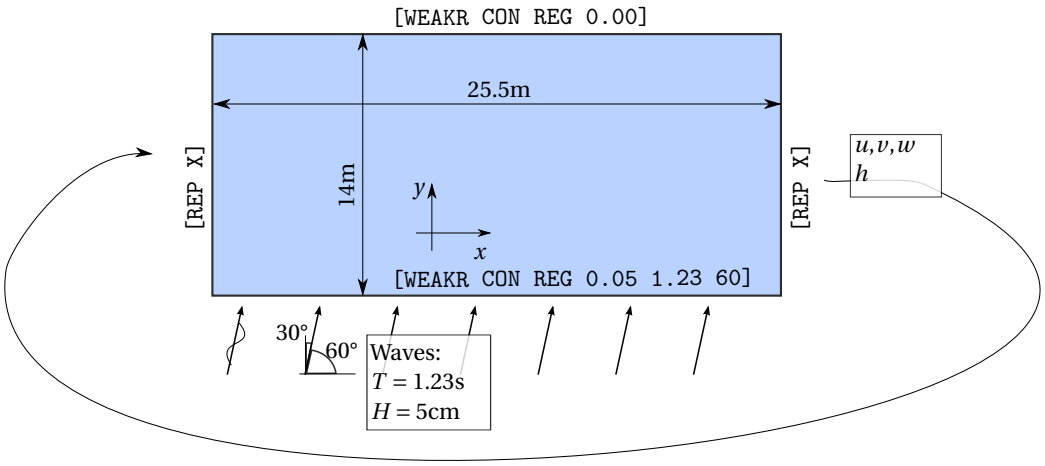

Figure 7.2: Principle of the SWASH domain for wave computations including the domain and the boundary conditions.

DOMAIN AND GRID

The numerical domain in case of waves is in the basic case $l_x \times l_y = 25.5\text{m} \times 14\text{m}$. The basic grid resolution is set to $\Delta x \times \Delta y = 0.05\text{m} \times 0.05\text{m}$. For the computation of waves, about 50-100 grid cells are recommended per wave length (The SWASH team, 2014). The incoming regular wave has a length of about $L = 2\text{m}$. A grid resolution in wavedirection of at least 0.04m is desired in wave direction. As the imposed wave is regular, a resolution of 0.05m is sufficient to simulate the propagation properly.

WAVES

The waves are implemented from the offshore boundary (south) with an angle of $\theta = 30°$ with respect to the cross-shore axis y. They are prescribed as regular waves with a wave height of $H = 0.05\text{m}$ and a period of $T = 1.23\text{s}$. Variations are mentioned in the context.

BOTTOM PROFILE

The bottom is sloping with an averaged slope of about 1:55. In principle, the bottom is given as *Bottom1* in Figure 7.3. However, as for reasons described in Section B.2.1, two other bottom files have been developed, see *Bottom2* and *Bottom3* in Figures 7.3a and 7.3b respectively.

BOUNDARY CONDITIONS

In the longshore direction, a periodic boundary is prescribed to avoid reflection from these boundaries back into the domain. With the periodic boundary, the information that leaves the domain on one side enters the domain at the opposite side, thus prolonging the effective length of the domain. This may be applied when the forcing and the bathymetry is uniform in that direction. The length of that domain should be an integer number of longshore component of the wave length of the imposed waves. Therefore, the domain has been extended by 0.5m compared to the current simulations. Between the water level at the outgoing boundary and at the incoming boundary, no discontinuity should be present for a correct transfer of information between the boundaries. Figures 7.4a and 7.4b display the connection at the periodic boundary showing that no discontinuity is visible.
The waves are entering the domain from the southern (offshore) boundary. The waves with the characteristics as mentioned above are implemented as weakly reflective harmonic waves.
The boundary at the north is subject to discussion as follows. There are generally two options tested. On the one hand,

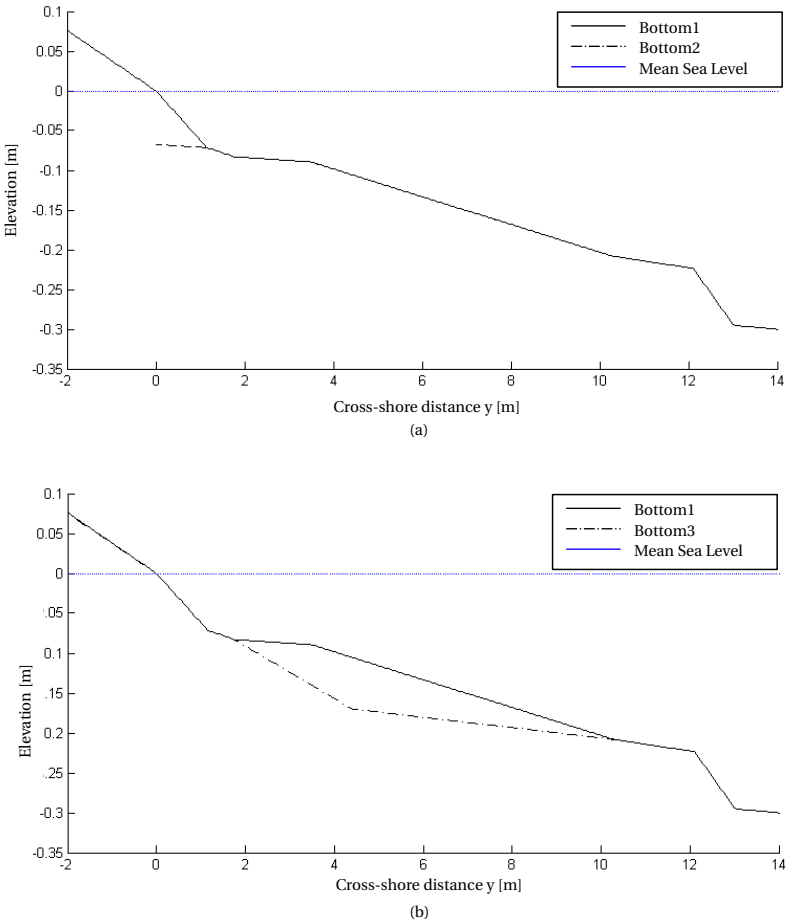

Figure 7.3: Bathymetry files used in the analysis of the flow field under wave forcing. (a) compared Bottom1 and Bottom2, (b) compares Bottom3 to Bottom1.

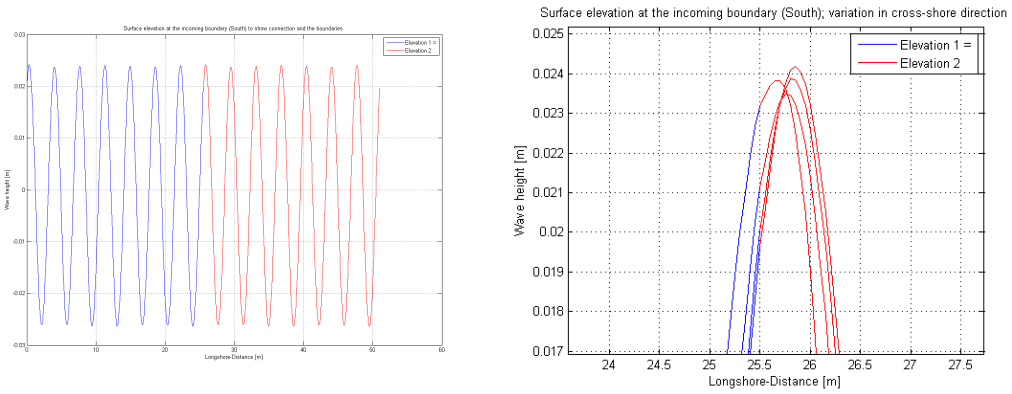

(a) Surface elevation at the waveboundary (south)

(b) Close up at the boundaries

Figure 7.4: The left figure shows the surface elevation at the southern boundary over the domain. The same elevation is plotted two times behind each other to show the difference in water level at the east and west boundary. As the water level at the two boundaries goes over to each other w.r.t the elevation itself and the first derivative, it is concluded that the periodic boundary is chosen correctly. The right figure shows a close up of the boundary for several longshore sections close to the southern boundary.

a bottom file that imitates a beach profile, thus with a dry part above mean sea level. In that case no boundary has to be prescribed (valid for *Bottom1* and *Bottom2*). On the other hand, *Bottom3* is adjusted close to the shoreline in such a way that the cells are wet in any case; the domain additionally stops at the shoreline in cross-shore direction. At this boundary,

a boundary has to be prescribed at the north when using *Bottom3* (`[WEAKR CON REG 0.00]`).
This latter alternative has firstly been chosen as the cells at the shoreline were the source of numerical instabilities when varying between being wet or dry cells and a practical solution was to be found. *Bottom3* consists of only wet cells, thus not giving instabilities. This bathymetry profile is mainly used for the sensitivity analysis (Appendix B). The reason for the instabilities appears to be found within the specification of the numerical preconditioner. The more robust conditioner ILU provides stability at the interface of wet and dry cells, whereas the first used ILUD-preconditioner appears to give the instabilities at the interface.

NUMBER OF LAYERS

With a small amount of layers over the vertical, wave characteristics and transformations might not be correctly computed. The number of the layer is related to the dimensionless depth kh. The wave number k is derived by

$$k = \frac{2\pi}{L} \tag{7.1}$$

with L the wave length, which is approximately $L = 1.83$m in intermediate waterdepth. This yields $k = 3.3781/$m. At the waveboundary, the waterdepth is $h = 0.30$m, therefore $kh = 1.01$. One or two layers should be sufficient according to the manual (The SWASH team, 2014).
The incoming waves are harmonic with a frequency of $f = 1/1.23\text{s} = 0.813$Hz. In order to be on the conservative side, the maximum frequency of a developed spectrum would be between 1.5 and 2 times the peak frequency, hence 1.6Hz. In case of 1m water depth, this can be modelled with three layers (The SWASH team, 2014). In the present case with regular waves, the shape of the spectrum is narrower than for a wave field. A small amount of layers (one to three)can be considered as sufficient.

7.4. SIMULATIONS WITHOUT GROINS

7.4.1. ANALYTICAL CONSIDERATIONS

The results from the numerical model are compared to analytical considerations and approximations for verification of the model results besides comparing to laboratory experiments.

WAVE BREAKING

According to the reference in Trampenau (2000), the waves are breaking when they reach a height at breaking of $H_B = 0.07$m. Assuming a breaker index of $\gamma = 0.78$, the water depth at breaking should be $h = 0.09$m.
When using analytical considerations, the point of wave breaking can be calculated according to the procedure in Bosboom and Stive (2013) with the following input of known data:

- $T = 1.23$s
- $H_0 = 0.05$m
- $\phi_0 = 30°$
- and a guessed water depth at wave breaking $h_b = 0.075$m.

It is calculated that

- a wave with a wave height at breaking $H = 0.055$m is breaking at a waterdepth of $h_b = 0.073$m when assuming $\gamma = 0.75$,
- a wave with a wave height at breaking $H = 0.070$m is breaking at a waterdepth of $h_b = 0.090$m when assuming $\gamma = 0.75$.

WATER LEVEL SET-UP AND SET-DOWN

For a wave height at breaking of $H_b = 0.055$m and $H_b = 0.070$m, the range of set-up and set-down is evaluated, each for a breaker index of $\gamma = 0.7$ and $\gamma = 0.8$ for spilling breaker (Section 2.3.1), see Table 7.1. This range is for waves approaching normal to the shore. For waves approaching with an angle, the setup will reduce due to the additional term $\cos(\theta)$. This reduction value is in the range of 1-2mm.

Table 7.1: Set-up and set-down for different wave heights at breaking H_b for a range of the breaker index γ between $\gamma = 0.7$ to 0.8, for normally incidenting waves.

	$H_b = 0.0055$m	$H_b = 0.0070$m
Set-down, equation 2.13	[-2.4; -2.7]	[-3.1;-3.5]
Maximal set-up, equation 2.12	[12.0; 13.8];	[15.3; 12.5]
Maximal water level difference, equation 2.14	[14.4; 16.5]	[18.4; 21.0]

LONGSHORE CURRENT CONSIDERATIONS

There are several ways to describe the longshore current (Section 2.3.1). The most important figures are the values of the longshore current in the middle of the surfzone and the theoretical maximum without lateral mixing. For the different approaches, these values have been evaluated for two different wave heights to give the range of the realistic magnitude of the longshore current (Table 7.2). In the measurements, Trampenau (2000) found a velocity of about $v = 0.23$m/s in the middle of the surf zone for a waveheight of $H_b = 0.07$m which is in accordance with the calculated results.

Table 7.2: Values for the longshore current velocity for different wave heights at breaking. The formulas 2.15, 2.16 and 2.17 have been used to evaluate the theoretical maximum velocity (Bosboom and Stive (2013), and Longuet-Higgins) and the velocity in the middle of the surf zone Komar (1998)

Velocity [m/s]	$H_b = 0.07$m	$H_b = 0.055$m
Theoretical maximum without mixing, eq. 2.15 (Bosboom and Stive, 2013)	0.8140	0.640
Maximal, eq. 2.16(Longuet-Higgins, 1970a)	0.4273	0.3787
Middle of surf zone, eq 2.17 (Komar, 1998)	0.2125	0.1884

7.4.2. BASIC SETTINGS OF THE NUMERICAL MODEL SET-UP

The basic model set-up has been evaluated with the standard SWASH settings for the viscosity, friction, advection schemes. These standard settings are:

- Friction: Manning ($m = 0.019$s/m$^{1/3}$)
- Viscosity: Smagorinsky ($c_s = 0.2$)
- Horizontal advection of momentum: BDF scheme
- Number of layers: 1
- Bathymetry file: *Bottom1* (Figure 7.3)

7.4.3. RESULTS

WATERLEVEL SETUP AND SET-DOWN

The set-up and set-down of the averaged water level in the numerical computation are qualitatively as expected. Just at wave-breaking the water is setting down and after wave-breaking setting up (Figures 7.5a and 7.5b). Trampenau (2000) measured the set-up only up to close to the shore but not at the beach itself. Therefore the measurements do not reach the theoretical maximal set-up. In the SWASH computations, the set-up is about 1cm in case of the extended beach profile. About 0.50m away from the original shoreline (i.e. where the water level is measured in the experiments), the set-up difference is about 3mm. This is the value as obtained by the measurements (red line in Figure 7.5a).
The set-up of the computation coincides well with the expectation according to the simplified models (Table 7.1) for a wave height at breaking of $H_b = 0.055$m while being lower than those results. This is in accordance with the assumption that the set-up and set-down is lower for waves approaching with an angle different than shore normal (Section 2.3.1).

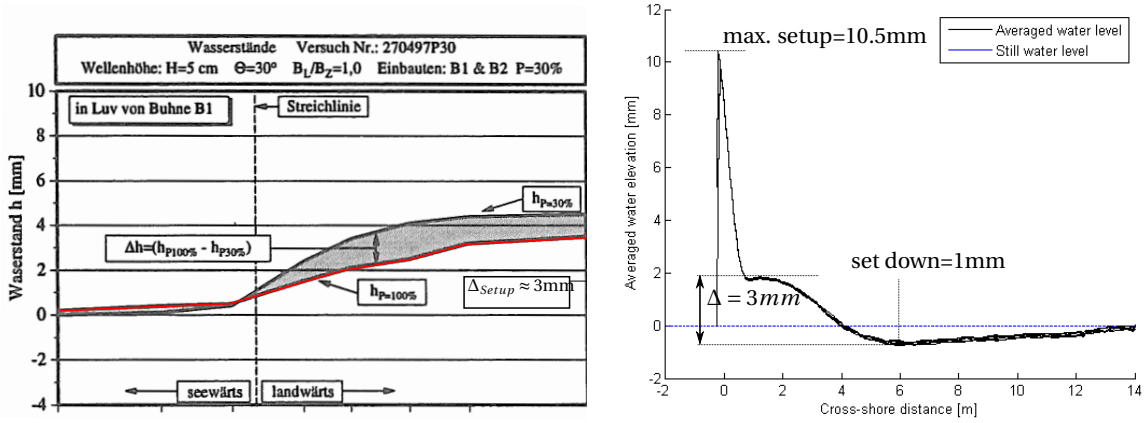

(a) Mean water level, adopted from Trampenau (2000) (b) Mean water level, numerical simulation

Figure 7.5: The mean waterlevel (set-up and set-down) in the experiments by Trampenau (2000) (a) and for the basic setting at several cross-sections in the numerical simulation (b). In (a), the red line indicates the reference case without groins (Permeability P=100%)

WAVE BREAKING AND LONGSHORE CURRENT

Differences between the measurements and the computations are found in the behaviour of the wavebreaking and the characteristics of the longshore current. In the SWASH computations, the wave breaking occurs $y = 6$m away from the shore at a waterdepth of about $h = 0.14$m. In the measurements, the waves are breaking at $y = 3.5$m away from the shoreline where the waterdepth is somewhat less than $h = 0.10$m (the exact value of the local waterdepth is not obtainable). This leads to a wider longshore current in the numerical computation as the breaking waves are initiating the longshore current (Section 2.3.1). This leads to another breaking behaviour from what Trampenau suggests and different waveheights than in the SWASH calculation. Trampenau indicates a breaker height of 7cm instead of 5.3cm which is the regular wave height. In his measurements, the waves are breaking in a waterdepth smaller than 10cm, but approximated from his depth profile not smaller than 9cm.
The longshore current is evaluated when averaging the velocities parallel to the shore over a sufficient amount of time to even out the instantaneous velocity which varies throughout the wave cycle (Figure 7.6). In the experiments by Trampenau (2000), this time is $t = 60$s; in the numerical computation, a period of $t = 120$s is used. Figure 7.7 gives an impression of the current velocity of the longshore current over the whole domain: The average is uniform over the longshore axis. The peak current velocity is lower in the numerical computation than in the measurements. This however is often a question of calibration by means of the bottom roughness. The magnitude of the longshore current in both cases is close to the value as obtained with equation 2.17. It is recommended for further laboratory experiments to include fine measurement resolution also close to the shore. Especially when considering morphology this second peak gets importance.

In the SWASH calculation, it seems that the waves are starting to break earlier as the longshore current is generated further offshore.

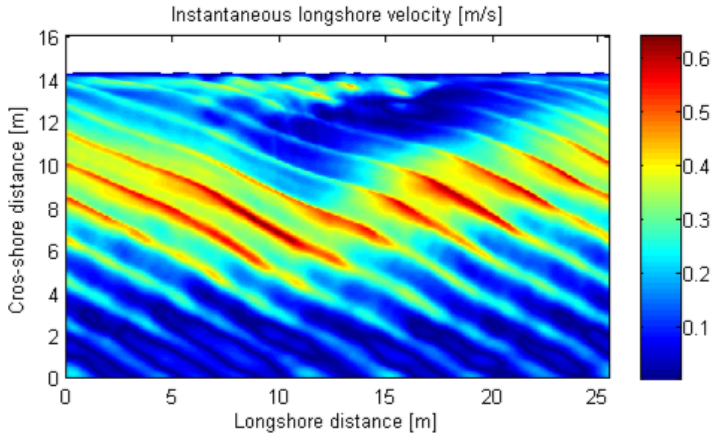

Figure 7.6: Instantaneous longshore velocity component obtained with SWASH for the testcase with the standard settings.

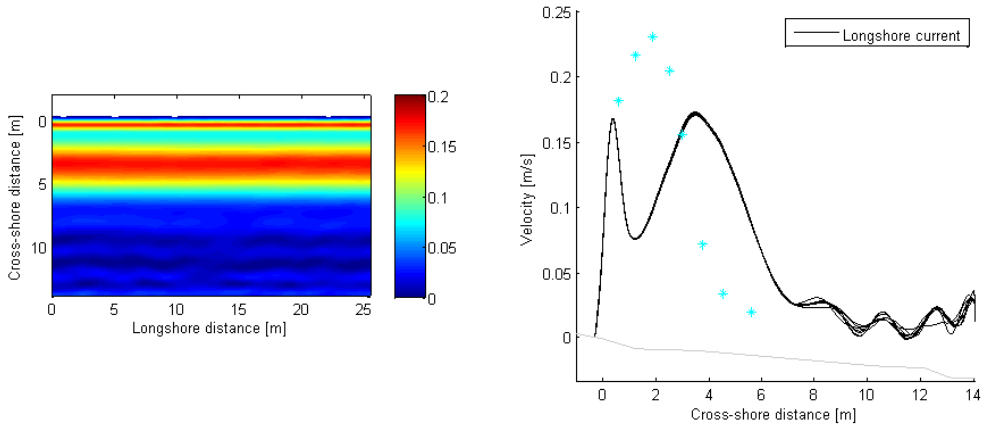

Figure 7.7: Longshore current velocity distribution averaged over $t = 120$s for the simulation with standard setting. Left figure shows the whole domain, the right figure for several cross-sections compared to the measurements.

7.4.4. DISCUSSION ON THE DIFFERENCES BETWEEN MEASUREMENTS AND SIMULATIONS

The basic settings in the numerical simulation do not lead to a wavebreaking and longshore current that coincides with the measurements by Trampenau (2000) (see Section 7.4.3 above). The waves break further offshore in the simulations, leading to a wider longshore current profile. The maximal velocity is lower in the numerical simulation.

POSSIBLE ORIGINS OF THE DIFFERENCES

Both the computations and the measurements can be the origin of the differences. In the numerical model, the parameters can be chosen with wrong values or that processes are not included in the model. For example, the magnitude of the longshore current is often adjusted by varying the bottom roughness. Another origin could be found in the measurements or their interpretation. On the one hand, there could have been a systematic error not seen. E.g., the basin could have had contained less water and therefore initiate wave breaking further onshore. On the other hand, the results were only available in paper format which leads to another insecurity in interpreting and comparing this data[1]. The digitizing can explain why a difference in the magnitude can be observed, yet, it cannot explain the different location, waterdepth and waveheight at wave breaking.
Another reason for the difference in magnitude could be the way of determining the mean velocity over the vertical. The exact location for the measurement device is not noted. According to the sketch, the measurement device is at one-third of the waterdepth above the bottom which, according to Reniers (1999), coincides very well with the velocity averaged over the vertical. It is assumed in this thesis that the measurements where taken at this height and can be compared to the mean velocity from the numerical results. If it was measured differently, it could explain differences in the magnitude, but not the width of the longshore current.

REFERENCE DATA FOR FURTHER RESEARCH

For the absolute values and the relative velocity for a groin with $P = 50\%$, only vector images are given in Trampenau (2000). For a comparison with the numerical data, this data has to be digitized which leads to possible errors: The print can give inaccuracies and the interpretation from scanning as well, e.g. how the vectors are to be interpreted.
To evaluate the accuracy in digitizing the measurement data, a comparison has been made to identify the effect of how to interpret the vector. In principle, the starting point of the vector should be the middle. However, the range of possible velocities has been measured by assuming a different starting point of the vector. For graphical clarification, see Figure 7.8b. The green line is a digitization of the principle sketch in Figure 5.1. The result can be seen in Figure 7.8a: It shows that the current should be more towards the offshore according to the principle sketch. The velocity magnitude of the sketch is closest to the "maximum" vector length case. However, it is not completely clear, how accurate that specific sketch (Figure 5.1) is supposed to be. For further analysis, the sketch and the medium pile length is set as first estimate but the range is taken into account as range of possible output. For Figures with only one given reference, it is referred to the sketch in Figure 5.1.

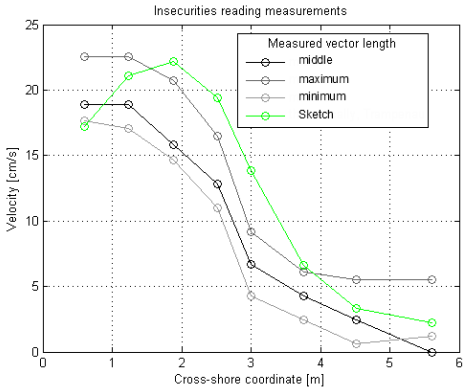

(a) Velocity profiles

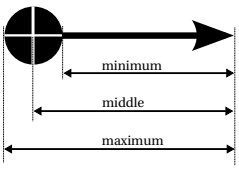

(b) Definition velocity vector

Figure 7.8: Insecurity of obtaining digitized version of measurement data. (a) shows the dependency of the interpretation of the arrows as in Figure 5.2 and the profile out of the more theoretical profile given by Trampenau (2000), see Figure 5.1. (b) shows the definitions of the velocity vector

[1] Digital data was not available any more

7.4.5. SENSITIVITY ANALYSIS

To evaluate the range of numerical results, a sensitivity analysis on environmental parameters such as the wave characteristics and the bathymetry, and on numerical parameters such as the bottom roughness approach and value, and viscosity is made. Detailed results are presented in Appendix B; a list of simulations can be found in Table B.1.

Though certain features of the longshore current are varying depending on the numerical parameter, it is not possible to change the place of the maximum longshore current or the place of wavebreaking significantly. This is desirable on the one hand, as it shows that the numerical model is consistent in itself. On the other hand, it leaves the question open why the waves are breaking further offshore.
The physical parameters have more importance on the wavebreaking and magnitude of the longshore current than the numerical parameters. Varying the wave height changes the location of breaking but influences the magnitude of the longshore current as well (Appendix B). When keeping the incoming wave height at $H = 0.05$m, the wave breaking can be influenced only by means of a change in the bottom file. An adjusted bathymetry profile *Bottom3* is used. It forces the waves to break at the same location as in the measurements by deepening the profile up to the point of desired wavebreaking (Figure 7.3).

Summarized, the most important finding of the sensitivity analysis are that:

- Most important parameters:
  The environmental parameters wave height and the ratio waveheight/bottomdepth are the most important parameters to adjust the wavebreaking and distribution of the longshore current.
  A change in the waveheight does not yield comparable results. Changing the bathymetry, the same results on wavebreaking can be obtained as in Trampenau (2000), therefore this bottom file is used for the up-following simulations including groins (Compare Figures B.9 and B.10).
- Numerical schemes:
  The BDF scheme becomes unstable for certain numbers of layers and for a too smooth bottom. The MINMOD scheme is more stable and is used for the groin computations, compare Figure B.3 and B.3.
- Bottom friction:
  The magnitude of the longshore current varies significantly when changing the friction approach (Manning or Chézy). The approach by Manning takes into account the local waterdepth (assuming a constant value for the friction is chosen as input) and is therefore more suitable for a coastal simulation, compare Figures B.4 and B.1.
- Turbulence/Viscosity:
  When schematizing viscosity, the chosen value for the coefficient in the Smagorsinky approach do not effect the longshore current. Using the mixing length approach influences the distribution of the longshore current but no proper value was found in this study. Smagorinsky gives reasonable results without the need for a study on proper values and is used further on, compare Figures B.5 and B.7.
- An important command is `[BREAKING]` that initiates breaking for a small amount of layers (less than six, according to The SWASH team (2014)). The usage is indispensable, yet the exact value does not play a role,
- When using multiple vertical layers, the k-epsilon model can be used to simulate the vertical viscosity. It showed to not have a major impact whether it is used or not,
- Using ILU for the iteration process can make unstable calculations stable. It though is slower than ILUD
- One layer is sufficient

7.4.6. FINAL SETTINGS AND COMPARISON TO MEASUREMENTS AND ANALYTICAL CONSIDERATIONS

MODEL SET-UP

Based on the conclusions of the calibration and sensitivity analysis presented above and in Appendix B, the final settings, that reproduce the longshore current profile and other characteristics the closest to theory and measurements, for the simulations under wave forcing are:

- Friction: Manning ($m = 0.019\text{s/m}^{1/3}$)
- Viscosity: Smagorinsky ($c_s = 0.2$)
- Horizontal advection of momentum: MINMOD scheme
- Number of layers: 1
- Bathymetry file: *Bottom3* (Figure 7.3)

The simulation with the barred beach profile (Section 7.2) shows that the breaking can be influenced and forced at a certain location with a longshore current close to measurements. Waves in SWASH are breaking at a waterdepth of about $h = 0.14$m. The bottom profile has been adjusted in such a way that wave breaking takes place at the same location as in the experiment by Trampenau (2000), see *Bottom3* in Figure 7.3. By varying the friction coefficient by Manning, the

current profile can be computed closely to the measurements (as seen in the profile Figure 7.10). This method is chosen as it remains unclear why the wave breaking behaviour differs from the measurements. For the further research on the effect of the groins, it is important to have obtained an undisturbed flow field a close as possible to the measurements for a better comparison of those simulations to the measurement results.
In order to be able to compare the effects to measurements, the adjusted bottom file has been chosen to provide a similar reference velocity profile in the measurements and in the numerical model.

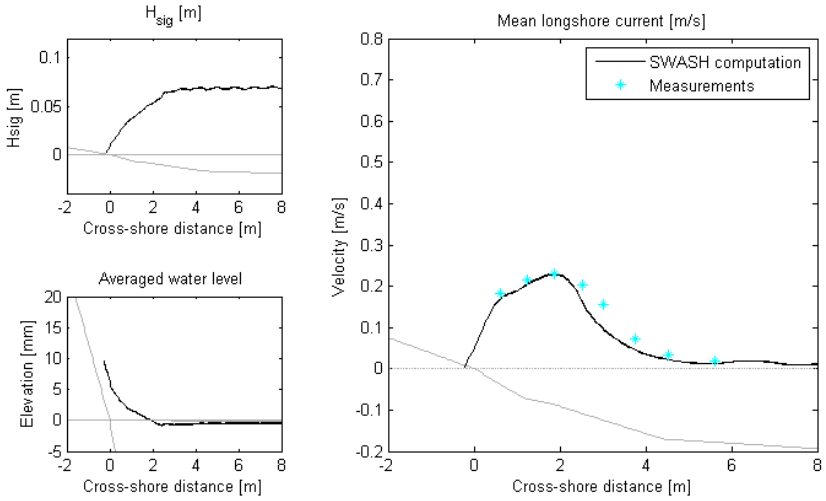

Figure 7.9: Significant wave height,averaged water level and longshore current velocity for the reference case compared to the measurements. This simulation shows good consistency between the measurements and the results from SWASH. A bottom roughness of Manning $m = 0.019\text{s/m}^{1/3}$, one layer and the MINMOD scheme has been used. Measurements refers to the profile obtained from Figure 5.1.

RESULTS

The water level difference between the minimal water level and at $y = 1.24$m (Measurement point Y1) is 2mm in the computations. In the measurements, this difference is 3mm. The maximal set-up in SWASH is 11mm, the analytical calculation gives 14-17mm. Figure 7.11 shows the averaged water level in the numerical computation compared to the measurements by Trampenau (2000) at three measurement points. As the measurement results do not show a set-down, the comparison has also been evaluated for the numerical computation raised for the lowest point to be at MSL. The two outer points show good agreement with the numerical computations. The mean water level differs for the computations and the experiments at $y = 3$m. The difference at this point can be explained by the change in the bottom file at this location.
It is concluded that the numerical results show good agreement with the measurements and analytical calculations.
The wavebreaking starts somewhat closer onshore than the measurements, between $y = 3.20$m and $y = 3.50$m. A closer study on the longshore current could be executed to adjust the wavebreaking even more. For the further study on the effect of the groins, it is assumed to be sufficient close.

It is concluded that with this setting, the results obtained in the experiment by Trampenau (2000) can be reduced accurately and are used for further simulations including the groins.

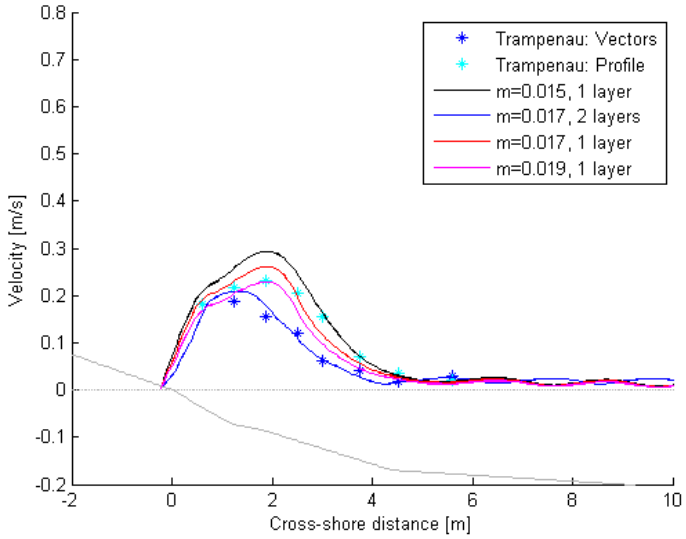

Figure 7.10: Longshore current velocity for different settings compared to the measurements. The number of layers and the friction parameter by Manning is varied, m is given in $s/m^{1/3}$. The most consistency shows the run with 1 layer and a friction of $m = 0.019 s/m^{1/3}$. The reference profile refers to Figure 5.1

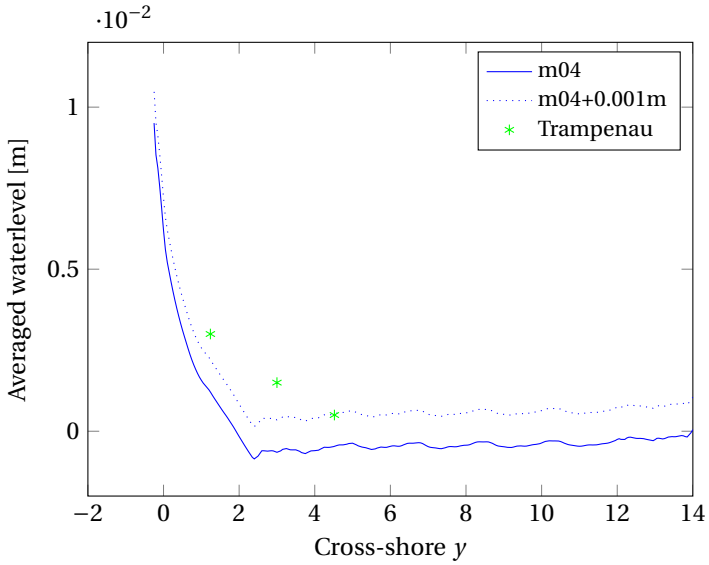

Figure 7.11: Averaged water level for simulation m4 along the cross-shore. The water level in the measurements of Trampenau (2000) is not setting down at point of breaking, the dashed line is raised by 1mm to have its minimum at 0mm

7.5. COMPUTATIONS INCLUDING GROINS

With a setting that results in a comparable longshore current as in the measurements by Trampenau (2000), the effect of groins on the longshore current and current paths can be evaluated. Firstly, a comparison of the different possibilities of implementing one groin is evaluated for a permeability of $P = 50\%$ and which one is closest to the measurements (this Section 7.5). Secondly, the effect of varying wave and groin parameters is evaluated (Section 7.6).

7.5.1. AVAILABLE REFERENCE DATA TRAMPENAU

The reference data for the relative velocity is available for the eight measurement points over the cross-section for a groin with a permeability of $P = 50\%$ for two lengths of the groin with respect to the place of wavebreaking (Table 7.3). In Trampenau (2000), it is mentioned that the measurement point next to the groin was showing the highest relative velocities. As a consequence the most offshore points were not taken into account for evaluating the relative velocity (blank fields in Table 7.3).

Table 7.3: Relative velocity reference data for a groin with a permeability of $P = 50\%$ for different lengths w.r.t the breakerline. Blanc fields indicate that this data is not available. Adapted from Trampenau (2000)

Measurement point	Y_0	Y_1	Y_2	Y_3	Y_4	Y_5	Y_6	Y_7
Distance to shoreline [m]	0.6	1.24	1.88	2.52	3	3.76	4.52	5.6
Relative velocity for a groin length until the breakerline	0.75±0.04	0.75±0.04	0.75±0.04	0.75±0.04	0.75±0.04	2.1	n.n.	n.n.
See or landwards of groin head	l	l	l	l	l	s	s	s
Relative velocity for a groin length until 0.833x the breakerline	0.75±0.04	0.75±0.04	0.75±0.04	0.75±0.04	2.0	1.6		
See or landwards of groin head	l	l	l	l	s	s	s	s

7.5.2. NUMERICAL SETTINGS AND SIMULATIONS

The numerical settings as described in Section 7.4.6 are used. Additionally, the following is implemented:
To avoid boundary effects, the domain needs to be prolonged for the simulations including groins as the influence of the groins reaches the boundaries. In longshore direction, twice the original length is used ($l_x = 51\text{m} \times l_y = 16\text{m}$).
For the bathymetry used (*Bottom3*), the wavebreaking now seems to occur a little closer onshore so that the width of the longshore current is somewhat narrower than in the measurements. To achieve a better comparability of the relative velocities in disturbed flow (between simulations and measurements), the groins are also shortened towards the breaker point and compared to simulations with the original length.
The groins can be implemented in different ways: As cylinders resolved on the grid, as averaged cylinders (subgrid feature) or as exception values. The overview on the different runs is listed in Table 7.4. The distinction of these terms is used as described in Section 6.2.3
The groin piles themselves in the input file are defined as piles with a diameter of $D = 1\text{cm}$ and a drag coefficient of $C_D = 1.5$ and emerged piles.

Table 7.4: Overview of simulations to test implementation of groin. The width in y-direction contains 2m of beach.

Name	Domain ($x \times y$ [m × m])	$\Delta x \times \Delta y$ [m × m]	Length of groin [m]	Groin
wg01	25.5x16	0.05 × 0.05	3.5	vegetation, resolved
wg02	51 × 16	0.05 × 0.05	3.5	vegetation, resolved
wg03	51 × 16	0.05 × 0.05	3.5	vegetation, averaged [10,000 stems/m^2]
wg04	51 × 16	0.05 × 0.05	3.5	exception values
wg05	51 × 16	0.05 × 0.05	2.7	vegetation, resolved
wg06	51 × 16	0.05 × 0.05	2.7	vegetation, averaged [5,000 stems/m^2]
wg07	51 × 16	0.05 × 0.05	2.7	vegetation, averaged [2,500 stems/m^2]
wg08	51 × 16	0.05 × 0.025	2.5	vegetation, resolved
wg09	51 × 16	0.05 × 0.05	3	vegetation, resolved
wg10	51 × 16	0.05 × 0.025	3	vegetation, resolved

7.5.3. OUTPUT ANALYSIS FOR DIFFERENT WAYS OF IMPLEMENTING THE GROIN

FLOW FIELD

The general flow field can be described as follows. Windward of the groin, the undisturbed longshore current profile develops. The flow is partially deflected offshore at the groin and partially flows through the groin. Leeward of the groin, the original current profile starts to redevelop. The undisturbed velocity profile is nearly recovered at the downstream boundary. The flow field as obtained for simulation wg05 is given in Figure 7.12. To avoid boundary effects, the domain is extended in longshore direction.

Using an averaged value for the amount of piles in the groin over the cross-shore leads to a significantly different flow pattern. The deflection is higher and some eddy-like structures are visible close to the shore and at the cross-shore height of the groin head. This flow field is obtained for different amounts of piles per m^2. The simulation wg06 should lead to a theoretical permeability of $P = 50\%$ with 5000 stems per m^2, while wg03 doubles the amount of piles and wg07 halves the amount, see Figures C.5, C.6 and C.2.

Using exception values leads to a similar flow field seawards of the groin as for the resolved version. Closer to the shore wind- and leewards of the groin, some accelerations and decelerations are observed similar to the less permeable groin which suggests that using exception values is leading to a less permeable groin, though the groin should be at least 50% open as it blocks half of the cells, see Figure C.3.

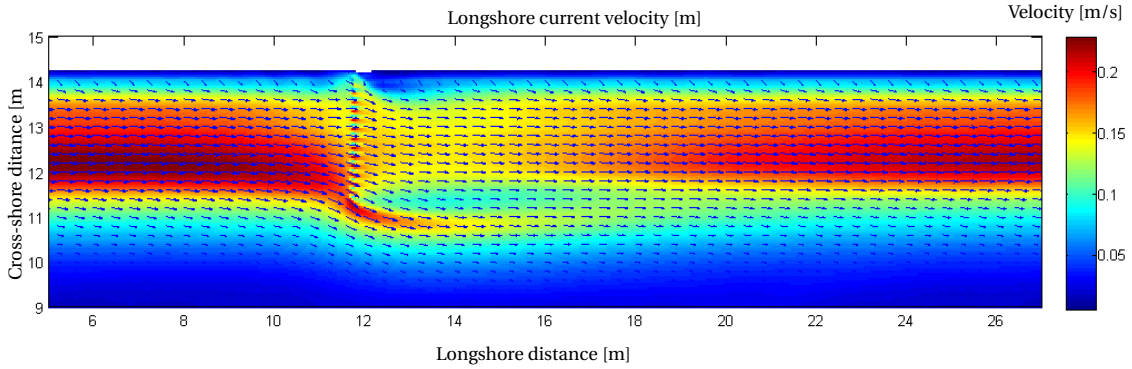

Figure 7.12: Flow field for wg05, including velocity vectors

LONGSHORE VELOCITIES

The absolute and relative velocities for the principle possibilities are presented in Figures 7.13 to 7.17 and compared to the measurements by Trampenau (2000) (Table 7.3). The velocities are evaluated 0.5m behind the groin as it should deliver the most comparable results to the measurements. It suggests that the schematisation as cylinders on the grid is the most promising one (wg05 and wg09). As a difference between those two runs, the length of the groin can be identified. The run wg05 with the shorter groin ($L_g = 2.70$m) corresponds to the values of the measurements for a groin/ breaker line ratio of $L_g/L_s = 0.833$, run wg09 corresponds to a groin reaching until the breaker line. Only the velocities up until a distance of about 5m away from the original shoreline are considered. Further offshore, there are slight deviations from a zero-averaged velocity which lead to high relative velocities which are not of further interest for evaluating the functioning of the groin.

From the simulations, wg05 and wg09 show certain advantages over other settings: A groin with 3.5m length in the numerical simulation reaches too far beyond the breaker line. Due to the adjustments in the bottom, the breaking occurs somewhat further onshore than in the experiments. As no comparison for a groin of $L_g/L_s > 1$ has been analysed in the experiments by Trampenau (2000), it is chosen to shorten the groin to compare the results of the same relative length to the breaker line (Figure 7.14).

Using exception values leads to similar results as the measurements and to the resolved piles (Figure 7.13) at the cross-section 0.50m behind the groin. In the flow pattern (Figures C.3), the groin attracts also a flow from the lee-side of the groin. This different behaviour suggests that either the permeability corresponds to a lower effective permeability or that the resolution is not fine enough to allow for the use of exception values (Figures 7.13 and C.3).

Using an averaged value of piles over the whole width of the groin needs more adjustments on the amount of piles. Both wg06 and wg07 lead to higher relative velocities next to the groin. The permeability is theoretically $P = 50\%$ for wg06 and the amount of piles of wg06 is halfed for wg07. Though for wg07 the relative velocity is close to the measurements, the pattern within the groin field differs (Figures 7.16, C.5 and C.6). At the shoreline, a high negative velocity is found and the relative velocity at $x = 2$ to 3m is lower than found in the measurements (Figure 7.17).

Comparing a grid with a resolution of $\Delta y = 0.05$m and $\Delta y = 0.025$m in the cross-shore direction y and a groin of $L_g = 3$m, differences are present. But especially when comparing the absolute velocities, they are close to each other in qualitative behaviour and in quantitative values (Figures 7.15, C.8 and C.9).

Run wg05 is used for further evaluating the dependency of the flow field on boundary conditions and groin characteristics.

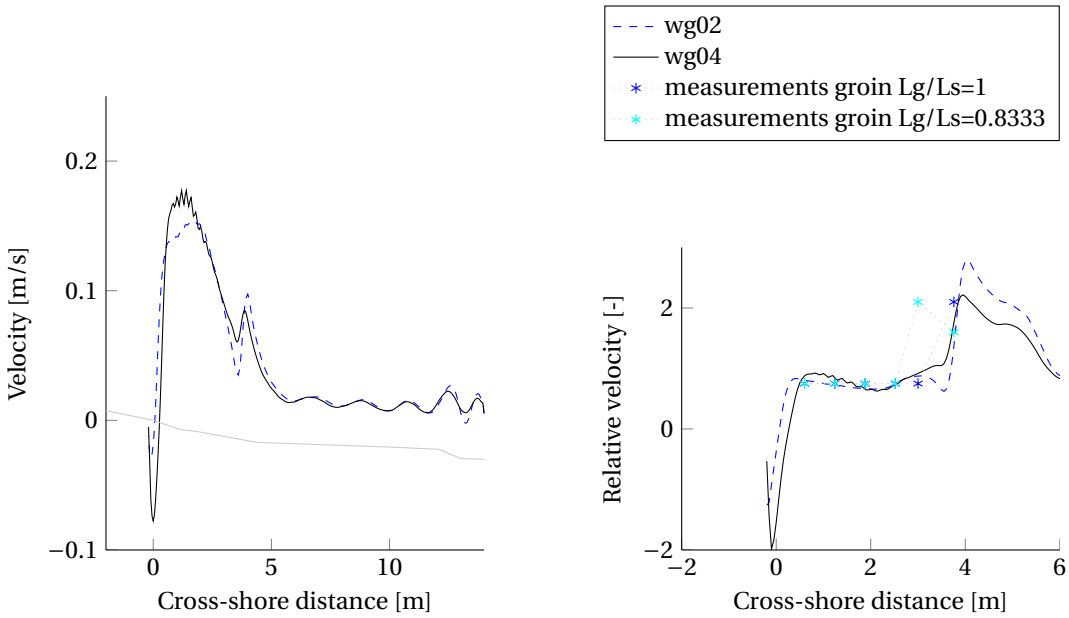

Figure 7.13: Longshore current velocity 0.5m behind the groin for absolute velocities (left) and compared to the undisturbed velocity (right). The simulations compare the usage of resolved piles on the grid (wg02) or the usage of exception values (wg04).

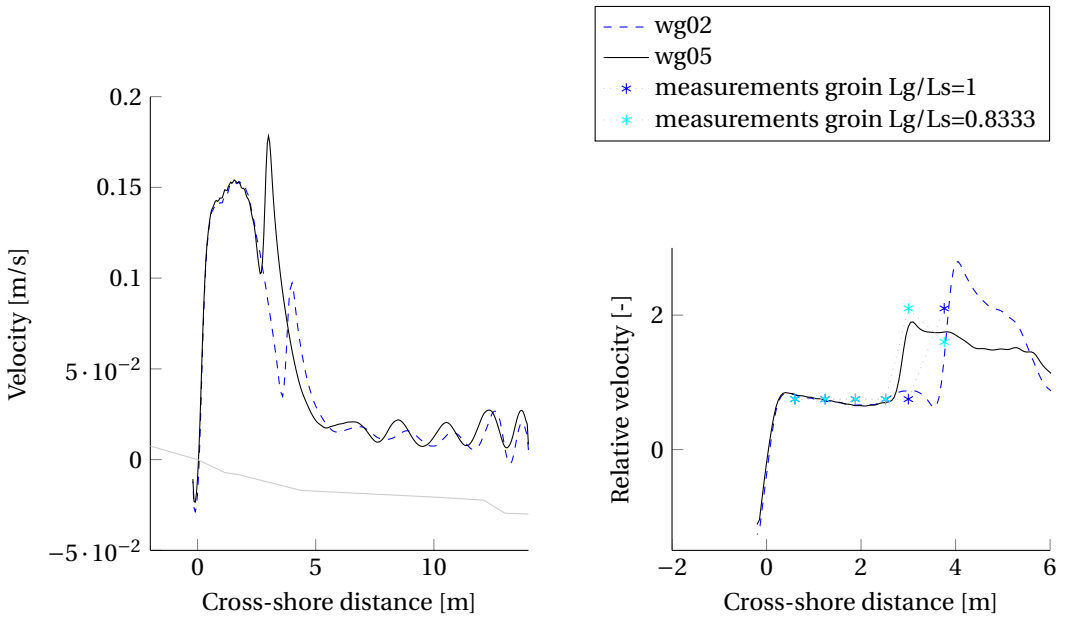

Figure 7.14: Longshore current velocity 0.5m behind the groin for absolute velocities (left) and compared to the undisturbed velocity (right). The simulations compare the effect of the length of the groin. For wg02: l_g = 3.50m, for wg04: l_g = 2.7m.

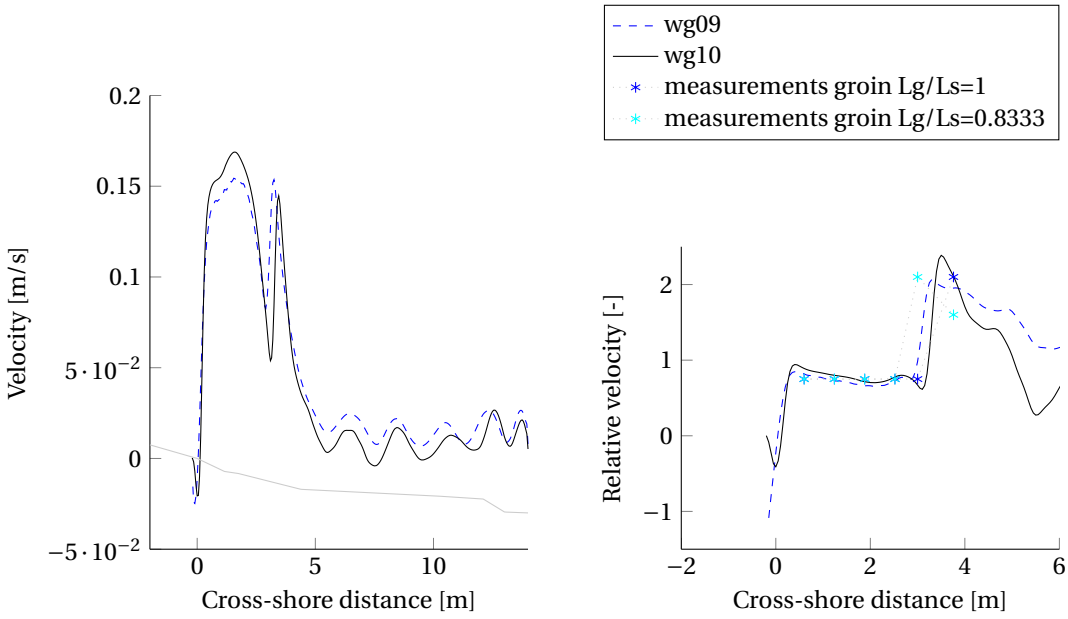

Figure 7.15: Longshore current velocity 0.5m behind the groin for absolute velocities (left) and compared to the undisturbed velocity (right). The simulations compare the resolution in the cross-shore direction. wg09 offers $\Delta y = 0.05$m and wg10 $\Delta y = 0.025$m.

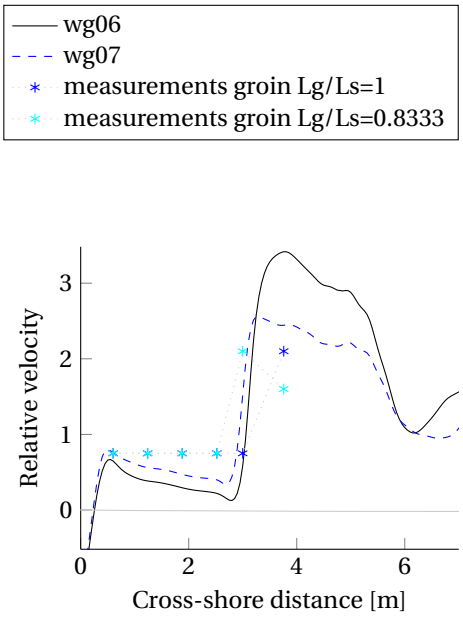

Figure 7.16: Longshore current velocity 0.5m behind the groin for absolute velocities (left) and compared to the undisturbed velocity (right) for testcases wg06 and wg07, comparing the dependency on the amount of piles implemented.

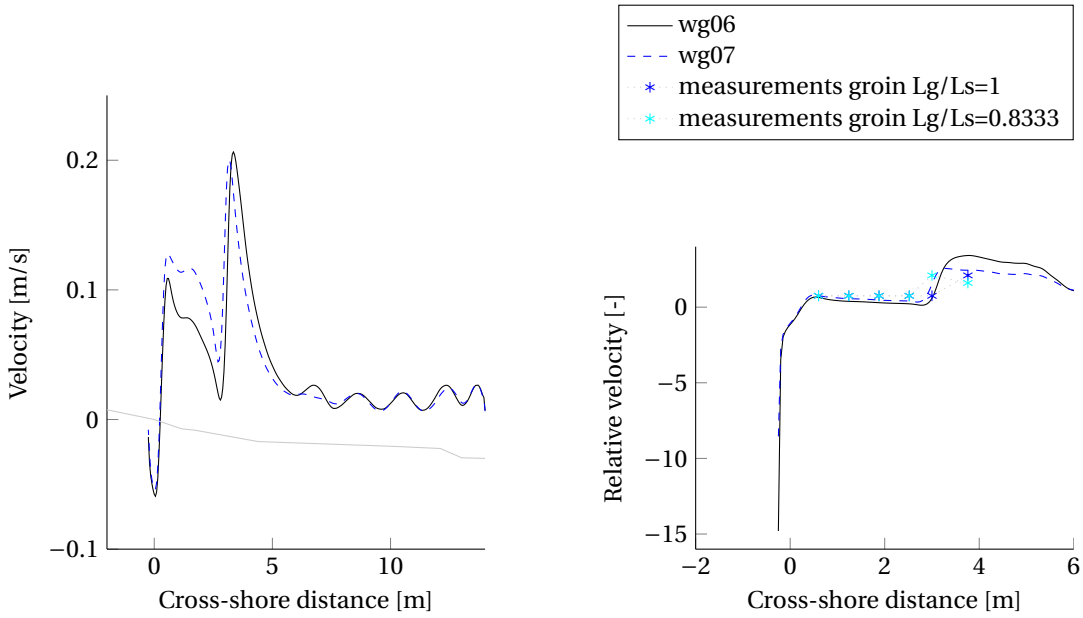

Figure 7.17: Longshore current velocity 0.5m behind the groin for absolute velocities (left) and the relative velocities compared to the undisturbed velocity (right). The testcases wg06 and wg07 compare the number of piles per m^2 in the average mode implementation.

7.5.4. FURTHER OUTPUT FOR TESTCASE WG05

WATER LEVEL DIFFERENCE

The water level difference in front of and behind the groin is evaluated for the testcase wg05 (Figure 7.18). The line indicates the value according to Trampenau which is close to the measurements. The difference in the water level is about the same value behind the groin over the whole length according to Trampenau (2000). From further available diagrams, the difference along the groin has a deviation of as well up to 0.5mm in the measurements.

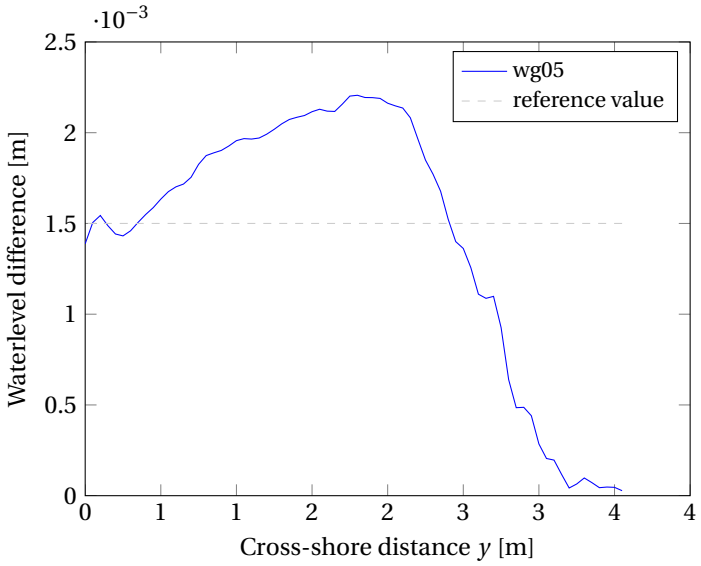

Figure 7.18: Water level difference in front and behind the groin over the cross-shore. The reference line indicates the averaged value for the water level difference according to Trampenau (2000).

LONGSHORE WIDTH OF INFLUENCE

The longshore distance of influence is important to determine how far windward and leeward of the groin the velocity is reduced and when it reaches the undisturbed velocity again. Depending on the desired reduced velocity, the distance between the groins can be chosen. Figure 7.19 shows how quickly the velocity is recovered compared to the original

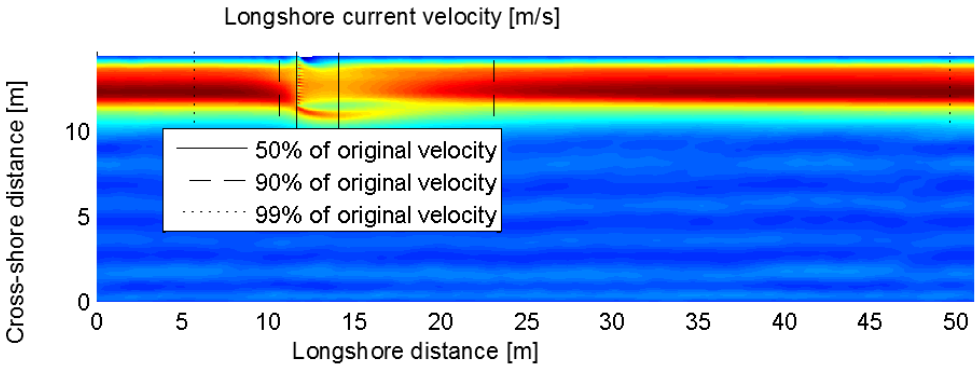

Figure 7.19: Locations in the profile where the maximal velocity wind- and leewards of the groin reaches a certain percentage (50, 90 and 99%) of the peak undisturbed velocity. For a groin with a length of $L_g = 2.70$m.

velocity. 90% of the velocity is regained about three groin lengths leeward while it needs up to 40m to obtain the original velocity.

CROSS-SHORE WIDTH OF INFLUENCE

For the influence in the cross-shore direction, two characteristics are of interest: The length how much the peak velocity shifts L_{peaks} and how far away from the shore an influence is given L_{infl}. For the latter, the place where the velocity crosses a value of $v = 0.025\text{m s}^{-1}$ is chosen and compared to the measurement data of Trampenau (2000). The exact way to determine this width is not given, so this threshold velocity is chosen as this is the maximal averaged velocity for the deeper part of the domain. For a groin with a permeability of $P = 30\%$, the range of influence is given with $L_{infl} \leq 0.2 \cdot L_g$ by Trampenau (2000) (L_g the length of the groin). In the numerical model, the width is $L_{infl} = 0.4$m, which is about $L_{infl} = 0.15 \cdot L_g$ (Figure 7.20).

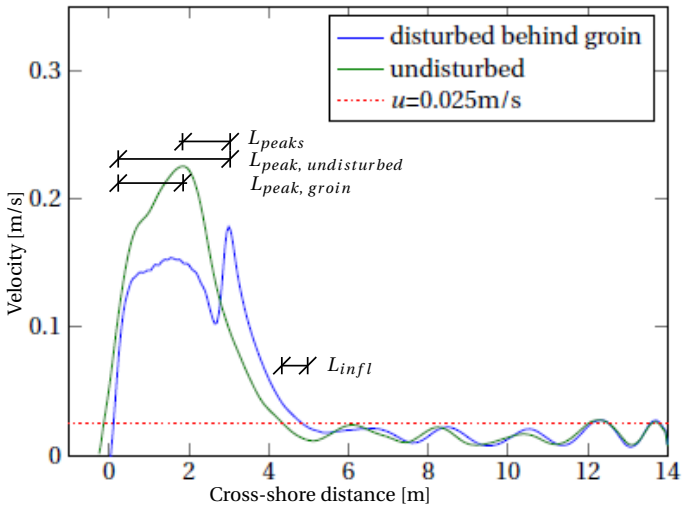

Figure 7.20: Disturbed and undisturbed velocity for the reference case wg05. The horizontal red line indicates a velocity of $u = 0.025\text{m s}^{-1}$. The difference between the current profiles for that velocity is identified as width of influence in cross-shore direction.

7.5.5. SUMMARY

Both using exception values and a resolution of the piles on the grid gives promising results. When using the pile variation, the output is smoother than the one obtained with exception values. An averaged value over the whole groin blocks too much of the discharge and does not lead to any visible flow deflection. Varying the amount of piles per cells (e.g. reducing the amount to reach a lower permeability) does not give better results. Even a permeability much lower than the theoretical 50% gives to high velocities next to the groin.
Using clusters of piles in cells next to empty cells, good consistency between the numerical results and the measurements were found. When reducing the grid size in cross-shore direction to half of the size, only minor changes are visible. This indicates that this approach is possible even though the grid size is higher than the pile size.

7.6. EFFECT OF VARYING PHYSICAL PARAMETERS

7.6.1. VARYING LENGTH OF THE GROIN

For waves approaching with an angle of $\theta = 30°$ to the cross-shore axis, the influence of the groin length is analysed on the the disturbed flow field. This comparison is based on the testcases wg02, wg05 and wg09 for a groin length of $L_g = 3.50$m, $L_g = 2.70$m and $L_g = 3.50$m respectively. The wave angle is kept constant at $\theta = 30°$. Therefore, the length of the groin varies with respect to the point of breaking and longshore current.

LONGSHORE VELOCITY PROFILE

The absolute and relative velocity profiles landwards of the groin in leeward direction are about equal for all three groin lengths. The shorter the groin, the larger the absolute velocities are seawards of the groin. For a groin reaching just out of the breaker zone, the relative peak velocity (i.e. compared to the undisturbed flow velocity) outside the groin field is higher than for the other groin lengths. However, the absolute velocity for this case is half of the other two cases (Figure 7.21).

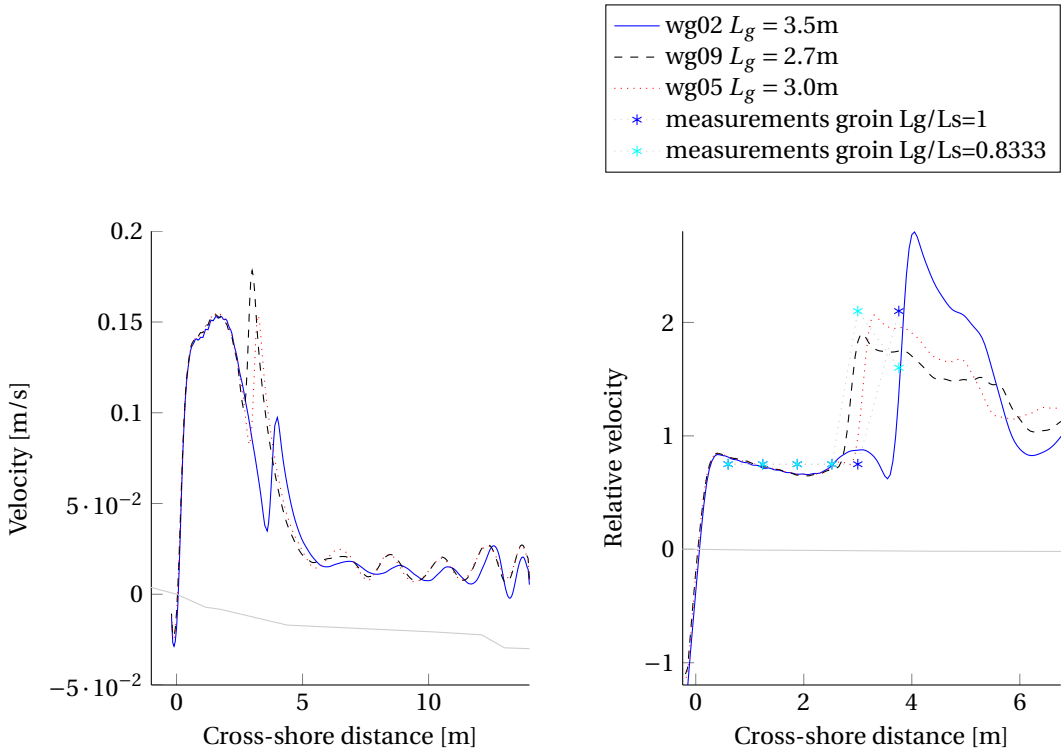

Figure 7.21: Longshore current velocity 0.5m behind the groin for absolute velocities (left) and compared to the undisturbed velocity (right) for testcases wg02, wg05 and wg09: influence of the groin length L_g.

CROSS-SHORE VELOCITY

The value of the maximal cross-shore velocity windward of the groin is not depending on the length of the groin. In all three cases under consideration, the maximal value is about $v = 0.10$m/s. It appears that the velocity for the groin with a length of $L_g = 3$m which is supposed to be the place of wave breaking produces slightly the highest cross-shore velocity. For the longer groin, the maximal velocity is lower, but persists over a longer distance and the peak is not only shifted further offshore (Figure 7.22).

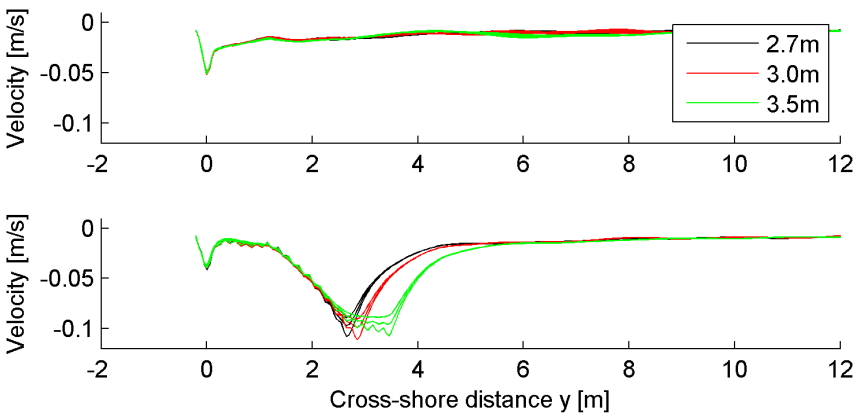

Figure 7.22: The cross-shore velocity in dependency of the groin length l_g. The upper Figure shows the undisturbed cross-shore velocity, the lower Figure the cross-shore velocity just windward of the groin. A negative velocity is offshore directed.

AREA OF INFLUENCE

The area of influence increases when the length of the groin increases. For the shortest groin with a length of $L_g = 2.70$m, the influenced area is the smallest. At a distance of 10m behind the groin, at most of the profile the original velocity is reached by 90% or more (Figure 7.19). For a groin of $L_g = 3.00$m length, the area of influence increases somewhat. At a distance of 10m behind the groin, at half of the cross-shore profile, 90% or more of the original velocity is reached. At a distance of 20m behind the groin, at the whole profile, 90% or more of the original velocity is reached. For a groin reaching further than the breaker zone, the area of influence increases significantly.
The exact length is wider than in the measurements which suggests more mixing forces in the laboratory experiment than in the numerical model.

SHEAR STRESS

The bottom shear stress is obtained in the numerical results. The given results are instantaneous shear stress values as they are depending on the orbital velocity of the wave which is time-dependent. For the evaluation, the shear stress is given at several cross-sections in a 1m band behind the groin and a 1m band in undisturbed flow.
The shear stress reduces for about 10% in the reference testcase with a groin length of $l_g = 2.70$m (Figure 7.23). For a different groin length, the maximal shear stress reduction remains at about 10%, so that the stirring up of material would not be effected by the choice of the length of the groin.

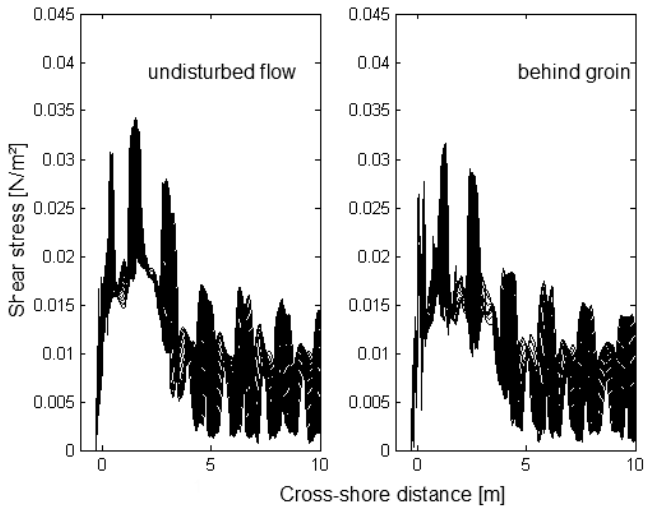

Figure 7.23: Shear stress for a groin length of $l_g = 2.70$m: The left figure shows the instantaneous shear stresses in a 1m band for several cross-sections, the right figure shows the reduced shear stresses behind the groin in a 1m band.

7.6.2. VARYING THE WAVE ANGLE

To evaluate the influence of the wave parameter wave height H, additional simulations with different angles are run (Table 7.5). The wave angle in this chapter is with respect to the cross-shore axis y.

Table 7.5: Testseries WG2: Simulations to observe the effect of the wave angle on the flow field and water level distribution. Other numerical settings are as given in Section 7.4.6.

Name	Wave angle w.r.t cross-shore
wg11	0°
wg12	15°
wg05	30°
wg13	45°
wg14	60°
wg15	75°

UNDISTURBED FLOW

For the wave height H_{RMS} and H_{SIG}, the wave height along the cross-shore is evaluated (Figures 7.24a and 7.24b). Depending on the angle, the wave heights vary. Yet, their point of breaking is roughly at the same location in cross-shore direction, especially for an angle between $\theta = 15°$ and $\theta = 45°$. The ratio between groin length and breaker zone is thus close to each other and reasonable comparable, implying that the results are mainly depending on the wave angle and less on the ratio groin length to width of breaker zone.

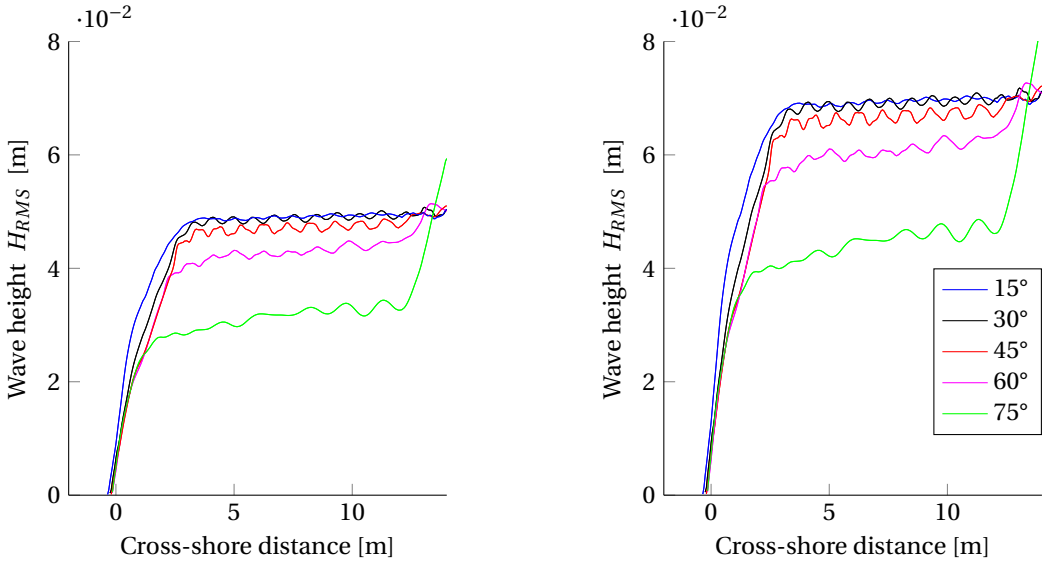

(a) H_{RMS} (b) H_{SIG}

Figure 7.24: Waveheight H_{RMS} and H_{SIG} in [m] along the cross-shore for different angles of the approaching waves.

The wave angle influences the cross-shore velocity component. For an angle of $\theta = 15°$ or less, the cross-shore velocity component becomes more significant in the surf zone and the longshore component vanishes.

SMALL WAVE ANGLES AND GROINS

For the wave angle of $\theta = 15°$, the influence of the groin on the flow field is small. For normal waves, the groin does not have any influence any more. This is as expected as groins act on the longshore direction. But for almost shore normally incident waves, no longshore current is induced.

CROSS-SHORE VELOCITY

The cross-shore velocity windward of the groin is compared to the undisturbed cross-shore current velocity (Figure 7.25). In the undisturbed flow, a major cross-shore component is found landwards of the original shoreline balancing the wave induced set-up of mean water level. The resulting velocities are nearly the same for all wave angles not normally approaching; for a wave angle of $\theta = 30 - 60°$, they increase slightly. For normally incident waves, the highest undisturbed cross-shore velocity is found, which additionally varies along the longshore unlike for waves approaching with an angle.

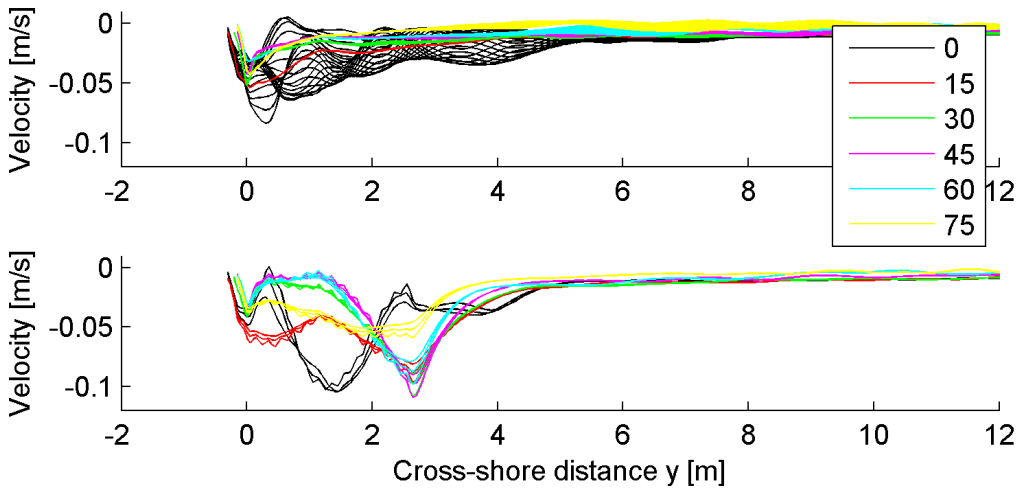

Figure 7.25: The cross-shore velocity in dependency of the wave angle θ [°] with respect to the cross-shore axis. The upper Figure shows the undisturbed cross-shore velocity, the lower Figure the cross-shore velocity just windward of the groin. A negative velocity is offshore directed.

The cross-shore velocity component in the disturbed flow field in front of the groin reaches the maximum at the same point in cross-shore direction with nearly the same value for wave angles between $\theta = 15 - 60°$. For shore-normal waves, the same value is reached, but closer onshore. The maximal value reaches the one of the disturbed flow, so it is assumed that it is a coincident that it reaches the maximal velocity of the other wave angles. For a wave angle of $\theta = 75°$, the distribution of the cross-shore velocity differs: The maximal velocity is lower compared to other wave angles, yet, its magnitude is higher closer to the shore (between 0.5 and 2m). This decreased velocity compared to the other wave angles is explainable by the lower wave height (and thus less wave energy) reached for $\theta = 75°$.
Except for the wave angles close to shore-normal, the presence of the groin is the origin of large cross-shore velocities. The highest velocity is reached just at the groin head. The magnitude and location are further not depending on the wave angle of the approaching waves. This is positive as it makes a permeable groin applicable for a wider range of main wave direction with the same consequences.

WATER LEVEL DIFFERENCES

The water level difference in front of and behind the groin is varying depending on the angle of the incident waves. This angle determines the intensity of the longshore current and discharge which is leading to the highest difference in the water levels for an angle of $\theta = 45°$ (Figure 7.26).

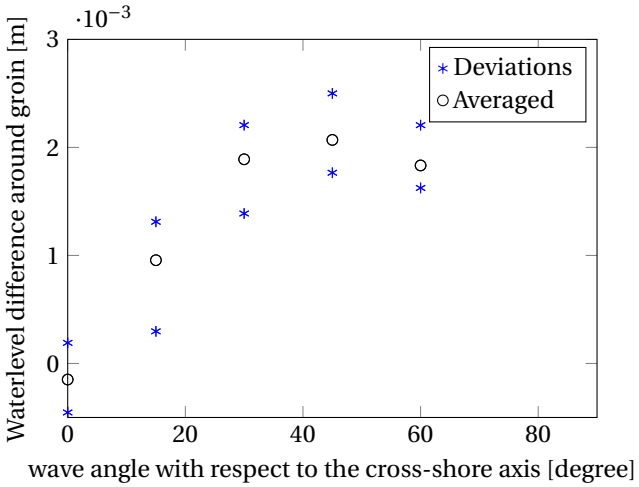

Figure 7.26: Water level difference in front and behind the groin for different wave directions. The wave direction with respect to the longshore axis. The groin has a length of $L_g = 2.70$m.

LOCATION OF MAXIMA, DEFLECTION OF THE FLOW

The location of the peak velocities of the longshore current is analysed and presented in Figure 7.27. As to be expected, the undisturbed longshore current reaches the widest profile for a wave angle of 45°, together with the peak the furthest away from the shoreline $L_{peak,undisturbed}$. In the disturbed flow, the peak seaward of the groin is due to the presence of the groin and the deflection that the groin is causing as it is an obstacle to the flow. The locations of the peak-velocity seawards of the groin $L_{peak,groin}$ for the different wave angles are in a closer range to each other than the locations of the peak-velocity in the undisturbed flow: 0.35m instead of 1.85m.
The distance between the peak of the disturbed flow compared to the peak of the undisturbed flow L_{peaks} is the smallest in case of the waves with an angle of 45°. This might be contra-intuitive as more water mass is deflected and a wider current would be expected. A mechanism behind this phenomenon is suggested to be the approaching waves. For an angle of 45°, the radiation stress is strongest and acting as a force on the flow limiting it into seaward direction.

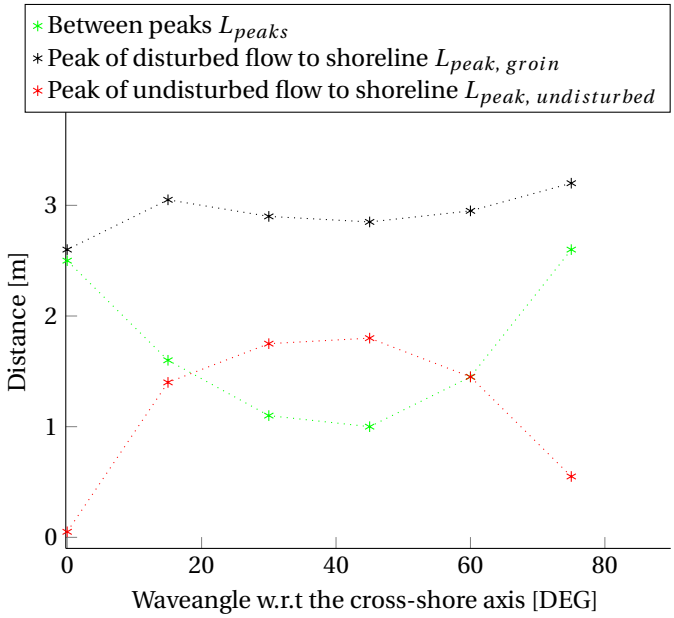

Figure 7.27: Comparison of the distances between the peak velocities of the undisturbed and disturbed flow. The peak of the disturbed flow is mainly depending on the length of the groin itself. The groin has a length of $L_g = 2.70$m. For the definitions of the lengths see Figure 7.20.

AREA OF INFLUENCE

The area of influence is varying with the angle of the approaching waves. First, the shadow area depends on the approaching waves due to diffraction. Second, the wave angle determines the location of wavebreaking, the longshore current profile and the maximal velocity, and the wave energy. For a wave angle of $\theta = 45°$, the current velocity and energy is reaching its maximum value. Therefore the area of influence behind the groin is least for this wave angle.

SHEAR STRESS

The bottom shear stress is obtained in the numerical results. The given results are instantaneous shear stress values as they are depending on the orbital velocity of the wave which is time-dependent. For the evaluation, the shear stress is given at several cross-sections in a 1m band behind the groin and a 1m band in undisturbed flow.
The reduction of the shear stress is depending on the angle of the approaching waves. Table 7.6 shows the reduced maximal shear stresses according to Figures in Appendix C.3. The most reduction is obtained for a wave angle of $\theta = 45°$ with 20%. For the other direction, the reduction is between 10-15%, except for the normally approaching waves, for which the shear stress is not reduced. If not taking the normal waves into account, the range of the absolute value of the shear stresses reduces to half of the range in the undisturbed flow.

Table 7.6: Shear stress in dependency of the wave angle. The first two columns give the maximal value found within a 1m band, the third compares the reduced shear stress.

Wave angle	max. value in undisturbed flow [N/m^2]	max. value leeward of groin [N/m^2]	Relative shear stress
0°	0.034	0.034	100%
15°	0.032	0.029	90.6%
30°	0.034	0.0315	92.6%
45°	0.040	0.032	80.0%
60°	0.038	0.033	86.8%
75°	0.035	0.032	91.4%
difference	0.008	0.004	

8

CONCLUSIONS AND RECOMMENDATIONS

To assess the application of permeable pile groins as part of the coastal protection system, they have been analysed under different forcing conditions based on a literature study, analytical considerations, a numerical model and comparison to available measurements. The waves have been analysed for a current-only and for a wave-only forcing. For the wave forcing, the effect of varying groin or wave characteristics are analysed.
This chapter provides insight on the research questions (Section 8.1) and recommendations on the usage of groins and their evaluation (Section 8.2). Suggestions for further research are given in Section 8.3.

8.1. CONCLUSIONS

8.1.1. RESEARCH OBJECTIVE

The objective of the research was defined to improve the understanding and predictability of permeable pile groins as coastal protection. With the research, it has been concluded that the usage of groins can be advised. The reproducibility and predictability of hydrodynamics around groins is shown for numerical and analytical models. Yet, more research is advised before the usage in engineering practise can be applied for specific questions based on a better reasoning. This step especially includes the effects of sediment transport and morphology.

8.1.2. RESEARCH QUESTIONS

What are the important hydrodynamic theories and concepts that have to be taken into account when analysing a groin system?
In the literature study (Chapter 2), important concepts on coastal processes with and without groins are evaluated. To evaluate the forcing on the groins, the longshore current induced by waves and the open channel flow formula for the current only forcing are the most important concepts. The wave induced longshore current derives mathematically from the concept of the radiation stress with curve fitting by calibration with experiments and field observations. It was shown that the Morison equation is an important concept to calculate the forces on a pile and evaluate the dissipation of energy. Important further aspects are the viscosity and horizontal mixing and the effect of bottom friction.
The most important concepts and theories applied are:
How do coastal groins effect currents and water levels from a global and local viewpoint?
The effects how groins influence the flow field are illustrated throughout the thesis: In the literature review, the principal effects on hydrodynamics and sedimentation and coastal development are illustrated and compared to numerical and experimental results in Chapters 6 and 7. For the forcing by waves, variations in the wave conditions and the groin length are evaluated on the significance on the effect.
The most important concept is that permeable pile groins act as an additional hydraulic resistance. In the part of stream containing the groin, the flow velocities will be reduced. Due to the partial blockage, the flow field will vary from the undisturbed flow field. A slight rip-current develops in front of the groin. The different flow resistance in the two streams leads to an increased discharge and flow velocity next to the groin. Compared to impermeable groins, the developed rip-current and flow velocity outside the groin field is lower in intensity. Inside the groin fields no eddies develop if the permeability is high enough. In front of the groin, the water will pile up favouring an offshore directed flow. Behind the groin, a depression in the water level can be found. The extend of this depends on the permeability of the groins.
The piles itself are an obstacle to the flow and reduce the area through which the discharge can flow. This will locally increase the velocity between the piles.

The effects of the permeable pile groins on the flow field are:

- Change on the flow field, causing cross-shore current components
- Reduction of flow velocity
- Increase of flow velocity next to groin
- Eddy formation for impermeable groins
- Piling up of water in front of the groin and depression of water level behind the groin

Under the influence of a wave forcing, the effect of the length of the groin L_g and the approach angle of the waves has been evaluated by means of the numerical model (Table 8.1). It can be observed that the influence of the approaching wave is higher than the effect of the groin length. For the evaluation of the boundary conditions, similar aspects are of interest as for the pure evaluation of the model. Those aspects of interest are:

- Area (Length and Width) of influence
- Longshore current reduction behind the groin
- Increase in the longshore current velocity beside the groin
- Cross-shore velocity
- Deflection of the flow
- Shear stress

EFFECT OF THE GROIN LENGTH L_g

The groin length is varied around the width of the surf zone. In this range, the area of influence remains close to each other. Also the velocity behind the groin reduces to approximately the same value. The maximal velocity is larger than the one in undisturbed flow for groins not reaching up until the breaker line. For a groin larger than the surf zone, the absolute velocity is smaller than the maximal undisturbed velocity (Table 8.1).

EFFECT OF THE WAVE ANGLE θ

For waves approaching with angles close to shore-normal ($\theta < 15°$), the groin does not yield a change in the flow field as the main component of those waves is cross-shore directed. For angles in the range of $\theta = 30 - 60°$, the groin is effective in reducing the longshore current velocity and the shear stresses without causing high rip-current velocities. For waves approaching with $\theta = 45°$, the effect is the highest. An exception is the width of the shadow zone leeward of the groin. The value of the reduced shear stress is close to each other for the various wave angles and in a closer range than those for the undisturbed flow. This is favourable as the shear stress is the responsible mechanism for making sediment available for transportation. Those findings suggest that permeable groins may be designed for a flow field with one or more main wave angles with one configuration (Table 8.1).

Table 8.1: Evaluation of varying physical parameters of the groin on the flow field in the wave simulations

Process	Remark
Varying groin length L_g	
Length of influence	The groin length is varied around the width of the surf zone. In this range, the length of influence remains close to each other
Width of influence	Depending on the length of the groin, the larger the groin length, the larger the width of influence.
Relative velocity behind groin	The longshore velocity reduces to approximately the same value
Absolute velocity seawards of groin	The maximal velocity is larger than the one in undisturbed flow for groins not reaching up until the breaker line. For a larger groin, the absolute velocity is smaller than the maximal undisturbed velocity
Relative velocity seawards of groin	For the larger groin, the relative velocity is the largest as the deflection is the most and the reference velocity is very small
Cross-shore velocity	Value only minor influenced by the groin length, reduces slightly for a longer groin, but persists over a longer distance
Shear stresses	No high dependency on the groin length
Varying wave angle θ	
Width of influence	Smallest for the waves approaching with $\theta = 45°$ as there is the most cross-shore force in the radiation stress to suppress the flow offshore
Deflection of the flow	Least deflection for $\theta = 45°$
Water level difference	Highest difference in front and behind the groin for $\theta = 45°$
Shear stresses	Reduces to approximately the same value for all wave angles

Can hydrodynamic processes around groin (fields) in coastal areas be reproduced?

By means of an analytical model:

An analytical model is developed which is able to reproduce the global effects on the water level and flow velocities by considering the Morison equation.

The analytical approach as presented in Chapter 3 for the forcing by a constant current is developed on the basis of the open channel flow concepts and an additional forcing by the piles approximated by the concepts of Morison et al. (1950). For the effect on the water level, the piles of the groin are approached as an additional flow resistance over the domain. The effect on the velocities is based on the idea that two one-dimensional streams are present; one including a groin, one not. For the evaluation of the water level it is assumed that exchange of the two streams will take place further away from the present obstacle. The discharge is assumed to distribute according to the flow resistance given in the two streams.

The analytical approach proofed to be a reasonable first estimate on the change on water level and velocity under a current forcing. As a one dimensional formula, it is a fast approach. Yet, the results cannot provide information on two dimensional flow characteristic in the horizontal domain. If there is a need to develop the analytical formula further, the effect of assuming a flat bottom and variable width of the two streams could be incorporated and analysed first.

By means of a numerical model:

The aim of the numerical study is to create a model set-up that leads to model results as close to reality (i.e. physical laboratory experiments) as possible for the specific settings of the experiment. A numerical model is intended to be a tool for research on additional cases with a higher variety as in laboratory experiments. A detailed study with more variations in the forcing and layout parameters is supposed to give additional insight into the effect of permeable pile groins at a coast. In this thesis, the effects of the groin length L_g and the wave angle θ have been analysed after the study on the available simulations by Trampenau (2000).

In the numerical model SWASH, the hydrodynamic processes in undisturbed flow can be reproduced and validated by comparison to measurements, to the analytical model and to further analytical considerations. The processes for the disturbed flow in the basic setting have been compared to measurements and show satisfying consistency. The increase in velocity between the piles of the groin can be simulated with the numerical model depending on the approach how the groin is schematized. To asset the possibilities of implementing the groins into the numerical model, it has been evaluated which flow characteristics in undisturbed and disturbed flow are well computed in the SWASH model and which less well. Overall, satisfying results were obtained. Some characteristics of the flow field are however closer to the measurements than other characteristics. An overview is given in Table 8.2 on the current forcing and in Table 8.3 on the wave forcing.

The processes of interest are:

- For undisturbed flow:
  - Water level distribution
  - Flow field
  - Discharge and velocity distribution
  - Wave induced water level set-up and set-down
  - Wave-induced longshore current
- For disturbed flow:
  - Water level distribution,
  - Flow field
  - Velocity reduction behind the groin
  - Velocity increase besides groins
  - Cross-shore velocity around the groin
  - Area of influence in cross- and longshore direction

GENERAL

For both the current and the wave simulations, reference cases for undisturbed flow have been compared to analytical considerations and available measurements. By this, it could be validated that the numerical model SWASH is able to satisfyingly calculate the flow field on the intended small scale.

It has further been shown that groins can be included into the SWASH model by means of exception values and by means of stiff cylinders ("Vegetation module") based on the Morison equation with a preference on the vegetation module. It has been concluded that an implementation as rubble mound breakwaters does not lead to suitable results.

CURRENT FORCING

For the current forcing, the reduction in velocity could be simulated by the vegetation module well compared to analytical considerations and available measurements.

The horizontal exchange of momentum seems to be weaker in the SWASH computations than in the measurements as the velocities in leeside of the groin recover earlier in the measurements. In the wave case with the additional force in horizontal direction, the current velocity recovers earlier and thus more realistically. Variations in the turbulence models

only showed minor influence on the amount of horizontal mixing. The choice of the turbulence model effects especially the temporal variations and has less effect on the mean flow velocity. However, for a higher viscosity, the mean flow velocity reduces compared to a lower value. Under current forcing, the flow field remains qualitatively the same and all turbulence models give close results to each other. When using several layers, preference is given to include the K-epsilon model. For a detailed study on the turbulent movement, more detailed laboratory measurements are advised.

WAVE FORCING

The wave forcing on a similar scale to the experiments by Trampenau (2000) in the SWASH model has been validated for a comparison of model results to the data source of Reniers (1999). For this latter source, the longshore current was satisfyingly computed.
Comparing the numerical model to the data source of Trampenau (2000) for undisturbed flow, a different behaviour in breaking and the longshore current profile is observed. The sensitivity analysis showed that the environmental parameters have a higher influence on the distribution than the numerical parameters. Out of the parameters under consideration, the ratio waveheight over local water depth is the one with the most influence on the wavebreaking and thus on the velocity profile development of the undisturbed longshore current. It has been identified as the only possibility to adjust the longshore current profile to meet the measurement data to further evaluate the effect of the groins on the flow field. Further possible explanations for the differences have been identified in the insecurity in the interpretation of the measurement data.
The friction model has a major influence on the value of the longshore current velocity in the wave simulations with a sloping bottom. Good results were obtained when using the Smagorinsky turbulence model. Varying the turbulence approach and parameters showed no major effect on the flow characteristics. The Prandtl-mixing length approach led to significantly different results less realistically than using the Smagorinsky model.
The groin implementation is evaluated on different aspects of the flow field (Table 8.2 and 8.3) to advise the optimized solution available. The optimized solution has been identified as resolving the piles on the grid and mimic permeability. Using an averaged value of piles per m^2 or exception values are less well suitable. The first initiates a too large deflection of the current for the theoretical permeability of $P = 50\%$; the applicability of the usage of the latter depends on the scale of consideration. In the present simulations, the grid could not satisfyingly be refined.

Table 8.2: Overview on how well SWASH is able to reproduce processes in the current testcases.

Process	Remark
Undisturbed flow	
Velocity field in undisturbed flow	Exactly as analytical calculations
Water levels in undisturbed flow	Exactly as analytical calculations
Implementing groins as vegetation	
Relative velocity behind groin	The decrease in velocity behind the groin is close to the analytical considerations and to measurements by Trampenau (2000)
Relative velocity seawards groin field	The relative velocity outside the groin field is close to the value in the measurements.
Width of influence	The cross-shore width of influence is in the range of the measurements by Trampenau (2000);

Table 8.3: Overview on how well SWASH is able to reproduce processes in the waves testcases

Process	Remark
Undisturbed flow	
Longshore current profile	Depends on wavebreaking; well reproduced in Reniers and Battjes (1997); for Trampenau (2000) adjustments in the bottom profile required
Longshore current, maximal velocity	Mainly depending on the value of the bottom roughness coefficient
Set-up/Set-down mean water level	Close to measurements and analytical expectations
Wavebreaking	Depending on the ratio waveheight over water depth
Implementing groins as vegetation	
Flow field	The general flow field is as expected
Relative velocity leewards of groin	For resolved vegetation, results are close to measurements For averaged vegetation, velocity is too low

Table 8.3: Overview on how well SWASH is able to reproduce processes in the waves testcases

Process	Remark
Length of influence behind groin	Closer to the measurements than current case due to additional cross-shore forcing
Width of influence	The width of influence is in accordance with the interpretation of the experiments in Trampenau (2000)
Implementing groins by exception values	
Flow field	For exception values, the results are close to the measurements, but with more wiggles. For the wave case, exception values are giving better results than under current forcing

What are advantages and possible shortcomings in numerical models?
Numerical models are always an estimation of reality and physics. The application boundaries resulting from shortcomings and restrictions in the numerical model are to be evaluated. On the other hand, numerical models offer opportunities as they can be time-saving comparing to physical experiment. They can deliver more detailed results compared to laboratory experiments and compared to simplified analytical models.
No explicit model to include piles exists, yet. The evaluation of piles is based on the dissipation based on the Morison equation or on the flow blockage by exception values. Especially the dissipation method leads to flow fields close to available comparison data. In SWASH, the resolution in space is restricted due to numerical expenses. This disfavours the usage of exception values on a small scale.
The usage of SWASH is evaluated compared to possibilities in other type of numerical models. In this thesis, preference is given to the SWASH model due to the possibility to include wave transformation in shallow water and flow phenomena. Compared to computational fluid dynamic models, it is assumed to be more efficient due to their required fine resolution and the possibility to extend the model set-up to nature scale is desirable for a future study. Compared to large circulation models, the possibility of a more detailed resolution inside the SWASH model is preferred including the different possibilities to include the pile groins.
A development advise for the SWASH model or an external tool is the inclusion of a sediment transport model to eventually evaluate the changes in morphology.

What kind of research and development is further needed to evaluate permeable groins?
On basis of the results, recommendations on potential further research are given. To increase the understanding of permeable pile groins further, more research is advised. This research should be a combination of laboratory experiments, analytical and theoretical considerations and numerical research, see Sections 8.2 and 8.3.

8.2. RECOMMENDATIONS

This thesis supports the opinion that permeable pile groins have a potential as part of the coastal protection. This thesis showed under different aspects, that the usage of permeable groins can be favourable over impermeable groins as a coastal protection system as the negative effects of impermeable groins such as rip-currents and large scale eddies are reduced while positive effects such as the reduced flow velocity inside the groin fields are kept. Further, the increased velocity offshore the groin is lower in case of permeable groins as the flow deflection is less. This is expected to be positive for the beach development, i.e. an accretion parallel to the original shoreline instead of a zig-zag coastline.
Further research on permeable groins is recommended with the aim to predict the suitability of permeable groins in specific situations and their design. The numerical research showed that satisfying results can be reached with present models and the analytical approach. For the usage within SWASH, the modelling of energy dissipation via the Morison equation (as vegetation) is recommended (or until a more suitable module is available). The present module in SWASH is suitable for the effect of the piles on the general flow field. It is not yet suitable for details of the flow close to the piles. This is related to the way piles are implemented into the dissipation model and not explicitly on the grid. For the evaluation of the effects on the mean flow field, this is less of importance, but might play a role once real groins are being build and detailed information on the erosion close to the piles is required to determine the embedment depth.

This study is based on laboratory scale. The effect on sediment transport and beach development is not directly evaluable: By means of Froude scaling, data on the flow field on laboratory data can be extrapolated to nature scales reasonably well. Due to changes in the physical behaviour of sediment depending on the diameter, a research of sediment transport on laboratory scale has to be evaluated with care and up-scaling of the results is less straight-forward. For a study on sediment transport, a numerical model on a larger scale is recommended.

8.3. FURTHER RESEARCH

In order to enhance the understanding of these groins and enhance the development of tools for the assessment of pile groins in nature, the following research aspects are recommended:
(1) For a further development of the analytical approach as presented in Chapter 3, it is advised to first focus on the effect of a variable depth in the cross-shore direction as at a natural beach and a variable width of the two streams to enhance the presence of the physical boundary conditions. In a second step, also additional terms yielding to energy loss or influence on the flow field may be considered such as turbulent terms.

For this presented research, mainly measurements on the mean flow characteristics were given. Unfortunately, those data is not digitally available. For a future research, more dedicated data should be made available by means of a laboratory experiment. This data can be used for the following aspects:
(2) Digital available data will improve the validation of numerical models as one error source (digitalization) can be excluded.
(3) Data with a higher resolution in space and time can be used to validate the model on the turbulent fluctuations. Turbulent movements are interesting as they will finally leads to energy loss, but also turbulence is important for the initiation of sediment movement. A higher resolution in space is advices close onshore where a second breaker line can be present. This second breaker line causes a second peak velocity which is of interest especially when considering effects on the sediment transport.
(4) For the research on the effect of piles on sediment transport processes and beach development, laboratory experiments are generally difficult due to scaling effects. In order to produce data, a laboratory experiment on a larger scale could be conducted or a field measurement.

Laboratory experiments are to be combined to a numerical research. To enhance the knowledge on the validation and reliability of numerical models, the following aspects are recommended:
(5) The further development of the Morison model (Vegetation model) inside the model SWASH. It showed to reproduce effects of piles well. Yet, a more dedicated model for this specific arrangement of piles could include an improved handling of the permeability of the pile groin. This model can also give better insight in the effect around the piles such as the increased velocity between the piles.
(6) Inside the model SWASH, the profile development is not yet available. For a study of the effect on morphology, an additional module is to be developed. This could be placed inside the model SWASH or as an external application. The numerical research should be combined with laboratory experiments as described in (4).
(7) In Civil Engineering practise, various models are being used. A study can evaluate the comparability of numerical results from different models to show which models are the most advanced concerning the implementation of pile groins.
(8) The numerical model can be used to evaluate the effect of changing further characteristics of the groins or of the forcing. The present research deals with regular waves with the same characteristics each. A more natural wave field is to be analysed. This will be of importance once the models are developed enough to include trustworthy sediment transport and beach development inside the model.

It is strongly advised to combine the numerical and laboratory research in a future study.

A

OVERVIEW ON AVAILABLE RESEARCH AND GUIDELINES

Most of the available research and guidelines on groins can be obtained in Dutch, British and German literature. This list gives an overview on what is already known about (permeable) groins and what are available guidelines with mentioning the most important concepts of these publications.

A.1. BAKKER ET AL. 1984

Bakker et al. (1984) summarized the Dutch experience with permeable groins since the 1960's in a positive way. On a global scale they summarized the advantages and disadvantages of permeable groins and differences compared to impermeable groins. They conclude that they should be considered a good alternative and subject to further research. They conducted some research on existing groin fields and laboratory experiments, but cannot derive universal guidelines. They found that there are significant differences whether permeable groins are built in a current only situation or a current-wave situation, i.e. the difference between a groin in a river and a groin at the coast.
They conclude:

- Advantages of permeable pile screens are:
  - Low cost
  - Reduced longshore current velocity (demonstrated by model tests)
  - Flexible construction, easily adjustable to beach changes
  - A more continuous beach line (as compared to the saw-tooth beach line with impermeable groins) as the safety of the coastal protection is related to the point of most erosion.
  - A more gradual velocity gradient and less turbulence near the seaward end as compared to impermeable groins
- Difficulties when using permeable groins:
  - Failure on the seaward side: washing-out of piles
  - Failure on the landward side: outflanking near the dune foot.
  - Mussels growing on the wooden piles can decrease the permeability of the groin and eventually turning it into an impermeable groin
  - Attraction of rip-channels, with consequent seaward sand loss
- Possible solutions to the difficulties are
  - Careful analysis w.r.t morphological changes in the coastal area
  - Embedding piles enough into the ground: they should be embedded for 60% of the total length below the lowest beach level to be expected.
  - Pile groins should be sufficiently extended landward of the existing dune foot to avoid outflanking
  - Regular removal of mussels.

A.2. FLEMING (1990)

This report can be advised as a guideline in designing groins and used for theoretical background information and experiences with groins.
The (British) CIRIA report 119 "Guide on the uses of groins in coastal engineering" (Fleming, 1990a) gives a clear overview

on coastal processes involved when designing a groin (field). In the report, the main hydrodynamic processes with and without groins are described, the influence of the beach type and beach material and the groin material are collected. The report lists the effects of a groin system and design guidelines, supported by existing groin systems and research. The focus in this report lies on the impermeable groins. Permeable groins are mentioned to have advantages but also Fleming (1990a) concludes that permeable groins are not intensively researched on.

A.3. EAK 1993

The German experience and general construction advices have been summarized in EAK (1993) with updated examples in EAK (2007).
Some general/ additional advise compared to Fleming (1990a) are:

- The length should be covering the main part of the width where longshore transport is taking place. A stable reef can be used as end point if applicable.
- The distance between the groins is a function of the length, i.e. the longer the groin, the longer may be the distance between the groins. For the German North Sea, they conclude a preliminary distance as a function of the expected orientation of the coastline and angle of wave incident.
- Possible lay-outs are described
- For groins only subject to waves in the Baltic Sea, general advise on the distance between groins as a function of the length, the permeability and the bottom slope is given
- In EAK (2007) also an overview on usable woods can be found

A.4. TRAMPENAU (2000)

Trampenau (2000) has focussed on evaluating the influence of different parameters in a groin (field) lay-out by means of laboratory experiments and field measurements. As a starting point, a representative beach profile has been evaluated and reduced to laboratory scale. On this profile, the effect of a current only and a wave forced situation has been evaluated. The model-set up and available data are described in Section 5.2.
The most important concepts are:

- The current velocity is reduced behind the groin without generating large scale eddies
- The current velocity seawards of the groin increases but less than for an impermeable groin
- Rip currents can occur also in case of permeable groins as consequence of partly deflection of the flow. These currents are less strong than in case of an impermeable groin.
- The water level distribution in the groin cells is different for permeable and impermeable groins: As permeable groins are not a hard obstacle to the flow, water level differences in cross- and longshore direction are less. The advantage is that a lower pressure gradient induces only weaker currents.
- Shorter groins are less effective than long groins reaching to the point of breaking.

B

SENSITIVITY ANALYSIS LONGSHORE CURRENT COMPUTATION

A sensitivity analysis has been carried out for the longshore current in the setup based on the experiment by Trampenau (2000) to show the influence of different setting in various parameters. The results are being compared to the velocity profiles as obtained from Figure 5.1 and to velocity profile obtained from Figure 5.2 when considering the middle arrow length as explained in Figure 7.8b. The nature of those variations can be of an environmental or a numerical parameter. This study is based on the findings of Section 7.4.4 and leads to the final settings used (Section 7.4.6) that are able to reproduce the measurements by Trampenau (2000). The sensitivity on the following variables has been evaluated:

- Environmental parameters (Section B.2)
  - Bottom profile
  - Wave height
- Numerical parameters (Section B.1)
  - Friction approach
  - Roughness
  - Scheme for horizontal advection of momentum
  - Horizontal and vertical viscosity
  - Number of layers

The bottom roughness can also be interpreted as an environmental parameter. As the bottom roughness (i.e. the value for the friction parameter) is often used for the calibration of a model, it is regarded as a numerical parameter in this specific study.
The following tests are referred to within this chapter (Table B.1):

Table B.1: Testseries G: Simulations on the longshore current on the sensitivity towards several parameters. The standard wave height is $H = 0.05$m, the standard horizontal viscosity model is Smagorinsky ($c_s = 0.2$).

G	*Bottom1*	$m = 0.0190\text{s/m}^{1/3}$	BDF	1	-
G2	*Bottom2*	$m = 0.0190\text{s/m}^{1/3}$	BDF	1	-
G3	*Bottom1*	$m = 0.0114\text{s/m}^{1/3}$	MINMOD	1	-
G4	*Bottom3*	$m = 0.0114\text{s/m}^{1/3}$	MINMOD	1	-
G5	*Bottom1*	$C = 70\text{m}^{1/2}\text{/s}$	MINMOD	1	-
G6	*Bottom2*	$C = 70\text{m}^{1/2}\text{/s}$	MINMOD	1	Wave height: $H = 0.03$m
G7	*Bottom1*	$C = 50\text{m}^{1/2}\text{/s}$	MINMOD	1	-
G8	*Bottom1*	$m = 0.0190\text{s/m}^{1/3}$	MINMOD	1	-
G9	*Bottom2*	$m = 0.0114\text{s/m}^{1/3}$	BDF	1	-
G10	*Bottom1*	$m = 0.0190\text{s/m}^{1/3}$	MINMOD	2 (33-67)	excluding k-epsilon model
G11	*Bottom1*	$m = 0.0190\text{s/m}^{1/3}$	MINMOD	2 (33-67)	including k-epsison model
G12	*Bottom1*	$m = 0.0190\text{s/m}^{1/3}$	MINMOD	2 (50-50)	excluding k-epsilon model

B.1. NUMERICAL PARAMETERS

B.1.1. FRICTION APPROACH

There are two (and more) ways to include the friction on the flow due to bottom roughness into the calculation. Two of those approaches, the one by Manning and the one by Chézy, have been evaluated. For both, a constant value has been used throughout the domain, implying that the bottom is getting rougher at lower waterdepth for Manning compared to Chézy according to formula 2.38 when using the same offshore roughness. Therefore, the current magnitude is larger using the Chézy approach. The cross-shore width of the longshore current and the wavebreaking are not influenced (Figure B.1).

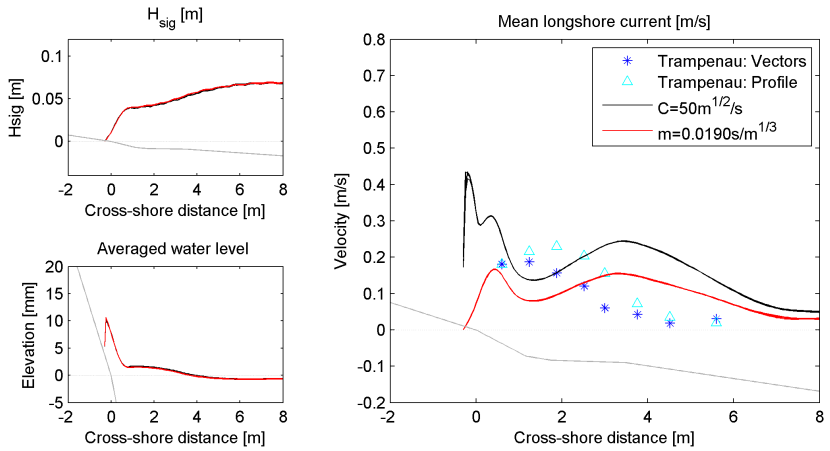

Figure B.1: Influence of the friction approach: The effect of changing the friction approach between the one of Chézy and the one of Manning. In both cases, a constant value over the whole domain has been implemented. The roughness represented by these values is the same effective roughness at the offshore boundary at a waterdepth of $h = 0.3$m. The scheme used is BDF for one single layer. The breaking and the averaged water level are not effected. The current profile is qualitatively similar, yet the values differ and the behaviour close to the shoreline.

B.1.2. FRICTION VALUE AND ADVECTION SCHEME

The primary, i.e. physical, effect of the value for the bottom roughness is the increase or reduction of the maximal (longshore) current velocity and its profile. As a secondary effect, a numerical, it influences the stability of the computation.
The more accurate BDF scheme gives rise to instabilities when using a smoother bottom (Figure B.2). The very wide longshore current and offshore breaking of the waves for the smoother bottom (using $m = 0.0114\text{s/m}^{1/3}$ and the BDF scheme) is not in the range of realistic expectation; for the rougher bottom (using $m = 0.0190\text{s/m}^{1/3}$), the BDF scheme yields more realistic results, closely to the results obtained with the MINMOD scheme (Figure B.2 and B.3).
When solving the horizontal advection of momentum by means of the MINMOD scheme, the value of the friction coefficient by Manning influences only the strength and width of the longshore current. Neither the stability nor the wavebreaking and initiation of the longshore current are influenced (Figure B.4).
Similar observations are made for using different bottom roughness values using the approach by Chézy, for both the BDF and the MINMOD scheme.

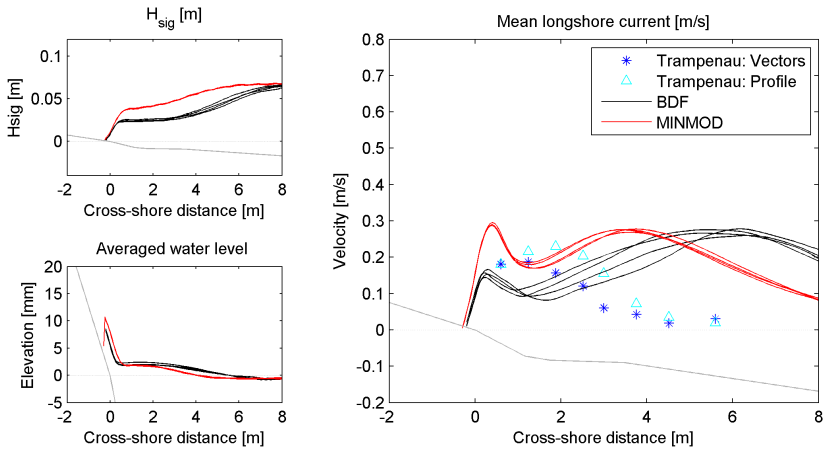

Figure B.2: Influence of the advection scheme for rough bottom: comparing the effect of using a different horizontal advection scheme of momentum (BDF and MINMOD) for a smooth bottom ($m = 0.0114\text{s/m}^{1/3}$) and a single layer.

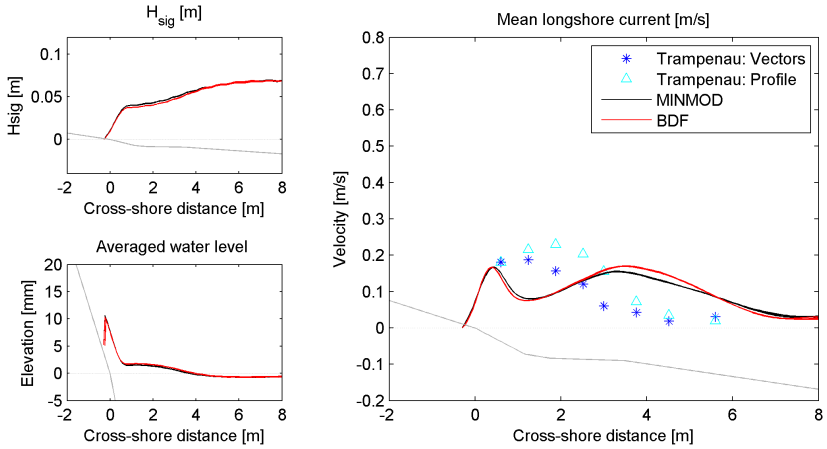

Figure B.3: Influence of the advection scheme for a rough bottom: comparing the effect of using a different horizontal advection scheme of momentum (BDF and MINMOD) for a rough bottom ($m = 0.0190\text{s/m}^{1/3}$) and a single layer. The wavebreaking is varying significantly for the two testcases leading to significantly different longshore current profiles.

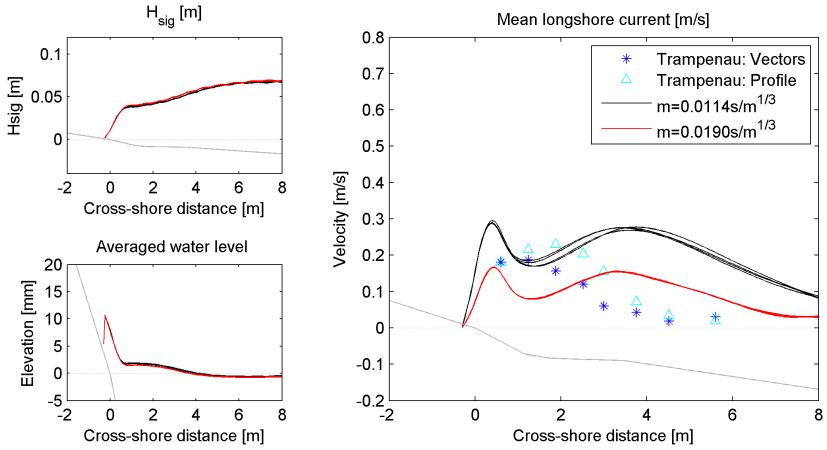

Figure B.4: Influence of the bottom friction: Using a higher friction value yields a rougher bottom and lower velocity but no visible effect on the wavebreaking and averaged water level. The MINMOD scheme is used for a single layer. The results for the waveheight, the averaged water level and the longshore current profile are practically the same.

B.1.3. NUMBER OF LAYERS

To evaluate the effect of the number of layers, this number has been varied between one and two. The most simple approximation is by only one layer over the vertical, i.e. a purely two dimensional approach. Secondly, two layers are used over the vertical, in which the upper layer (layer 1) has 33% of the waterdepth and the lower layer 67% of the local waterdepth. Thirdly, two layers with an even distribution over the vertical are used.
Choosing multiple layers and thus a 3D simulation, only influences the magnitude of the longshore current. The place of wave breaking and the width of the longshore current are not influenced. This indicates that the location of wave breaking is not varying from the measurements due to an unsatisfactory resolution in the vertical. Instabilities arose for a usage of four or more layers. Again, these are stabilized by using the preconditioner ILU instead of ILUD.

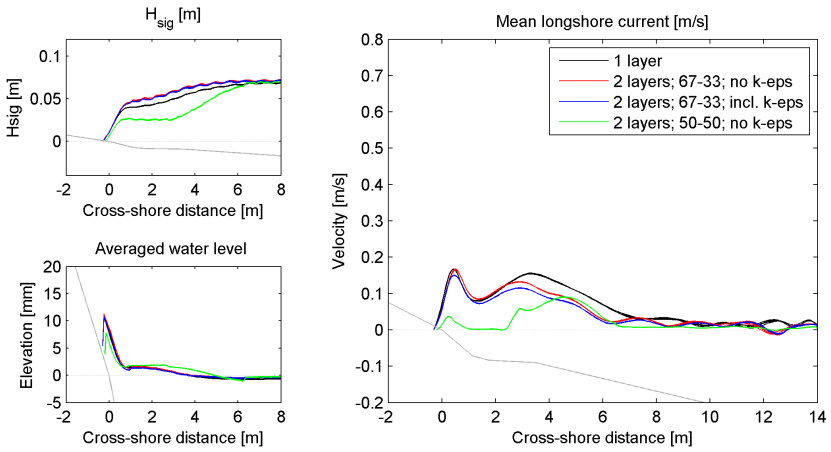

Figure B.5: Influence of the choice of number of layers: Using a single layer is compared to different options using two layers. Only using an evenly distribution of the layers gives a major change in wavebreaking and the longshore current distribution. That setting is not favourable as it can be declared as not realistic.

B.1.4. VISCOSITY

HORIZONTAL VISCOSITY

For the simulation based on the experiment by Reniers (1999), the horizontal mixing has been evaluated for all three available possibilities in the numerical model: The Smagorinsky, the mixing length and the constant eddy viscosity approach. It showed to be possible to obtain the same results for a Smagorinsky value of $c_s = 0.2$ and for a constant eddy viscosity of $\nu = 0.0005\text{m}^2/\text{s}$ (Figure B.6) which is a rather small value. Based on this experience, it is chosen that the Smagorinsky approach requires less adjustment and is used hereafter as viscosity model for the wave case.

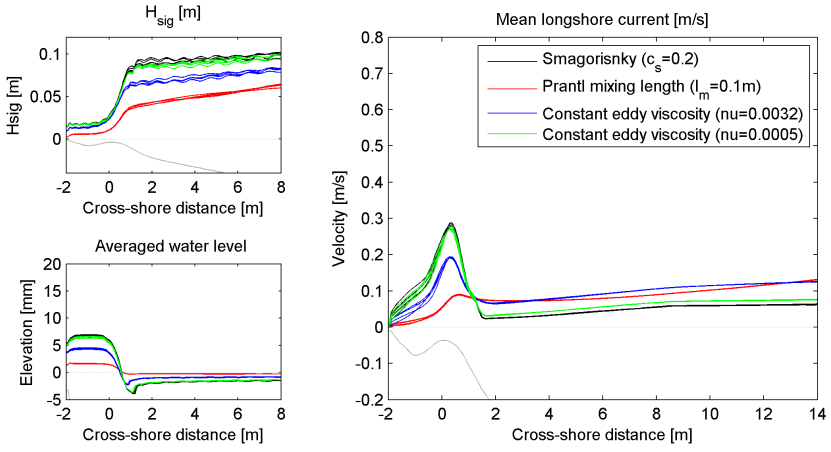

Figure B.6: Influence of schematizing horizontal viscosity: A Smagorinsky value of $c_s = 0.2$ has been compared to a mixing length of $l_m = 0.1$m and 0.1m. A friction of $m = 0.0124$ and one layer have been used. The high mixing length shows a strong horizontal mixing, whereas a smaller mixing length of $l_m = 0.01$m gives a comparable distribution to the Smagorinsky approach (For Reniers case).

VERTICAL VISCOSITY

In case of multiple vertical layers, a vertical viscosity can be included by means of the k-epsilon model; in a purely two dimensional simulation, it is not included. When including vertical viscosity, the separation of the layers is of importance (Figure B.7). For a division at half of the waterdepth, the vertical viscosity has a major influence, whereas for a division at 2/3 of the waterdepth with the smaller layer being the top one, there is no major influence visible (Figure B.8).

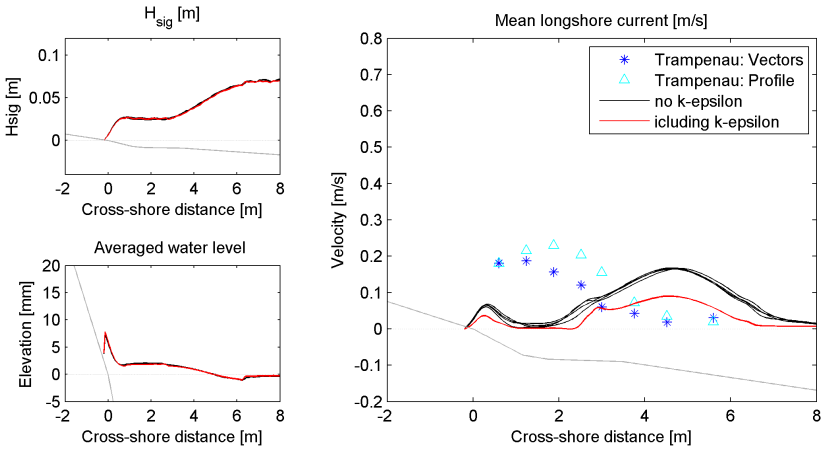

Figure B.7: Influence of the vertical viscosity model for two vertically evenly distributed layers. The simulation without k-epsilon model is for one single layer. The MINMOD scheme is used with a bottom roughness by Manning with $m = 0.0190\text{s/m}^{1/3}$

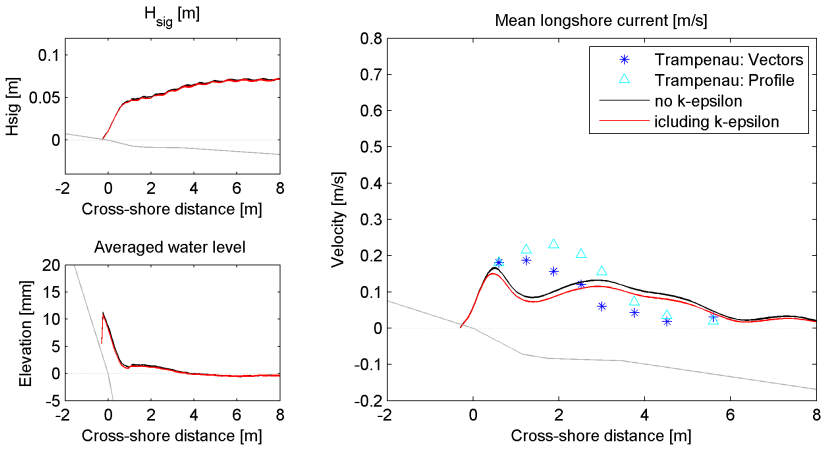

Figure B.8: Influence of the vertical viscosity model for a layer distribution of 1/3-2/3 (from top). The MINMOD scheme is used with a bottom roughness by Manning with $m = 0.0190\text{s/m}^{1/3}$. For this layer schematisation, there is no influence of including or excluding the k-epsilon model.

B.2. INFLUENCE ENVIRONMENTAL PARAMETERS

B.2.1. BOTTOM PROFILE

In the computational part of this thesis, three bathymetry profiles have been evaluated: (1) a bottom slope including the beach part of the profile (*Bottom2*); (2) a bottom profile not including the beach part as in a first approximation the beach part was not stable (*Bottom1*); and (3) a bottom that is adjusted to initiate wave breaking further onshore (*Bottom3*), see Figure 7.3a and 7.3b.

COMPARING BATHYMETRY PROFILES *Bottom(1)* AND *Bottom(2)*

As the original bottom profile (imitating the beach from the experiments by Trampenau (2000)) gave rise to instabilities in the computation, a second bottom profile is developed. It appeared that the transition between wet and dry cells can be identified as the origin of the instabilities. Therefore, the bathymetry profile has been adjusted in such a way that it does not include points on the threshold between being wet or dry by deepening the bottom close to the shore and ending the grid at the shoreline. For this profile, parts of the sensitivity analysis are presented. However, it proofed

that by changing the numerical method for solving the given matrix from the preconditioner ILUD to ILU, the transition cells can be stabilised in the original bathymetry profile. The preconditioner ILU offers more stability though it is on the cost of efficiency as it is computationally more expensive. There is no visible effect on the wavebreaking near the main breaker zone. The peak of the longshore current is at the same cross-shore distance. However, the shape is moved shorewards when not including the beach (Figure B.9). Due to the change in the bathymetry close onshore, effects are visible at this location. When including the beach, the waveheight is decreasing to zero including a second breaker line, which induces a second, smaller, peak in the longshore current profile close to the shoreline. Comparing those results to the measurements, the less exact schematisation seems to be closer to the measurements than the bottom including the beach.
The water level setup is higher for the profile *Bottom2* at the shoreline as the highest set-up with respect to the MSL occurs closer to the shoreline with lower waterdepths. An interesting observation is that the averaged water level is generally higher when including the shore line.

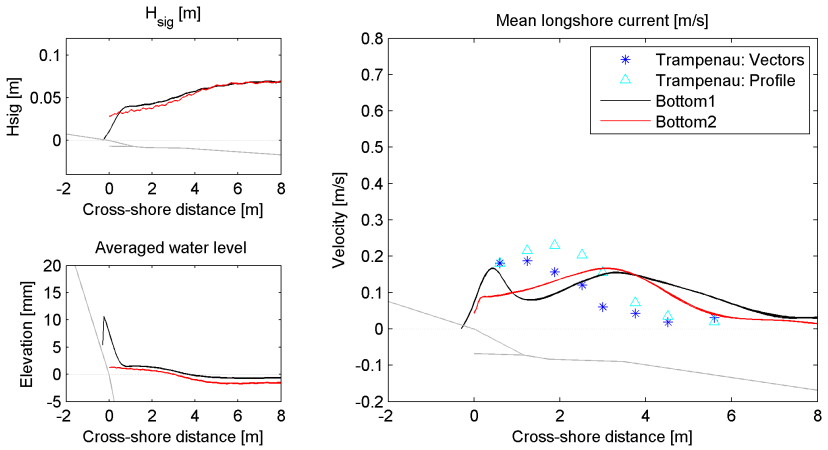

Figure B.9: Influence of the bottom schematisation: comparing *Bottom(1)* and *Bottom(2)*. The bottom including and excluding the original shoreline. The BDF scheme for one single layers and a Manning friction value of $m = 0.019\text{s/m}^{1/3}$ are used. The offshore breaking is not influenced, neither is the peak of the longshore current (magnitude and location). However, the set-up is influenced and the original bottom initiates a second breaker line.

COMPARING BOTTOM PROFILE (1) AND (3)

In bathymetry profile *bottom(3)*, the elevation has been lowered between the points where the waves are breaking in profile *bottom(1)* and where they should break according to the results by Trampenau (2000). Lowering the profile results in a later wavebreaking as the breaker parameter γ (ratio $\gamma = H/h$) reaches the possible maximum further onshore and thus an onshore shift of the longshore current occurs. With this bathymetry, the actual measurements can be reproduced reasonably well and are used for the evaluation of the groins (Figure B.10).

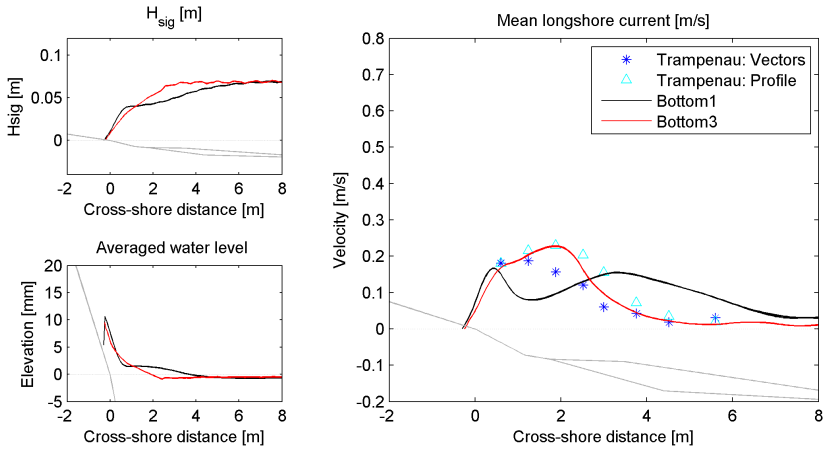

Figure B.10: Influence of the bottom schematisation: comparing *Bottom(1)* and *Bottom(3)*. The MINMOD scheme has been used for a single layer and a Manning friction coefficient of $m = 0.0114\text{s/m}^{1/3}$. For the adjusted bottom, the breaking is taking place closer onshore leading to an onshore shift of the longshore current compared to *Bottom(1)*.

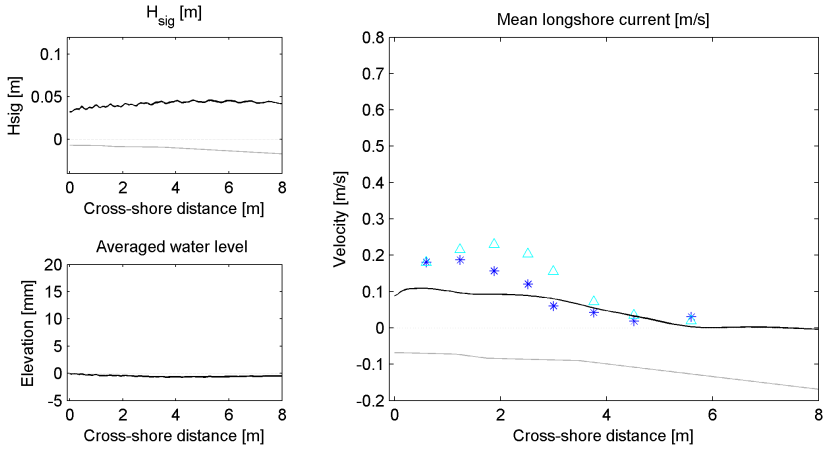

Figure B.11: Influence of the wave height: A smaller wave height ($H = 0.03$m is evaluated. The bathymetry *Bottom2* is used for the evaluation. The bottom friction is $C = 70\text{m}^{1/2}/\text{s}$.. The MINMOD scheme is used. The longshore current for the lower wave height starts further onshore as to be expected as the waves break more onshore in a lower waterdepth. On the other hand, the value for the longshore current is much lower.

B.2.2. WAVE HEIGHT

The waveheight is an important environmental parameter. It determines the location of wavebreaking (via the breaker index γ) and the magnitude of the longshore current. The influence of the waveheight has been tested for the bathymetry profile *Bottom(2)*. Also in the results from SWASH, the waveheight determines the location of the breaker line. The smaller waves break at a lower waterdepth closer to the shoreline. The magnitude of the longshore current is depending on the radiation stress induced by the wave. The lower wave height induces a lower radiation stress and therefore reduces the velocity of the longshore current compared to the higher wave. As there are two factors influenced by the waveheight, it does not seem to be usable to improve the relation between the measurements and the SWASH results. The (maximal) magnitude of the longshore current coincides well for the higher waves (with H=0.05m), but not for the lower waves ($H_0 = 0.03$m). The location of the wavebreaking coincides for the lower waves but not for the high waves.

B.3. SUMMARY AND FURTHER ADVISE

The following choices can be made according to this sensitivity analysis:

- The main influence on the wavebreaking is due to the waveheight and the local waterdepth. If the waveheight is supposed to remain unchanged, another bottom schematisation should be chosen. In future research by means of a numerical model, more insight could be gained if this is observable again. For the further report, the bathymetry profile *Bottom3* will be used,
- Using the Manning friction approach with a value of $m = 0.019\text{s/m}^{1/3}$,

- The Smagorinsky model is used to include horizontal mixing.

Furthermore, the following minor advices can be given without further detailed explanation:

- An important command is `[BREAKING]` that initiates breaking for a small amount of layers (less than six, according to The SWASH team (2014)). The usage is indispensable, yet the exact value does not play a role,
- When using multiple vertical layers, the k-epsilon model can be used to simulate the vertical viscosity. It showed to not have a major impact whether it is used or not,
- Using ILU for the iteration process can make unstable calculations stable. It though is slower than ILUD
- One layer is sufficient

C

ADDITIONAL FIGURES SIMULATION WAVES AND GROINS

C.1. FLOW FIELD FOR DIFFERENT IMPLEMENTATION OF GROINS

Figures C.1 to C.9 show the flow fields for simulations with one groin under wave conditions ($H_0 = 0.05$m, $T = 1.23$s, $\theta = 30°$) as discussed on Section 7.5.3.

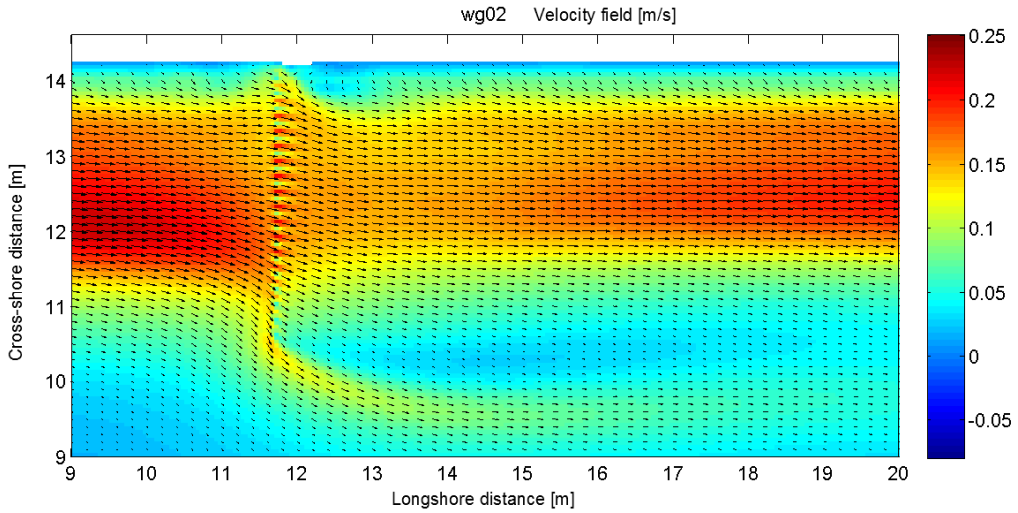

Figure C.1: Flow field and velocity for wg02: Groin with a length of $L_g = 3.5$m, piles resolved on the grid. Grid resolution $\Delta x = \Delta y = 0.05$m.

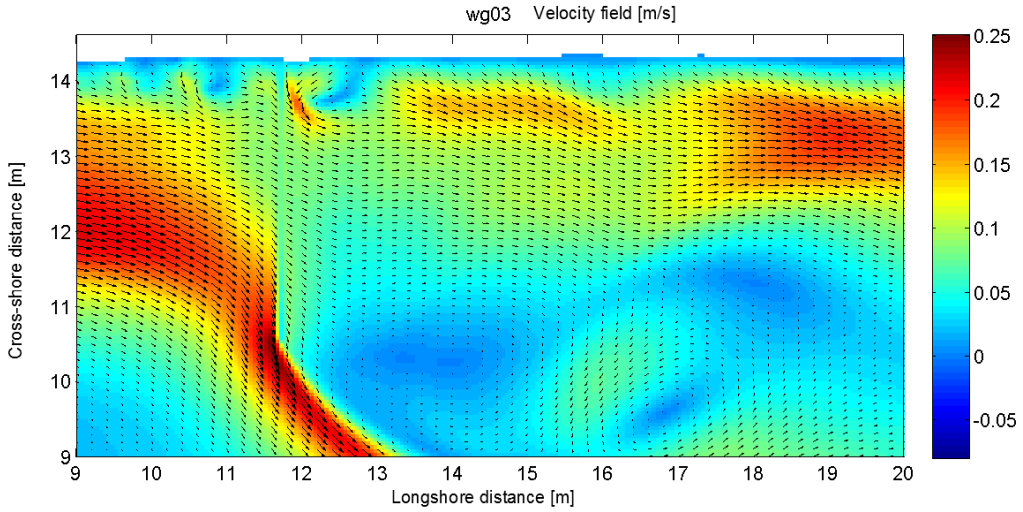

Figure C.2: Flow field and velocity for wg03: Groin with a length of $L_g = 3.5$m, piles averaged as subgrid feature (impermeable groin). Grid resolution $\Delta x = \Delta y = 0.05$m.

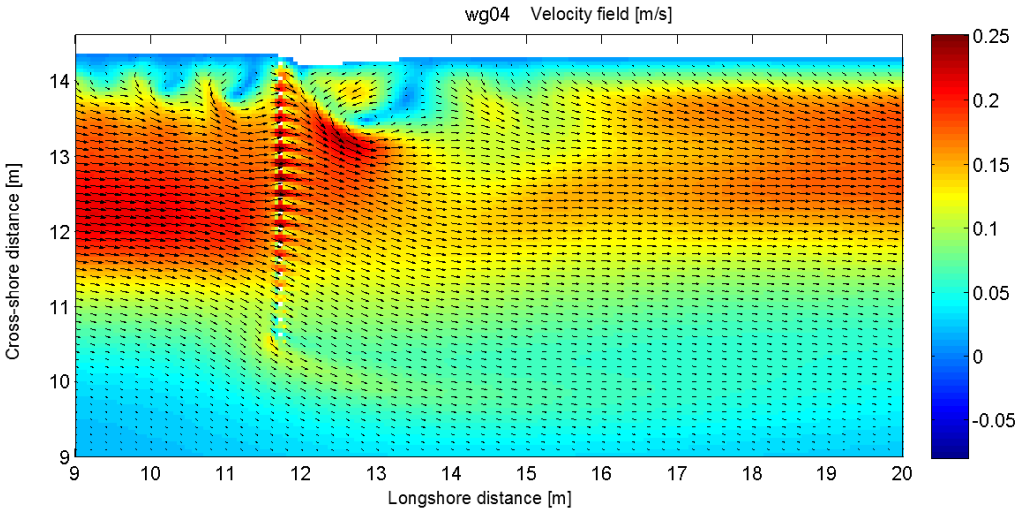

Figure C.3: Flow field and velocity for wg04: Groin with a length of $L_g = 3.5$m, piles are exception values. Gridresolution $\Delta x = \Delta y = 0.05$m.

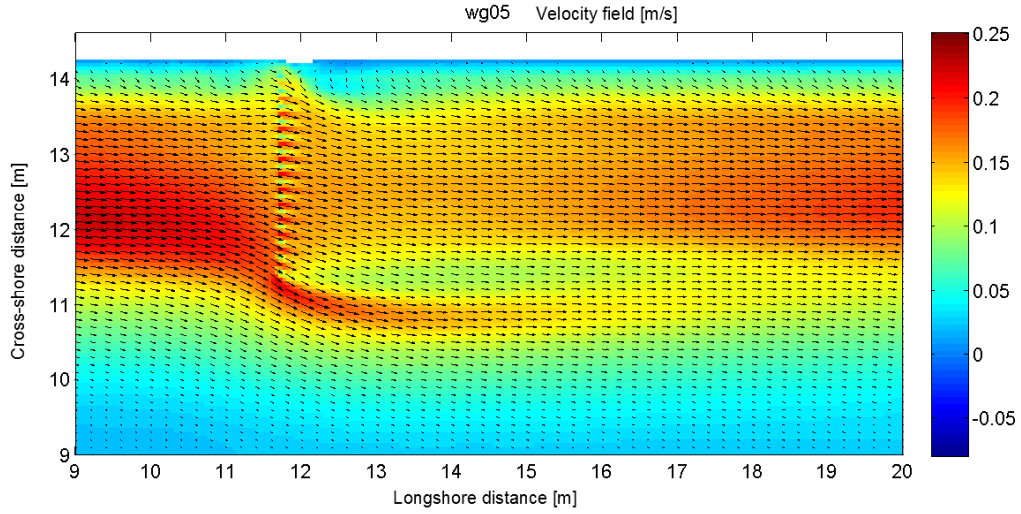

Figure C.4: Flow field and velocity for wg05: Groin with a length of $L_g = 2.7$m, piles resolved on the grid. Grid resolution $\Delta x = \Delta y = 0.05$m.

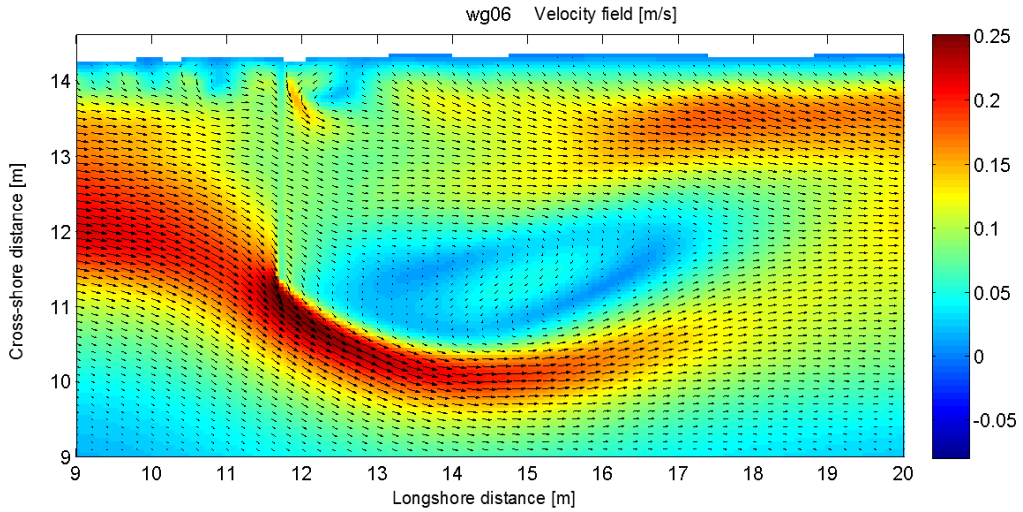

Figure C.5: Flow field and velocity for wg06: Groin with a length of $L_g = 2.7$m, piles are averaged as subgrid feature (Permeability theoretically 50%). Grid resolution $\Delta x = \Delta y = 0.05$m.

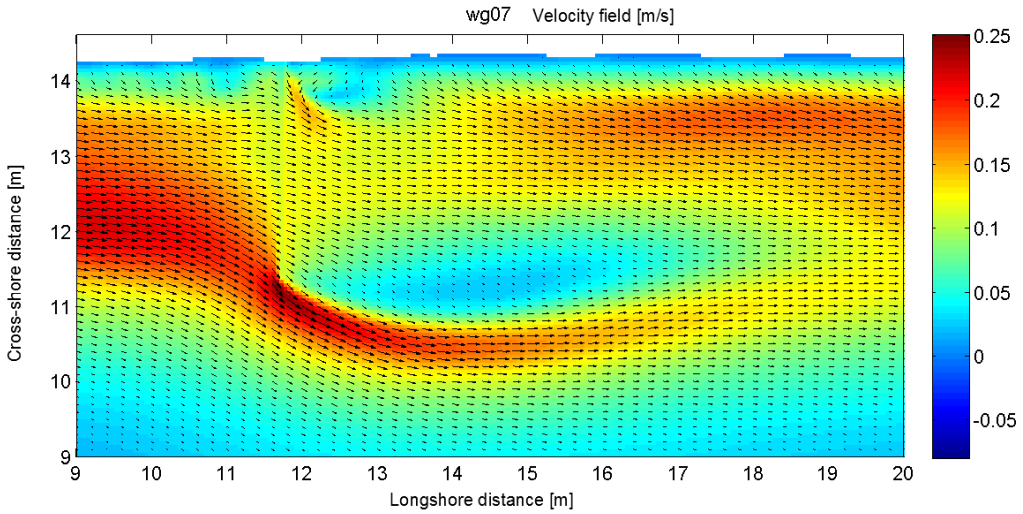

Figure C.6: Flow field and velocity for wg07: Groin with a length of $L_g = 2.7$m, piles are averaged as subgrid feature (Permeability theoretically 25%). Grid resolution $\Delta x = \Delta y = 0.05$m.

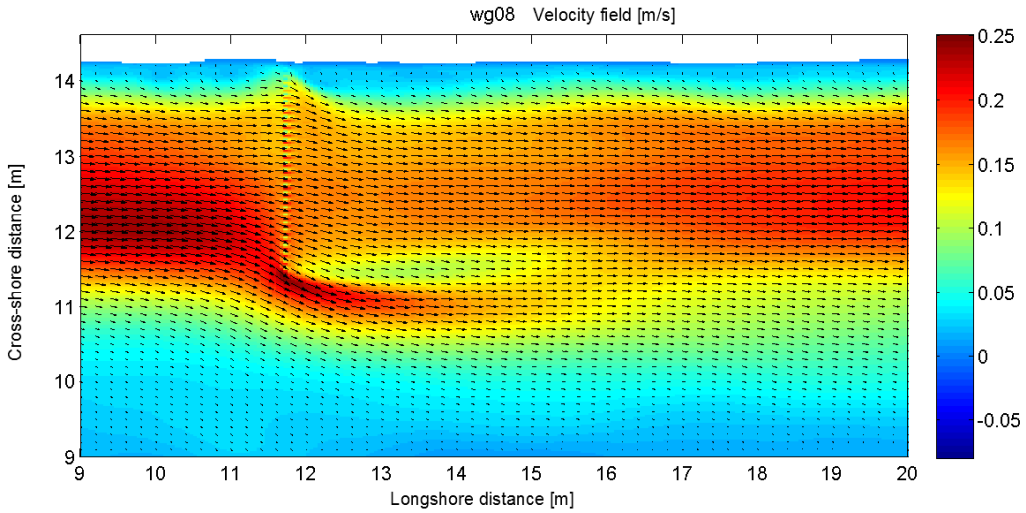

Figure C.7: Flow field and velocity for wg08: Groin with a length of $L_g = 2.5$m, piles resolved on the grid. Grid resolution $\Delta x = \Delta y = 0.05\text{m} \times 0.025\text{m}$.

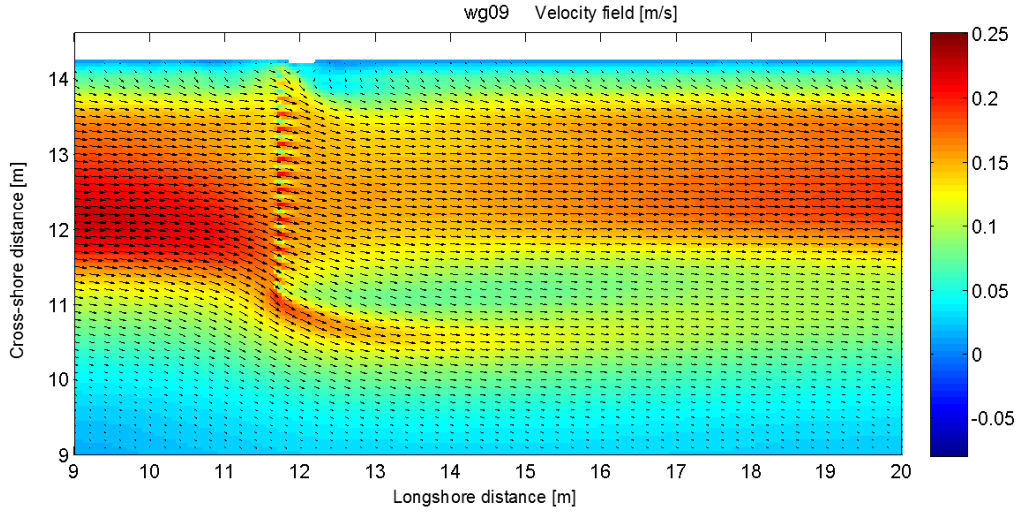

Figure C.8: Flow field and velocity for wg09: Groin with a length of $L_g = 3.0$m, piles resolved on the grid. Grid resolution $\Delta x = \Delta y = 0.05$m.

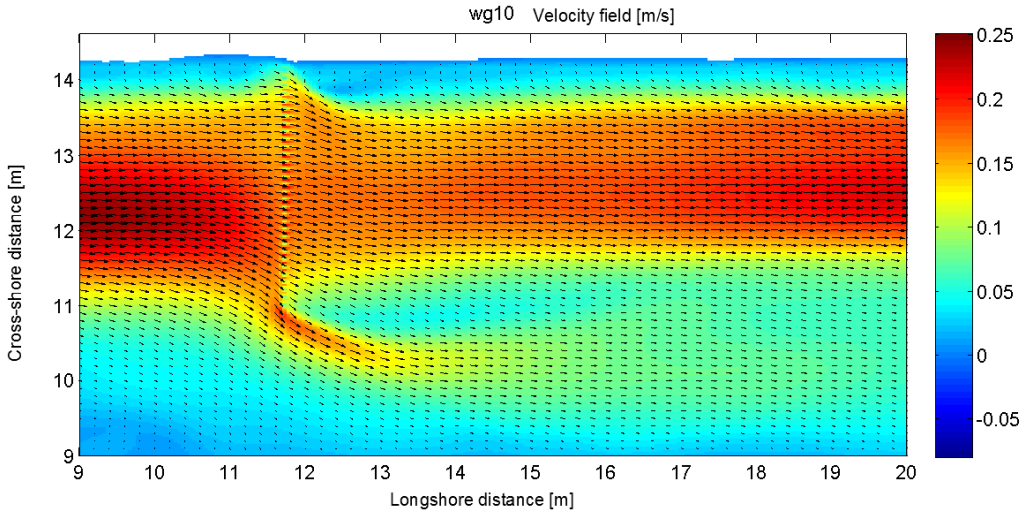

Figure C.9: Flow field and velocity for wg10: Groin with a length of L_g = 3.0m, piles resolved on the grid. Grid resolution $\Delta x = \Delta y$ = 0.05m × 0.025m.

C.2. LONGSHORE CURRENT VELOCITY FOR DIFFERENT WAVE ANGLES

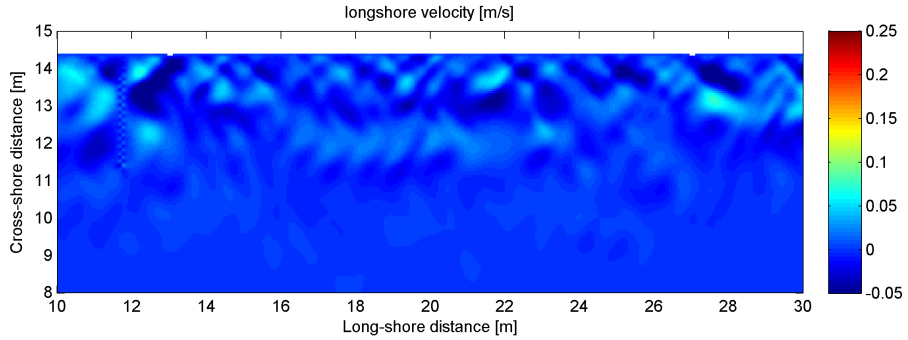

Figure C.10: Longshore current velocity for waves approaching with $\theta = 0°$ to the cross-shore.

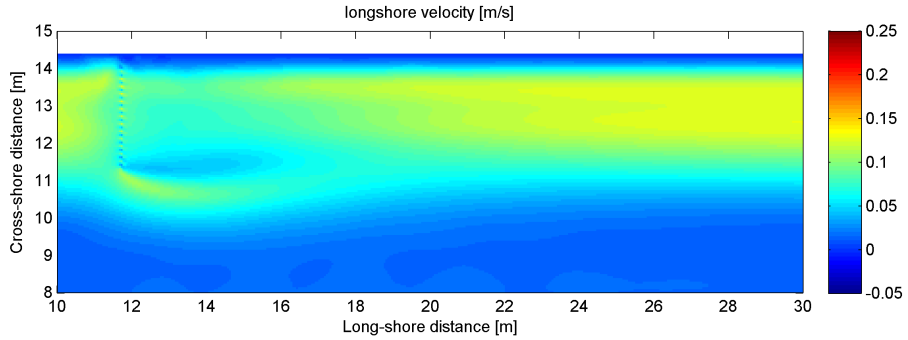

Figure C.11: Longshore current velocity for waves approaching with $\theta = 15°$.

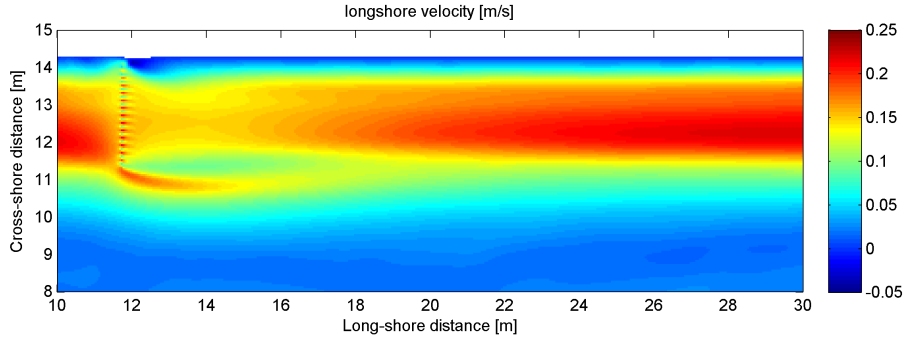

Figure C.12: Longshore current velocity for waves approaching with $\theta = 30°$.

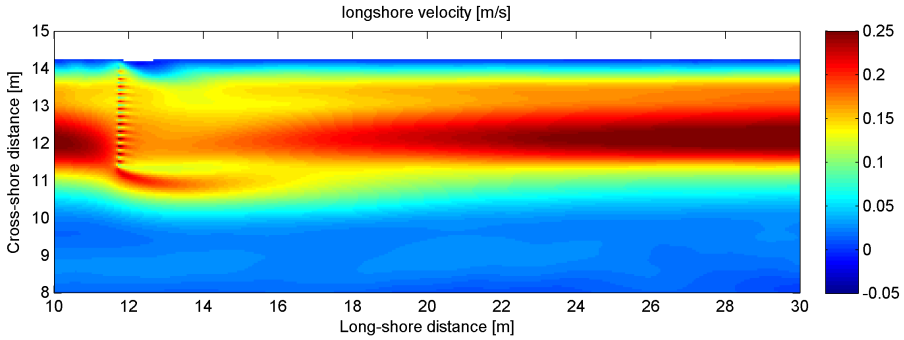

Figure C.13: Longshore current velocity for waves approaching with $\theta = 45°$.

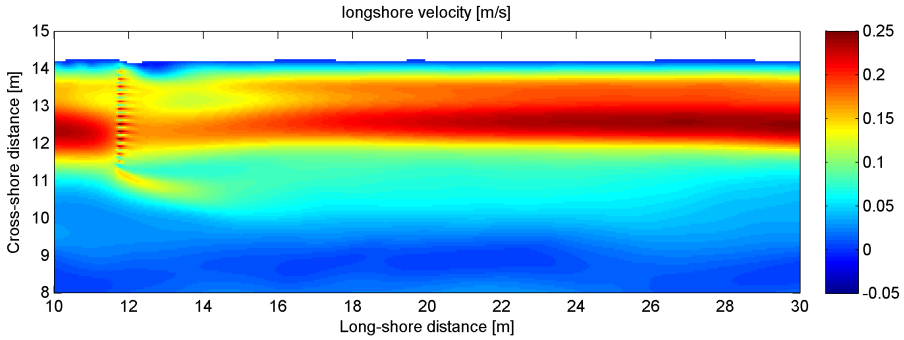

Figure C.14: Longshore current velocity for waves approaching with $\theta = 60°$.

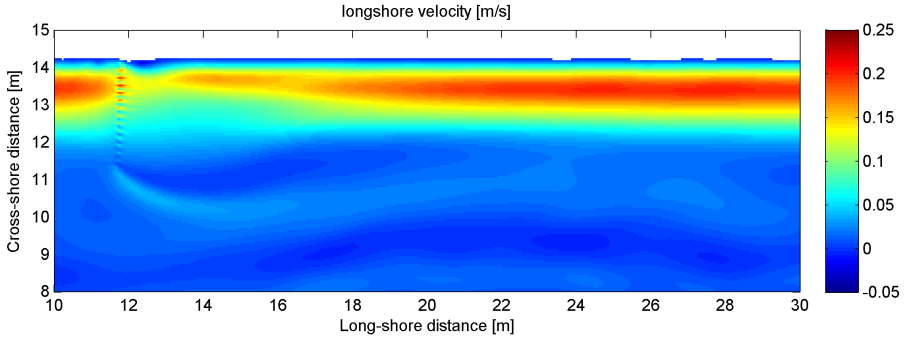

Figure C.15: Longshore current velocity for waves approaching with $\theta = 75°$.

C.3. SHEAR STRESS DEPENDENCY ON GROIN LENGTH AND WAVE ANGLE

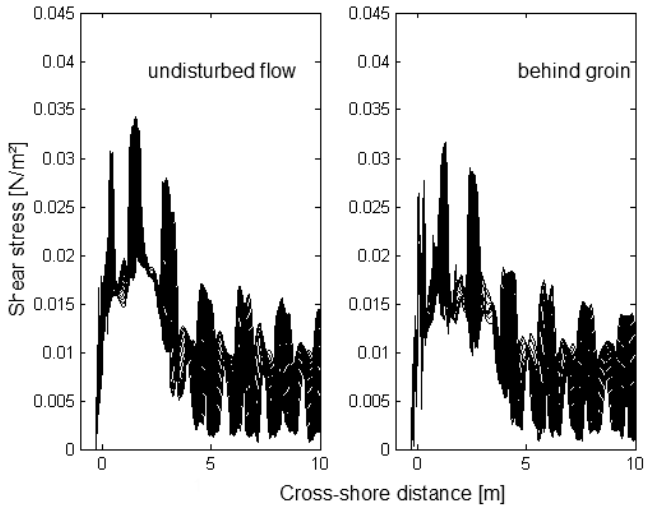

Figure C.16: Shear stress for a groin length of l_g = 2.70m: The left figure shows the instantaneous shear stresses in a 1m band, the right figure shows the reduced shear stresses behind the groin in a 1m band.

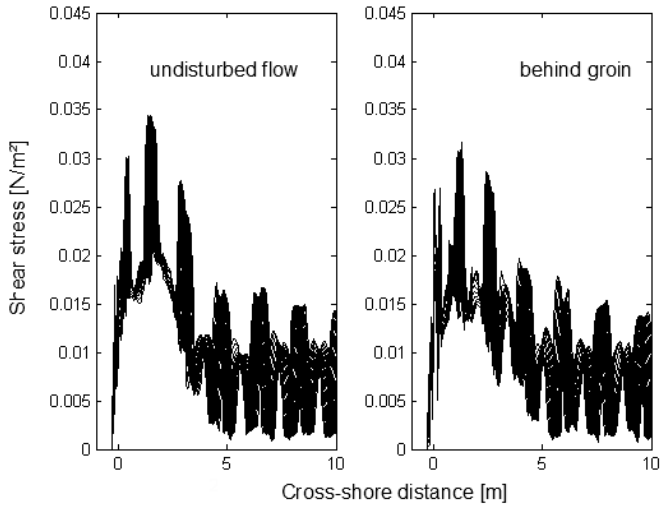

Figure C.17: Shear stress for a groin length of l_g = 3.00m: The left figure shows the instantaneous shear stresses in a 1m band for several cross-sections, the right figure shows the reduced shear stresses behind the groin in a 1m band.

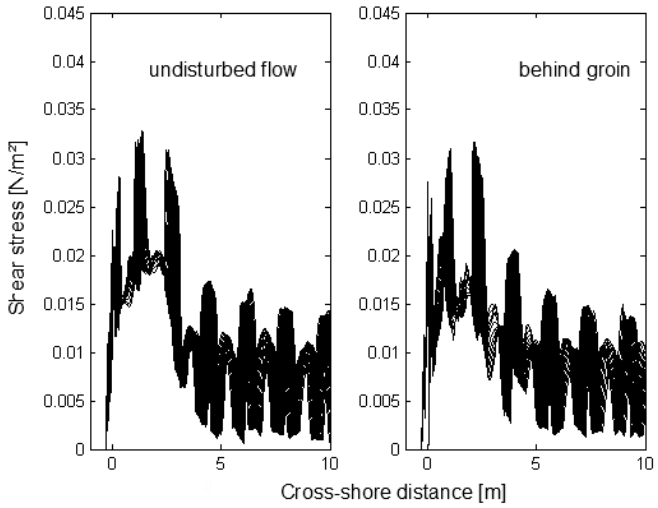

Figure C.18: Shear stress for a groin length of l_g = 3.50m: The left figure shows the instantaneous shear stresses in a 1m band for several cross-sections, the right figure shows the reduced shear stresses behind the groin in a 1m band.

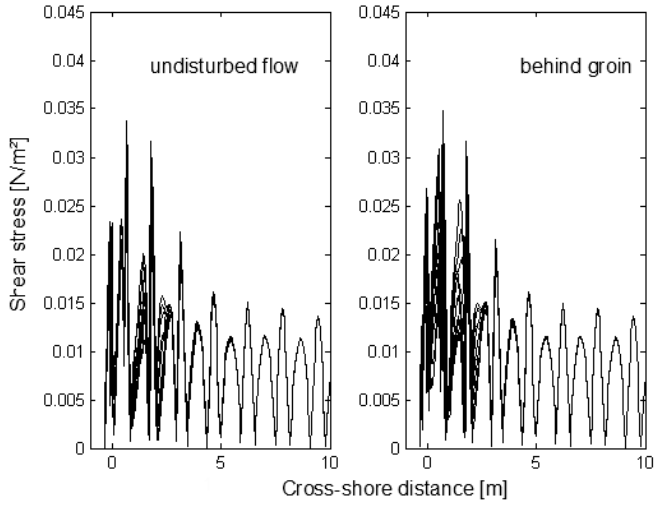

Figure C.19: Shear stress for waves approaching with θ = 0°: The left figure shows the instantaneous shear stresses in a 1m band for several cross-sections, the right figure shows the reduced shear stresses behind the groin in a 1m band.

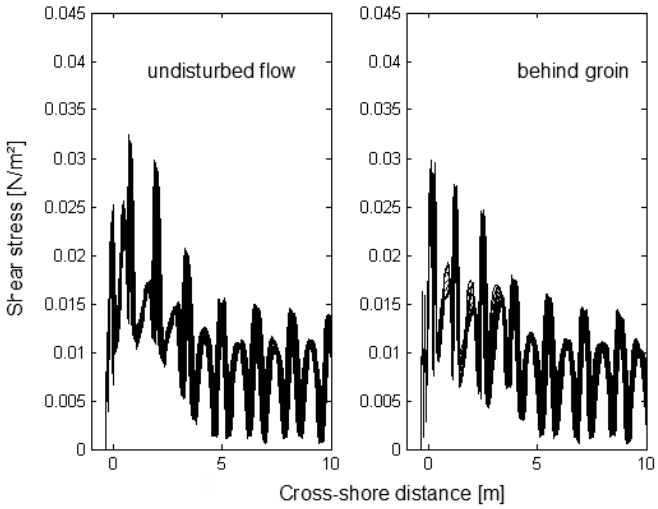

Figure C.20: Shear stress for waves approaching with $\theta = 15°$: The left figure shows the instantaneous shear stresses in a 1m band for several cross-sections, the right figure shows the reduced shear stresses behind the groin in a 1m band.

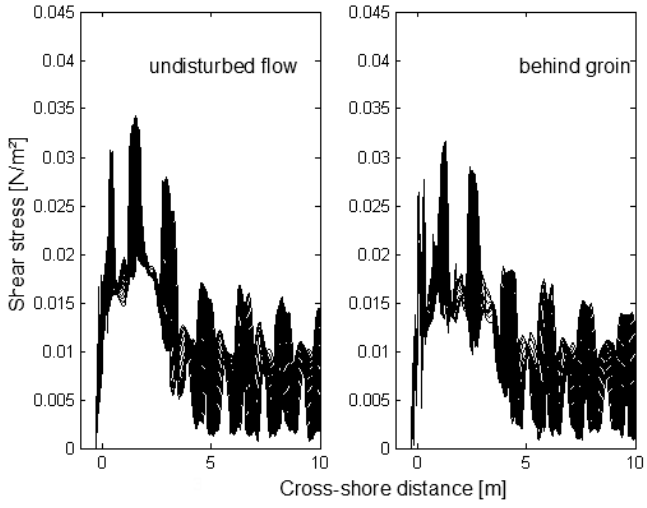

Figure C.21: Shear stress for waves approaching with $\theta = 30°$: The left figure shows the instantaneous shear stresses in a 1m band for several cross-sections, the right figure shows the reduced shear stresses behind the groin in a 1m band.

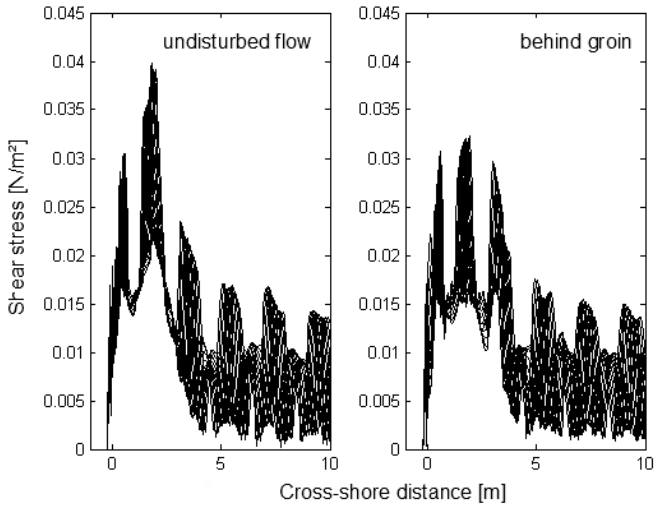

Figure C.22: Shear stress for waves approaching with $\theta = 45°$: The left figure shows the instantaneous shear stresses in a 1m band for several cross-sections, the right figure shows the reduced shear stresses behind the groin in a 1m band.

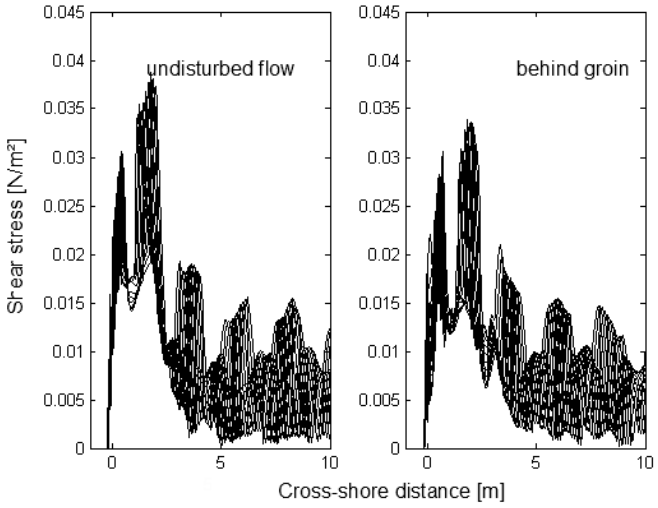

Figure C.23: Shear stress for waves approaching with $\theta = 60°$: The left figure shows the instantaneous shear stresses in a 1m band for several cross-sections, the right figure shows the reduced shear stresses behind the groin in a 1m band.

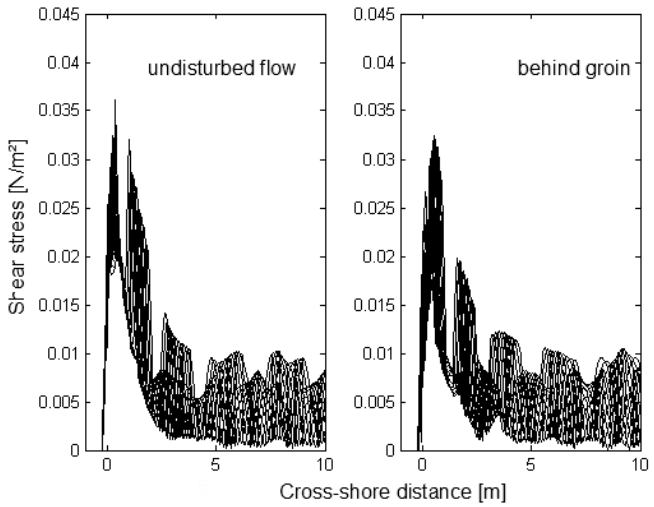

Figure C.24: Shear stress for waves approaching with $\theta = 75°$: The left figure shows the instantaneous shear stresses in a 1m band for several cross-sections, the right figure shows the reduced shear stresses behind the groin in a 1m band.

BIBLIOGRAPHY

A. Apotsos, B. Raubenheimer, S. Elgar, R. Guza, and J. Smith. Effects of wave rollers and bottom stress on wave setup. *Journal of Geophysical Research*, 112(C02003), 2007.

W.T. Bakker, C.H. Hulsbergen, P. Roelse, C. de Smit, and J.N. Svasek. Permeable groynes: Experiments and practice in the Netherlands. In *Proceedings of the 19th Conference on Coastal Engineering*, number C, pages 2026–2041, Houston, USA, 1984. Proceedings of the 19th Conference on Coastal Engineering.

J.A. Battjes. Surf similarity. *Proceedings of the 14th International Conference on Coastal Engineering*, 1:466–480, 1974.

J.A. Battjes. *Vloeistofmechanica*. TU Delft, Faculteit CITG, Delft, 2002.

K.G. Bezuyen, M.J.F. Stive, G.J.C. Vaes, J.K. Vrijling, and T.J. Zitman. *Inleiding Waterbouwkunde, Lecture notes*. VSSD, Delft, 2011.

Boekblad.nl. Fotografe richt monument op voor de Zeeuwse paalhoofden, 2007. URL http://www.boekblad.nl/fotografe-richt-monument-op-voor-de-zeeuwse.125355.lynkx.

J. Bosboom and M.J.F. Stive. *Coastal Dynamics I*. VSSD, Delft, 2013.

Deltares. CFD modelling of flows in hydraulic structures and process equipment using ANSYS-CFX, 2014.

EAK. *Die Küste Band 55*. Number 1993. Kuratorium für Forschung im Küsteningenieurwesen, 1993. ISBN 3804206506.

EAK. *Die Küste Band 65 Jahr 2002, korrigierte Ausgabe 2007*. Kuratorium für Forschung im Küsteningenieurwesen, 2007. ISBN 9783804210561.

C.A. Fleming. Guide on the use of groynes in coastal engineering. Technical report, Construction Industry Research and Information Association (CIRIA), Report 119, 1990a.

C.A. Fleming. Principles and effectiveness of Groynes. In K.W. Pilarczyk, editor, *Coastal Protection*, pages 121–156. Balkema, Rotterdam/Brookfield, Netherlands, 1990b. ISBN 90-6191-127-3.

Geschiedeniszeeland. De vijftig vensters, a. URL http://www.geschiedeniszeeland.nl/topics/zc_boekje.pdf.

Geschiedeniszeeland. Colofon geschiedeniszeeland.nl, b. URL http://www.geschiedeniszeeland.nl/tab_themas/meer/canon/colofon_canon/index?lng=nl.

D. Hinrichsen. *The Atlas of coasts & oceans, mapping ecosystems, threatened ressources and marine conservation*. Earthscan Ltd, Brighton, UK, 2011. ISBN 978-1-84971-207-1.

L.H. Holthuijsen. *Waves in oceanic and coastal waters*. Cambridge University Press, New York, 2007. ISBN 9780521860284.

J.M.J. Journée and W.W. Massie. *Offshore hydromechanics*. Number January. Delft University of Technology, Delft, first edition, 2001. URL http://ocw.tudelft.nl/courses/offshore-engineering/offshore-hydromechanics-1/readings/.

G.H. Keulegan and L.H. Carpenter. Forces on cylinders and plates in an oscillating fluid. *Journal of Research of the National Bureau of Standards*, 60(5):423–440, May 1958. ISSN 0091-0635. doi: 10.6028/jres.060.043. URL http://nvlpubs.nist.gov/nistpubs/jres/60/jresv60n5p423_A1b.pdf.

J.T. Kirby. Boussinesq Models and Applications to Nearshore Wave Propagation, surf Zone Processes and Wave-Induced Currents. In C. Lakhan, editor, *Advances in Coastal modelling, Elsevier Oceanography Series*, volume 67, pages 1–41. Elsevier Science B.V., 2003. ISBN 0444511490.

P.D. Komar. Beach-slope dependence of longshore currents. *Journal of Waterway, Port, Coastal and Ocean Division*, (ASCE 105(WW4)):460–464, 1979.

P.D. Komar. *Beach processes and sedimentation*. New Jersey, second edition, 1998. ISBN 0-13-754938-5.

J.B. Kuipers and J. Francke. *Geschiedenis van Zeeland, de Canon van ons Zeeuws Verleden*. 2009.

M.S. Longuet-Higgins. Currents Generated by Obliquely Incident Sea Waves, 1. *Journal of Geophysical Research*, 75(33): 6778–6789, 1970a.

M.S. Longuet-Higgins. Currents Generated by Obliquely Incident Sea Waves, 2. *Journal of Geophysical Research*, 75(33): 6790–6801, 1970b.

M.S. Longuet-Higgins and R.W. Stewart. Radiation stress and mass transport in gravity waves, with application to surf-beats. *Journal of Fluid Mechanics*, 13:481–504, 1962.

M.S. Longuet-Higgins and R.W. Stewart. Radiation stresses in water waves: a physical discussion with applications. *Deep-Sea Research*, 11:529–562, 1964.

G. Ma, J. T. Kirby, S.-F. Su, J. Figlus, and F. Shi. Numerical study of turbulence and wave damping induced by vegetation canopies. *Coastal Engineering*, 80:68–78, 2013.

Maritimejournal. Strengthening of coastal defences is underway at Eastoke Peninsular Hayling The Eastern Solent Coastal Partnership, 2014. URL http://www.maritimejournal.com/__data/assets/image/0005/818375/Strengthening-of-coastal-defences-is-underway-at-Eastoke-Peninsular-Hayling-The-Eastern-Solent-Coastal-Partnership.jpg.

R. Miche. Mouvements ondulatoires des mers en profundeur constante on decroisante. In *Annales des Ponts et Caussees*. 1944.

J.R. Morison, M.P. O'Brien, J.W. Johnson, and S.A. Schaaf. The Force Exerted by Surface Waves on Piles. *PetroleumTransactions, AIME*, 189:149–154, 1950.

S. B. Pope. *Turbulent Flows*. Press syndicate of the University of Cambridge, Cambridge, UK, 2000. ISBN 0521591252.

Provinciale Zeeuwse Courant. Kopzorgen over paalhoofden, 2007. URL http://www.pzc.nl/regio/walcheren/kopzorgen-over-paalhoofden-1.1812397.

A. Reniers. *Longshore current dynamics*. Delft, 1999. ISBN 90-9012742-9.

A.J.H.M. Reniers and J.A. Battjes. A laboratory study of longshore currents over barred and non-barred beaches. *Coastal Engineering*, 30:1–21, 1997.

RIZA. *Stromingsweerstand vegetatie in uiterwaarden, Deel 1, Handboek versie 1-2003*. RIZA Rijksinstituut voor Integraal Zoetwaterbeheer En Afvalwaterbehandeling, 2003a. ISBN 90-369-5642-0.

RIZA. *Stromingsweerstand vegetatie in uiterwaarden, Deel 2 Achtergronddocument versie 1-2003*. Riza Rijksinstituut voor Integraal Zoetwaterbeheer En Afvalwaterbehandeling, 2003b. ISBN 90-369-5643-9.

W. Rodi. Examples of calculation methods for flow and mixing in stratified flows. *Journal of Geophysical Research*, 92(5): 5305–5328, 1987.

G.J. Schiereck. *Introduction to bed, bank and shore protection*. Delft University Press, Delft, Netherlands, first edition, 2004. ISBN 9040716838.

A. Shields. Anwendung der Aehnlichkeitsmechanik und der Turbulenzforschung auf die Geschiebebewegung. *Mitteilungen der Preußischen Versuchsanstalt für Wasserbau und Schiffbau*, 26, 1936.

Y. Shimizu and T. Tsujimoto. Numerical analysis of turbulent open-channel flow over a vegetation layer using a k-epsilon turbulence model. *Journal of Hydroscience and Hydraulic engineering*, 11(2):57–67, 1994.

A. Stacey. A rock groyne, H12, below the car park, 2001. URL http://www.stacey.peak-media.co.uk/Highcliffe/800-10210015.jpg.

G.S. Stelling and M. Zijlema. Numerical modeling of wave propagation, breaking and run-up on a beach. URL http://swash.sourceforge.net/online_doc/dcse.pdf.

G.S. Stelling and M. Zijlema. An accurate and effcient finite-difference algorithm for non-hydrostatic free-surface flow with application to wave propagation. *Int. J. Numer. Meth. Fluids 2003;*, 43(May 2002):1–23, 2003. doi: 10.1002/fld.595.

T. Suzuki, G. Schramkowski, K. Verelst, T. Verwaest, and F. Mostaert. SWASH development for coastal safety: Part 2: Development of SWASH-VEG. Version 0_1. WL Rapporten, 00_108_1. Technical report, Flanders Hydraulics Research, Antwerp, Belgium, 2013.

The COMET programme. waveangle_smallstruct.jpg, 2012. URL http://apollo.lsc.vsc.edu/classes/comet/marine/ripcurrents/NSF/media/graphics/waveangle_smallstruct.jpg.

The MathWorks Inc. MATLAB and Statistics Toolbox Release 2013b.

The SWASH team. SWASH- Simulating WAves til SHore, 2013. URL http://swash.sourceforge.net/.

The SWASH team. USER MANUAL SWASH version 2.00A. 2014. URL http://swash.sourceforge.net/download/zip/swashuse.pdf.

T. Trampenau. *Hydraulische Wirksamkeit durchlässiger Buhnen*. Leichtweiss-Institut für Wasserbau, TU Braunschweig, Braunschweig, 2000.

W. Uijttewaal. *Turbulence in hydraulics, CT 5312, lecture notes*. Faculty of Civil Engineering and Geoscience, TU Delft, Delft, Netherlands.

Unknown. 5027543696_76c36e794e_o. URL https://www.flickr.com/photos/lollyman/5027543696/in/photostream/.

J. van de Graaf and M.J. Koster. Dune and beach erosion and nourishment. In K.W. Pilarczyk, editor, *Coastal Protection*, pages 99–120. Balkema, Rotterdam/Brookfield, Netherlands, 1990. ISBN 90-6191-127-3.

P. van Lyden. *A resistable force, when man meets the sea*. Stichting Visual Legacy, Doorn, 2007. ISBN 978-90-811850-4-2.

M.M. Zdravkovich. *Flow around circular cylinders, Volume 2*. Oxford university press, Oxford, UK, 2003. ISBN 0198565615.

M. Zijlema, G. S. Stelling, and P. Smit. SWASH: an operational public domain code for simulating wave fields and rapidly varied flows in coastal waters. *Preprint submitted to Coastal Engineering*, 2011. URL http://swash.sourceforge.net/online_doc/swash.pdf.